Microtubules in hyaloclasts from the Hawaii Scientific Drilling Project #2 phase 1 core, Hilo, Hawaii: evidence of microbe-rock interactions

By

Kimberly E. Metevier

Submitted to the Department of Geology and the Faculty of

the Graduate School of the University of Kansas in partial fulfillment of

the requirements for the degree of Master of Science.

_____

Anthony W. Walton, Co-Chairman

_____

Stephen T. Hasiotis, Co-Chairman

_____

Jennifer A. Roberts

Date Defended:

October 14, 2011

Kimberly E. Metevier

The Thesis Committee for Kimberly E. Metevier

certifies that this is the approved version of the following thesis:

Microtubules in hyaloclasts from the Hawaii Scientific Drilling Project #2 phase 1 core, Hilo, Hawaii: evidence of microbe-rock interactions

_____

Chairperson: Anthony W. Walton

_____

Stephen T. Hasiotis, Co-Chairman

Date approved:

October 14, 2011

Abstract

Minute tubules etched into basalt glass in hyaloclastites from the Hawaii Scientific Drilling Project #2 (HSDP) phase 1 borehole are interpreted as trace fossils formed by microbes, i.e. microendolithic borings. Such borings are one to a few micrometers in diameter and up to >100 µm long; they extend into glass shards from free surfaces (broken shards, vesicles, fractures). Morphologic characterization of microendolithic borings quantitatively describes them for comparison with other occurrences and aids in understanding the interactions between microorganisms and basaltic glass that result in the dissolution of the glass.

The first step in working with these features as trace fossils was to modify the ichnofabric index of Droser and Bottjer (1986) for use with minute features that extend into homogeneous material. The modification includes six semiquantitative classes of disruption and is scale-independent, applicable to any size feature. The second step was to apply the new microendolithic ichnofabric index (MII) to the HSDP samples. Analysis of the HSDP samples using the MII showed that the abundance of bioerosion varied throughout the core. Assigned MII values ranged from 1 to 3, average MII values ranged from 1 to 2.44, while the mean MII value of 1.2. Areas with the most bioerosion were located between 1,365.9 and 1,478.8 mbsl and a section of the core centered around 2,117.0 mbsl. The MII values of these locations ranged from 2 to 2.5. Areas with low bioerosion (all samples <2) were located between 1,079.0 and 1,320.0 mbsl, 1,799.0 and 1,900.0 mbsl, and all depths below 2,500.0 mbsl.

Lastly, such features as length, diameter, ornamentation, density, and complexity and tortuosity were measured to better describe the interactions between microorganisms and basaltic hyaloclastite media. The shortest measured 0.907 µm and the longest measured 129.22 µm. Lengths were approximately log-normally distributed with a geometric mean of 18.9 µm. The

tortuosity of borings had a median of 1.29 with a range of 1.227 to 1.37. The least tortuous measured 1.22 and the most tortuous measured 16.46. This was one of the first attempts to quantify the range of morphology and density, of euendolithic microborings in basalt glass. This study extends the sampling scale for ichnological study to what is near the minimum size range of trace fossils. It demonstrates that trace fossil abundance does not simply decrease with depth in ocean islands, unlike basalts of oceanic crust, but varies, probably as a result of variation of the rate of accumulation of suitable substrates.

Acknowledgements

This research was not possible without the support, encouragement, and generosity of many people. I owe my biggest thanks to my three thesis advisors, Tony Walton, Steve Hasiotis, and Jennifer Roberts for giving me endless amounts of time, support, guidance, encouragement, and advice. I also thank Gary Tockman with Boyce Scientific for assistance with photography.

I want to thank my family and friends. I big thank you to my husband for providing endless support and encouragement through the years. I want to thank all my friends for offering encouragement and providing assistance, especially fellow graduate students Julie Retrum, Pete Schillig, Brian Platt, Jon Smith, Paul Kenward, and Ezra Kulczycki. I also want to thank the faculty, staff, and students at Alpena Community College.

This research was partially supported by the National Science Foundation (EAR #0125495 to A. W. Walton).

TABLE OF CONTENTS

Figures

Chapter 2

FIGURE 1—Map of the Hawaiian Islands (inset) and the island of Hawaii showing the HSDP site just offshore of Hilo, in the flanks of Mauna Kea. Modified from DePaolo et al. (1996).

FIGURE 2—Lithostratigraphy of the lower part of the Hawaii Scientific Drilling Project #2 phase 1 core. Areas of alteration on the right are as listed in Walton and Schiffman (2003). Arrows on the left indicate the location of the analyzed samples. Modified from Walton (2008). mbsl = meters below sea level.

FIGURE 3—Comparison of the range of scale of various trace fossils. A) euendolithic microborings, B) ostracode burrows, and C) a sauropod footprint modified and used by permission from Platt and Hasiotis (2006).

FIGURE 4—Schematic diagrams of microendolithic ichnofabric indices 1–5 (top to bottom) with representative examples from the Hawaii Scientific Drilling Project #2 well; left = schematic of microborings, center = microborings in thin section, right = schematic ichnofabric index (from Droser and Bottjer, 1986). Scale bar in center = 5 μm. 1 = 0% dissolution, depth 2117 mbsl (meters below sea level); 2 = 8% dissolution, depth 2117 mbsl; 3 = 30% dissolution, depth 2117 mbsl; 4 = 50% dissolution, depth 2040 mbsl; 5 = 61% dissolution, depth 2117 mbsl.

FIGURE 5— Glass shard with a smectite-lined vesicle adjacent to a smectite-lined intergranular pore (blue). Note smectitic grain replacement (arrow); depth = 1350 mbsl.

FIGURE 6—Application of the MII to euendolithic microborings. A) Thin section of a sample from 2117 mbsl assigned an MII value of 3. Glass = unaltered basalt glass; Ol = olivine; Pal =

palagonite rim developed on hyaloclasts (note many euendolithic microborings); Pore = chabazite- and smectite-filled primary pore. B) Graphical representation of the use of the MII for the sample shown in Figure 6A; gray bar = average MII category. The assigned MII category is 3. See text and Table 1 or further explanation.

Chapter 3

FIGURE 1—Map of the Hawaiian Islands (inset) and the island of Hawaii with the HSDP site near Hilo, Hawaii. Modified from DePaolo et al. (1996).

FIGURE 2—Lithologic description of the lower part of the HSDP #2 phase 1 core. Modified from (Walton 2008); Average MII and Temperature data; Silica %; Porosity and PPT all vs Depth.

FIGURE 3—Alteration history. A) Palagonite alteration in a hyaloclastite from HSDP #2 phase 1 core from a depth of 2565.7 mbsl. The sample is imaged in plane-polarized light. B) Later phase of alteration, pore-filling chabazite and radiated masses of bladed phillipsite. The sample is imaged in plane-polarized light. (Walton and Schiffman 2003).

FIGURE 4—Euendolithic microborings observed in the thin sections of HSDP #2 samples.

FIGURE 5—Schematic diagrams of micro-ichnofabric indices 1 through 5 with representative examples, left = schematic, right = example. 5 μm scale bar in 1B is for 1-5. 1; 0% dissolution; depth 2117 mbsl. 2; 8% dissolution; depth 2117 mbsl. 3; 30% dissolution; depth 2117 mbsl. 4; 50% dissolution; depth 2040.1 mbsl. 5; 61% dissolution; depth 2117 mbsl (after Montague et al.,

2010)

FIGURE 6—Scanning Electron Microscope photomicrographs showing width of two different euendolithic microborings from a depth of 6902.4 mbsl. A) Tubular shaped boring, notice the texture on the inside of the boring is bumpy. Scale bar is 2 μm. B) Irregular shaped boring. Scale bar is 1 μm.

FIGURE 7—A) Delicate borings originating from a fracture. B) More robust borings originating from a vesicle. Scale bars are 50 μm.

FIGURE 8—Extreme lengths of euendolithic microborings. A) Shortest borings, 0.96 μm from a depth of 6902.4 mbsl, these microborings originate from a fracture. B) Longest borings, 129.2 μm from a depth of 4833.1 mbsl. Scale bars are 10 μm.

FIGURE 9— Plot of length of borings vs. abundance in six samples.

FIGURE 10—Explanation of tortuosity: U= total length and V= straight-line distance between the beginning and end of the boring. Modified from (Hembree and Hasiotis 2006).

FIGURE 11—Comparison of a highly tortuous boring to a non-tortuous boring. A) High tortuosity, T= 25. 7 μm/ 2.59 μm = 9.93. Microboring is from a depth of 5096.6 mbsl. B) Low tortuosity, T= 20.5 μm/ 17.6 μm = 1.16. Microboring is from a depth of 4833.1 mbsl. Scale bars are 10 μm.

Tables

Chapter 2

Chapter 3

Chapter 1

Introduction

While the study of macroscopic trace fossils in shale, sandstone, and limestone dates well back into the history of geological science (Baucon, 2010), the idea that microorganisms could live by boring into tholeiitic glass and leave traces has emerged only in the past few years (Thorseth et al., 1992, 1995b; Staudigel et al, 1995, 1998). Early reports concentrated on occurrences in subglacial lava flows in Iceland and the oceanic crust, but the structures are also common in submarine ocean-island basalts from Hawaii (Fisk et. al., 2003; Walton and Schiffman, 2003; Walton, 2008). The fact that these features exist in subsurface environments is no longer in question. However, new questions arise: what is the distribution of these traces, and if they are truly trace fossils, what is the morphology of these features?

Any euendolithic structures must meet three criteria to be considered trace fossils (McLoughlin et al., 2007): (1) geological context that demonstrates the syngenicity of possible biological traces, though such trace fossils can be emplaced much later than the time the medium was produced, such as at an unconformity or at a modern surface long after the formation of the rock, resulting in overprinting (e.g., Hasiotis et al., 2002; Hasiotis, 2007; Walton, 2008); (2) evidence of biological morphology and behavior; and (3) geochemical evidence for biological processing. A common form of microbial ichnofossils in basalt glass is hollow or mineral-filled, micrometer-scale tubules that extend into glass from surfaces of pillows or glass fragments, i.e. hyaloclasts, or from fractures and vesicles in them. Such tubules are thought to be euendolithic microborings or ichnofossils generated by boring microorganisms because they: (1) correspond with sizes of modern microorganisms; (2) display features inconsistent with known inorganic processes; (3) are associated with low $\delta^{13}C$ values (Torsvik, et al., 1998; Banerjee and Muehlenbachs, 2003; Furnes et al., 2005) and elevated concentrations of vital such elements as

C, N, P, K, and S (Furnes et al., 2001; Banerjee and Muehlenbachs, 2003); and (4) display evidence of behavior (Walton, 2008).

Samples used in this study come from the phase one core of the Hawaii Scientific Drilling Project (HSDP) #2, which was taken near Hilo, Hawaii. The lower two thirds of the core, from 1,079 meters below sea level (mbsl) to total depth at 3,109.4 mbsl, contains submarine lava flows, both massive and pillowed, hyaloclastites, and intrusions from Mauna Kea (DePaolo et al. 2000). Rocks in this portion of the core range in age from ~413 to ~635 kyr (Sharp and Renne 2005). Rocks from the phase 2 core, drilled in 2004–5 are generally similar in lithology and alteration, both inorganic and organic, to the bottom of the core at 3,519.5 mbsl. Most samples studied here were from thick hyaloclastite beds, some of which were laminated and probably resedimented from their original emplacement in lava deltas. A few samples were from pillow lavas, both from the margins of the pillows and inter-pillow hyaloclast breccias.

This thesis first develops a semiquantitative method for systematically characterizing euendolithic microborings as bioerosion in basaltic glass in order to address the question of bioerosion distribution. The use of the petrography of hyaloclastite samples from the HSDP #2 phase one core, along with microscopic examination of euendolithic microborings, aided the characterization of the morphology of the microborings and relative percentages of bioerosion of mineral and rock grains. Prior to this study, no method existed to estimate the degree of bioerosion or distribution in other euendolithic microboring-bearing media. Consequently, the ichnofabric index (ii) of Droser and Bottjer (1986) was modified to be a scale-independent, orientation-independent, semiquantitative classification scheme of the disturbance of primary texture to document the extent of bioerosion recorded in HSDP #2 volcanic samples. This new, microendolithic ichnofabric index (MII) is based on the percentage of glass dissolution and is

divided into six distinct categories. When used in conjunction with petrographic data and descriptive ichnology, this classification scheme can determine changes in the nature and concentration of bioerosion in basaltic glass from different strata. This new method also allows quantification of bioerosion at any scale, in homogeneous as well as layered media. Such quantified descriptions will assist in demonstrating that the microborings meet the criteria to be traces of life in that they establish that the tubules are evidence of biological morphology and behavior.

Second, this thesis describes and quantifies some morphological and abundance characteristics of euendolithic microborings found in cores from the Hawaii Scientific Drilling Project. Then quantitative data are presented on the bioerosion using the microendolithic ichnofabric index (MII; Montague et al., 2010). This thesis provides quantitative description of the euendolithic microborings, including length, tortuosity, complexity, and abundance and distribution throughout the core rather than expanding on the taxonomy of any microorganism(s) responsible for producing the euendolithic microborings.. Such descriptions, may be a basis for determining if different organisms have adopted the same life style in different environments or over geologic time. The paper considers possible controls on the distribution of microborings with depth in the core and compares this ocean-island system to similar microborings found in oceanic crust.

References

BANERJEE, N.R., and MUEHLENBACHS, K., 2003, Tuff life: Bioalteration in volcaniclastic rocks from the Ontong Java Plateau: Geochemistry, Geophysics, Geosystems, v. 4, p. 1-22, doi: 10.1029/2002GC000470.

BAUCON, A., 2010, Leonardo Da Vinci, The Founding Father of Ichnology: PALAIOS, v. 25, n. 6, p. 361-367, doi: 10.2110/pala.2009.p09-049r.

DEPAOLO, D., THOMAS, D., STOLPER, E., and GARCIA, M., 2000, Scientific Drilling Project: Core logs and summarizing data report: Pasadena, California Institute of Technology, p. 1-8.

DROSER, M.L., and BOTTJER, D.J., 1986, A semiquantitative field classification of ichnofabric: Journal of Sedimentary Petrology, v. 56, p. 558–559.

FISK, M.R., STORRIE-LOMBARDI, M.C., DOUGLAS, S., POPA, R., MCDONALD, G., and DI MEO-SAVOIE, C., 2003, Evidence of biological activity in Hawaiian subsurface basalts: Geochemistry, Geophysics, Geosystems, v. 4, p. 1-24, doi: 10.1029/2002GC000387.

FURNES, H., BANERJEE, N.R., MUEHLENBACHS, K., and KONTINEN, A., 2005, Preservation of biosignatures in metaglassy volcanic rocks from the Jormua ophiolite complex, Finland: Precambrian Research, v. 136, p. 125-137.

Furnes, H., Staudigel, H., Thorseth, I., H., Torsvik, T., Muehlenbachs, K., and Tumyr, O., 2001, Bioalteration of basaltic glass in oceanic crust: Geochemistry, Geophysics, Geosystems, p. 1-30, doi: 2000GC000150.

HASIOTIS, S. T., 2007, Continental ichnology: fundamental processes and controls on trace-fossil distribution, *in* Miller, W. III (ed.), Trace Fossils—Concepts, Problems, Prospects, Elsevier Press, p. 268-284.

HASIOTIS, S. T., ROGERS, J. R., AND GOLDSTEIN, R. H. 2002. Traces of Life: Macro- and Microscopic Evidence of Past and Present Biogenic Activity Potentially Preserved in Extraterrestrial Sediments and rocks: XXXIII Lunar and Planetary Science Conference, March 11-15, 2002, Houston, TX, Abstract 2054.pdf (CD-ROM).

MCLOUGHLIN, N., BRASIER, M.D., WACEY, D., GREEN, O.R., and PERRY, R.S., 2007, On Biogenicity Criteria for Endolithic Microborings on Early Earth and Beyond: Astrobiology, v. 7, p. 10-26.

MONTAGUE, K. E., WALTON, A.W., HASIOTIS, S. T., 2010, Euendolithic Microbroings in Basalt Glass Fragments in Hyaloclastites: Extending the Ichnofabric Index to Microbioerosion, PALAIOS, v. 25. p. 393-399, doi: 10.2110/palo.2009.p09-025r.

SHARP, W.D., and RENNE, P.R., 2005, The 40Ar/39Ar dating of core recovered by the Hawaii Scientific Drilling Project (phase 2), Hilo, Hawaii: Geochemistry, Geophysics, Geosystems, v. 6, p. 1-18, doi: 10.1029/2004GC000846.

STAUDIGEL H., CHASTAIN, R.A., YAYANOS, A., AND BOURCIER, W., 1995, Biologically mediated dissolution of glass, Chemical Geology, v. 126, p. 147-154.

STAUDIGEL, H., YAYANOS, A., CHASTAIN, R., DAVIES, G., TH. VERDURMEN, E.,A., SCHIFFMAN, P., BOURCIER, R., AND DE BAAR., H., 1998, Biologically mediated dissolution of volcanic glass in seawater, Earth and Planetary Science Letters, v. 164, p. 233-244.

THORSETH, I.H., FURNES, H., and HELDAL, M., 1992, The importance of microbiological activity in the alteration of natural basaltic glass: Geochimica et Cosmochimica Acta, v. 56, p. 845–850.

THORSETH, I.H., TORSVIK, T., FURNES, H., and MUEHLENBACHS, K., 1995, Microbes play an important role in the alteration of oceanic crust: Chemical Geology, v. 126, p. 137-146.

TORSVIK, T., 1998, Evidence for microbial activity at the glass-alteration interface in oceanic basalts: Earth and Planetary Science Letters, v. 162, p. 165-176.

WALTON, A.W., 2008, Microtubules in basalt glass from Hawaii Scientific Drilling Project #2 phase 1 core and Hilina slope, Hawaii: evidence of the occurrence and behavior of endolithic microorganisms: Geobiology, v. 6, n. 4, p. 351-364.

WALTON, A.W., and SCHIFFMAN, P., 2003, Alteration of hyaloclastites in the HSDP 2 Phase 1 Drill Core 1. Description and paragenesis: Geochemistry, Geophysics, Geosystems, v. 4, p. 1-31, doi: 10.1029/2002GC000368.

Chapter 2

Introduction

A large portion of the Earth's biomass may live in subsurface environments (Fisk et al., 2003). One form of evidence for the existence of life in such rocks is euendolithic microborings (Thorseth et al., 1992, 1995; Furnes et al., 1996; Giovannoni et al., 1996; Furnes and Staudigel, 1999; Fisk et al., 2003; Storrie-Lombardi and Fisk, 2004). Euendolithic microborings are microscopic tunnels or tubules made by organisms in various media, including carbonate and siliciclastic rocks as well as basaltic glass (Golubic et al., 1981, 2005; Fisk et al., 1998; Furnes et al., 2002, 2005; Banerjee and Muehlenbachs, 2003; Staudigel et al., 2006).

Borings are a type of trace fossil in which an organism or organisms mechanically or physiochemically bore through rock, mineral, or bioclastic grains. In contrast to the rich literature on macroscopic trace fossils in sedimentary rocks (e.g., Droser and Bottjer, 1986; Hembree and Hasiotis, 2006; Lockley et al., 2007; Miller, 2007; Hasiotis, 2008; Platt and Hasiotis, 2006, and references therein), there have been few morphological descriptions of euendolithic microborings in basaltic glass and there are still very few papers that actually refer to these features as trace fossils (e.g., Torsvik, 1998; Hasiotis et al., 2002; McLoughlin et al., 2007, 2008, 2009; Walton, 2008). Fisk et al. (2003) and Walton and Schiffman (2003) concluded that tubules in hyaloclastite samples from the Hawaii Scientific Drilling Project (HSDP) #2 phase one core were the result of biotic activity and thus likely borings. They resemble tubular structures described and interpreted as biogenic by Banerjee and Muehlenbachs (2003) and Furnes et al. (2005) in basalt pillows and hyaloclastite fragments from oceanic crust. Walton (2008) discussed the importance of observing the behaviors of microorganisms recorded as ichnofossils in hyaloclastites, but the same behavior by different organisms may be recorded as the same ichnofossil. McLoughlin et al. (2009) provided the first systematic description of

microbial ichnofossils in volcanic glass, erecting two ichnogenera and five ichnospecies. Their morphological descriptions assist in documenting that microborings meet the criteria to be traces of life (i.e., trace fossils) in that they establish that these tubules can be evidence of biological morphology (McLoughlin et al., 2008, 2009).

Three criteria were proposed by McLoughlin et al. (2007) for any euendolithic structures to be considered trace fossils: (1) geological context which demonstrates the syngenicity of possible biological traces; (2) evidence of biological morphology and behavior; and (3) geochemical evidence for biological processing. A methodology that helps resolve the distribution and density of tubular structures in hard media could be used to provide evidence of biological morphology and behavior represented by putative borings. Such a methodology could be applied to microtubules of any provenance.

This paper develops a semiquantitative method for systematically characterizing euendolithic microborings in basaltic glass. We utilize petrography of hyaloclastite samples from the HSDP #2 phase one core, along with microscopic examination of euendolithic microborings, in order to characterize the morphology of the microborings and relative percentages of bioerosion of mineral and rock grains. Prior to this study, no method existed to estimate the degree of bioerosion here or in other euendolithic microboring-bearing media. We modify the ichnofabric index (ii) of Droser and Bottjer (1986), to be a scale independent, orientation-independent, semiquantitative classification scheme of the disturbance of primary texture to document the extent of bioerosion recorded in HSDP #2 volcanic samples. This new, microendolithic ichnofabric index (MII) is based on the percentage of glass dissolution and is divided into six distinct categories. When used in conjunction with petrographic data and descriptive ichnology, this classification scheme can determine changes in the nature and concentration of bioerosion in basaltic glass from different strata.

Geologic Setting

Samples used to develop the MII come from the phase one core of the HSDP #2 well taken near Hilo, Hawaii (Fig. 1). The lower two-thirds of the core (Fig. 2), from 1,079 m below sea level (mbsl) to total depth at over 3,109 mbsl, contains submarine lavas, hyaloclastites, and intrusions from Mauna Kea (DePaolo et al., 2000). The age of the rocks at the top of the submarine section of the core is < 413 ka (Sharp and Renne, 2005). Hyaloclasts form in two ways: (1) when lava enters water or ice, is quenched, and shatters, or (2) by spalling of vitreous margins of basalt pillows. Most samples are not bedded and poorly sorted, with no evidence of transport or resedimentation. Some layers are clearly bedded and well sorted, and these have been reworked and deposited by submarine currents. Fragments are composed of basaltic glass, or sideromelane, phenocrysts, microlites, and quench crystals. Compositionally, the samples are olivine-phyric tholeiites (Stolper et al., 2004).

The unstable glass undergoes successive alteration to smectite and palagonite, with precipitation of smectite, zeolites, and Ca-silicates in pores, apparently by a combination of biogenic and abiotic processes. Microborings begin to form after the hyaloclastites are emplaced and fractured, and after formation of one layer of grain-coating smectite, but before zeolites and palagonite as well as later grain-coating and grain-replacing smectite form (Walton and Schiffman, 2003; Walton, 2008).

Current Ichnofabric Parameters

Semiquantitative or quantitative techniques for describing trace fossils include their length, width, ornamentation, and abundance (Droser and Bottjer, 1986), as well as their complexity and tortuosity (Meadows, 1991; Hembree and Hasiotis, 2006). The ichnofabric index (ii) is a semiquantitative approach to determine the percent of bioturbation in marine strata (Droser and Bottjer, 1986), with values ranging from 1–6:

1. No bioturbation recorded.

2. Discrete, isolated trace fossils; up to 10% of original bedding disturbed.

3. Approximately 10%–40% of original bedding disturbed.

4. Approximately 40%–60% disturbed.

5. Bedding is completely disturbed, but burrows are still discrete in places and the fabric is not mixed.

6. Bedding is nearly or totally homogenized.

When using the existing ii, percent of bioturbation is sampled using a 50 cm x 35 cm vertical cross-sectional area (Droser and Bottjer, 1986). Unfortunately, this scheme is limited to macroscopic burrows in sedimentary units and cannot currently be applied to small burrows, microborings in basalt glass, large dinosaur footprints, or large diameter burrow networks because of the differences in medium, scale, and orientation.

Development of the MII

To address the scale issue of the euendolithic microborings (Fig. 3A), the size of trace fossils must be considered. Ostracode burrows are some of the smallest recognized, being, 1 mm in diameter and, 2 mm deep. Ostracode crawling traces (Fig. 3B) are 1 mm wide and upwards of 5 cm long (Retrum et al., 2005). At the opposite end of the spectrum are dinosaur footprints (Fig. 3C) and large-diameter burrow networks. The largest known sauropod track is 125 cm long and, 50 cm deep from Upper Jurassic deposits in Asturias, Spain (Lockley et al., 2007), whereas some of the largest burrows are 30 cm x 50 cm in diameter and 200 cm to 300 cm long (Hembree and Hasiotis, 2008). It is clear that the current ii sampling interval cannot be applied to these three different sizes of trace fossils. The area of measurement should be consistently related to the scale of the bioturbating agents.

The categories of the MII are based on the percent disruption of the primary fabric, whether expressed as disruption of bedding, boring of hardgrounds, or as in this case, dissolution of glass. The six categories used in this study are specific to dissolution of glass in hyaloclastites (Fig. 4):

1. No dissolution of glass, no bioerosion.
2. Discrete, isolated borings, < 10% dissolution of glass.
3. About 10%–40% dissolution of glass; borings are generally isolated.
4. About 40%–60% dissolution of glass; borings overlap, but do not intersect.
5. Dissolution of glass > 60%; borings are hard to distinguish one from another.
6. Complete dissolution of glass.

These six categories correspond to the six categories of the ii (Droser and Bottjer, 1986). A schematic diagram for the sixth category of MII has not been created for inclusion here, although complete bioerosion does occur in some HSDP #2 samples. One example of this is in samples with smectitic grain replacement (Fig. 5) and hints of category 6 are common in grains with complete dissolution, as described by Walton and Schiffman (2003). Category 6 also applies to granular textures observed in other basaltic glass samples (Banerjee and Muehlenbachs, 2003; Furnes et al., 2006; Staudigel et al., 2006), as they are similar in scale to the euendolithic borings used in this study.

Methods

Six samples from different levels of the HSCP #2 core were analyzed (Fig. 2), totaling 322 different slide locations. Standard petrographic thin sections containing euendolithic microborings were examined using a Nikon Eclipse E600 optical microscope. A total of 60 thin sections were examined and six were used to develop the MII. Following the development of the

MII, all 60 thin sections were assigned MII categories, and those results will be reported separately. To determine the best sampling dimensions for euendolithic microborings, squares with dimensions of 10 µm, 30 µm, and 100 µm were placed on scaled photomicrographs of the thin sections where borings were observed. This progression of dimensions approximately preserves any logarithmic patterns that might be observed. The square gives calculations based on an equal surface area and samples the circular field of view more completely than a rectangle. The concentration of borings in each square was then estimated by using a line corresponding to the length of each box: 10 µm, 30 µm, and 100 µm. The number of borings intersecting the line was recorded.

The final modification of the ii of Droser and Bottjer (1986) was for the type of medium examined. Hyaloclasts do not display sedimentary bedding at the microscopic scale of the microborings. Instead, the scale of bedding in HSDP #2 hyaloclastites, even that of the finely bedded, well-sorted units, is much greater than the scale of observation. Grain surfaces are examined, not bedding surfaces or vertical cross sections. The situation is similar to that of borings in boulders in conglomerates. The main components of hyaloclastites are fragments of homogeneous glass, with or without vesicles, quench crystals, microlites, and phenocrysts, and the boundaries of glass fragments are the key surfaces. The microborings extend from boundaries of glass fragments, just as burrows or borings in sedimentary rocks extend from bedding surfaces. In measuring the MII, locations should be randomly selected so as not to introduce a sampling bias, although only places where borings are present can be analyzed. Measurable locations are areas once open to pore waters such as vesicle walls, margins of shards, and fractures.

The schematic diagrams in Figure 4 were constructed by assembling black lines to cover the desired percentage of area of the diagram. The black lines represent borings into basaltic glass, and they are the approximate width and length of borings in the hyaloclastite samples, relative to the size of the sampling template. The diagrams were analyzed using analySIS 3.1, an image-analysis program. Statistical analysis of the total number of measurements made for each slide used in this study was necessary to determine the number needed to lead to detectable differences between samples at a 95% confidence level. This was done using the formula to determine the sample size necessary for estimating the mean, $n = (Z_{\alpha/2} * \sigma)/E)^2$; with Z =1.960, E = 0.25, and $\sigma = 0.95$ (Weiss, 2005). Statistical analysis of the bioerosion data shows that 60 locations on a thin section will lead to detectable differences between samples at a 95% confidence level. The standard error of the mean (SEM) was calculated for each thin section using the MII and each was found to be small; < 1.25. The SEM is the standard deviation of the difference between the measured or estimated values and the true values.

Results

The tubules observed in thin sections from HSDP #2 samples extend into the glass from free margins, specifically edges of vesicles, margins of shards, or along fractures in the sideromelane and smectite fragments of the hyaloclastites. These surfaces were open to pore waters and indirectly to the surface at one time. Tubules ,1–2 μm in diameter and 1 to > 100 μm long are present in many of these samples. The abundance of tubules varies with depth (Walton, 2008). The HSDP #2 samples studied herein lack euendolithic microborings in open or filled pores, unfractured interiors of large hyaloclast shards, phenocrysts within shards, and glass-free fragments of basalt. These types of locations are considered immeasurable.

The concentration of borings in the 10 µm square was too great to be useful, as every location would have been assigned an MII of 5. The concentration of borings in the 100 µm square was too variable to be useful, as each location would have been assigned a MII of 1. The 30 µm square was determined to be the optimal sampling interval for borings of the size range of euendolithic microorganisms, as well as for providing the most information about percent of bioerosion. At this size the assigned MII was closest to the average MII for the largest number of samples. The process of comparing the three different-sized square templates was performed on the 322 different locations to confirm the optimal size of the template as 30 µm by 30 µm. Our results and the success of the ii (Droser and Bottjer, 1986) suggest that the ratio between the size of traces and the measuring template should be 30:1, whether the traces are microborings or dinosaur footprints six orders of magnitude or larger (Figs. 3A–C). For example, determination of the ichnofabric index of an ostracode burrow 0.5 mm in diameter would require a template 15 mm by 15 mm, while a sauropod footprint 1.0 m in diameter would require a 30 m by 30 m template.

Analysis of the schematic diagrams showed that bioerosion in the category 2 schematic (Fig. 4) covers 8% of the 30 µm by 30 µm box. Bioerosion is 30% in the category 3 schematic, 50% in category 4, and 61% in category 5. Enlargements of the schematic diagrams of MII categories 1–5 were used in petrographic studies of hyaloclastite thin sections to quantify bioerosion. Like Droser and Bottjer (1986), we used comparison charts to estimate the abundance of trace fossils. Preliminary use of the MII has produced favorable results. Figure 6A is a photomicrograph of a sample from 2,117.0 mbsl showing the euendolithic microborings measured. Figure 6B is a graphic representation of the assigned MII category versus number of observations calculated for a sample at 1,396.7 mbsl. The overall MII category assigned to this sample by visual observation was 3, whereas the weighted average MII category measured

quantitatively on a number of different sites in that thin section was calculated as 2.4 (Fig. 6B, gray bar). The assigned MII for each of the six thin sections analyzed to develop the MII compared to the average MII is shown in Table 1.

Discussion

This study suggests that the MII works well for estimating the degree of disruption produced by tubular microborings. The difference between the estimated and measured MII values illustrates that biases are introduced by the observer in the way that observations are made and in how pattern recognition is intuitively processed to estimate percentages of disruption. The actual average value of MII is not as important as the consistent use of the MII technique to illustrate the variation in bioerosion from one sample to another or to communicate the degree of bioerosion. The application of MII is similar to the application of ii to core and outcrop, where ii can vary between the different lithofacies and between researchers making the observations. The average ii for one section of an outcrop is not the significant piece of information for the entire outcrop; it is the variability of ii within and between different types of lithofacies and how this variability can be used to deduce variations in sedimentation rate, the frequency of sedimentation events, and the oxygenation of bottom and pore water (e.g., Droser and Bottjer, 1986, 1989). The low value of the SEM for the MII of HSDP #2 samples used in this study, < 1.25, statistically means that variability in the MII for the sample is small.

The MII is useful for studies of euendolithic microborings in basaltic glass, but can be adapted for any rock type, media configuration, and scale of bioturbation, provided that the scale of sampling is compatible with the size of the measured features. This study determined that a

ratio of ~30:1 for sampling window to feature dimension is satisfactory. This is a value slightly smaller than the ratios 35:1 to 50:1 suggested by Droser and Bottjer (1986) for burrows that disrupt bedding, or Miller and Smail (1997) for features visible on bedding planes. For tubular structures, like those studied here and those envisioned by Droser and Bottjer (1986), the reference dimension is the diameter of the tubes (i.e., the trace fossil). For equant features, the reference dimension is the diameter of the features. For example, determination of the ichnofabric index of sauropod footprints would require a template 30 times the size of the footprint, or a square template of 15–30 m on a side if the prints range from 0.5 to 1.0 m in diameter (e.g., Platt and Hasiotis, 2006), while a 15 m template would be required to study large networks with burrow diameters of 35–50 cm (e.g., Hembree and Hasiotis, 2008). Widely available percentage-estimation diagrams would be useful for studies where existing comparison charts are not appropriate.

Conclusions

We developed a semiquantitative technique to systematically measure the intensity of euendolithic microbioerosion in order to better understand and quantify interactions between microorganisms and basalt glass, based on core samples from Hawaii. Previously, no such system existed. Percent disruption of primary fabric is the basis of the MII, unlike percent disruption of bedding of the original ii (Droser and Bottjer, 1986). The six categories range from no disruption of primary fabric (MII < 1) to complete disruption (MII > 6).

MII schematic diagrams (Fig. 4) provide a basis for a semiquantitative estimate of the density of bioerosion when used during analysis of petrographic thin sections in the laboratory. The use of the MII also allows for comparison of bioerosion densities from different samples of

basaltic glass and facilitates the comparison of euendolithic microborings with much larger borings and larger diameter trace fossils in a variety of media, as long as a scale ratio of area of measure to trace fossil size is maintained at 30:1. Statistical analysis verifies that analyzing 60 random locations will give detectable differences between samples at a 95% confidence level.

Like any other semiquantitative classification, even though no two persons will necessarily assign the same category of disruption, the use of MII schematic diagrams can reduce the range of variability between observers of euendolithic microbial borings. This semi-quantitative system is also useful because it facilitates comparison between microborings and the degree of bioerosion in samples from different sections within a particular core or rock sample as well as between samples from different sites.

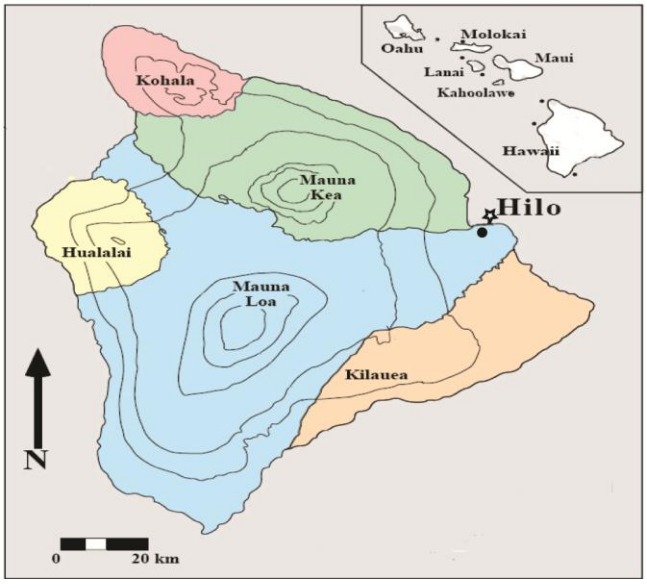
Oahu
Molokai
Maui
Lanai
Kahoolawe
Hawaii
Kohala
Mauna Kea
Hilo
Hualalai
Mauna Loa
Kilauea
N
0
20 km

Figure 1

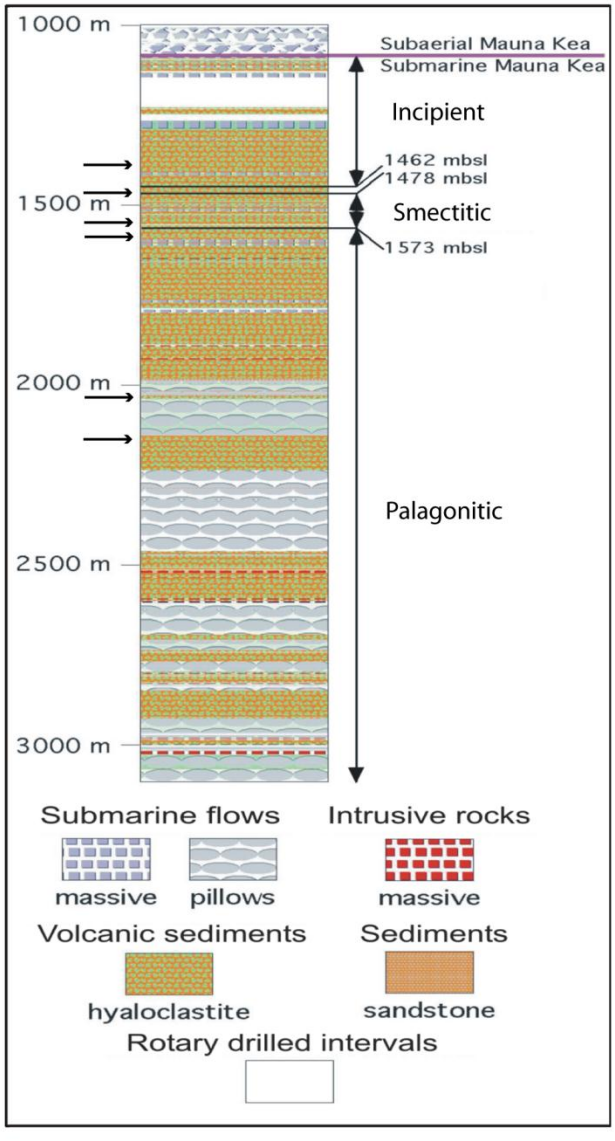
1000 m
Subaerial Mauna Kea
Submarine Mauna Kea
Incipient
1462 mbsl
1478 mbsl
1500 m
Smectitic
1573 mbsl
2000 m
Palagonitic
2500 m
3000 m
Submarine flows
Intrusive rocks
massive
pillows
massive
Volcanic sediments
Sediments
hyaloclastite
sandstone
Rotary drilled intervals

Figure 2

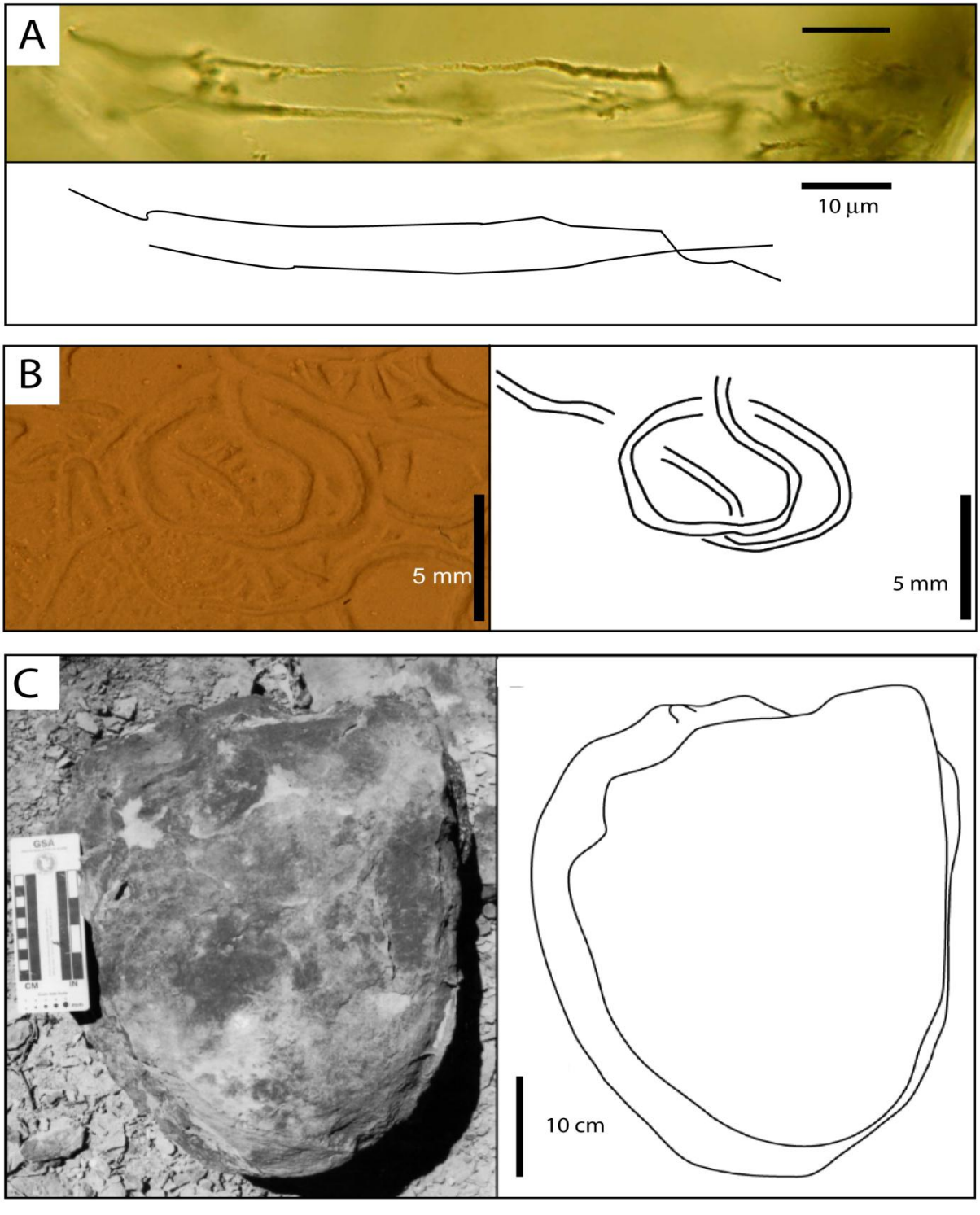

Figure 3

Figure 4

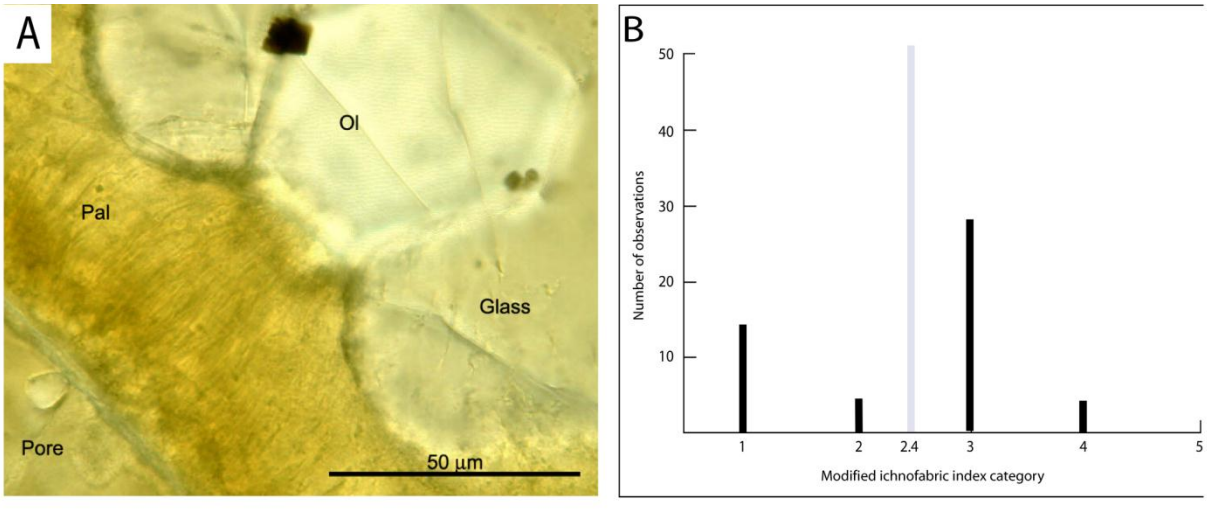

Figure 5

mbsl	Estimated MII	Average MII	No. of locations measured
1365.9	3	2.34	67
1478.8	3	2.88	60
1560.1	2	1.64	47
1597	2	2.1	20
2040.1	2	2.07	58
2117	3	2.81	70

Table 1

FIGURE 1—Map of the Hawaiian Islands (inset) and the island of Hawaii showing the HSDP site just offshore of Hilo, in the flanks of Mauna Kea. Modified from DePaolo et al. (1996).

FIGURE 2—Lithostratigraphy of the lower part of the Hawaii Scientific Drilling Project #2 phase 1 core. Areas of alteration on the right are as listed in Walton and Schiffman (2003). Arrows on the left indicate the location of the analyzed samples. Modified from Walton (2008). mbsl = meters below sea level.

FIGURE 3—Comparison of the range of scale of various trace fossils. A) euendolithic microborings, B) ostracode burrows, and C) a sauropod footprint modified and used by permission from Platt and Hasiotis (2006).

FIGURE 4—Schematic diagrams of microendolithic ichnofabric indices 1–5 (top to bottom) with representative examples from the Hawaii Scientific Drilling Project #2 well; left = schematic of microborings, center = microborings in thin section, right = schematic ichnofabric index (from Droser and Bottjer, 1986). Scale bar in center = 5 μm. 1 = 0% dissolution, depth 2117 mbsl (meters below sea level); 2 = 8% dissolution, depth 2117 mbsl; 3 = 30% dissolution, depth 2117 mbsl; 4 = 50% dissolution, depth 2040 mbsl; 5 = 61% dissolution, depth 2117 mbsl.

FIGURE 5— Glass shard with a smectite-lined vesicle adjacent to a smectite-lined intergranular pore (blue). Note smectitic grain replacement (arrow); depth = 1350 mbsl.

FIGURE 6—Application of the MII to euendolithic microborings. A) Thin section of a sample from 2117 mbsl assigned an MII value of 3. Glass = unaltered basalt glass; Ol = olivine; Pal = palagonite rim developed on hyaloclasts (note many euendolithic microborings); Pore = chabazite- and smectite-filled primary pore. B) Graphical representation of the use of the MII for

the sample shown in Figure 6A; gray bar = average MII category. The assigned MII category is 3. See text and Table 1 or further explanation.

TABLE 1—Visually estimated MII and calculated average MII. mbsl = meters below sea level.

References

BANERJEE, N.R., and MUEHLENBACHS, K., 2003, Tuff life: Bioalteration in volcaniclastic rocks from the Ontong Java Plateau: Geochemistry, Geophysics, Geosystems, v. 4, no. 4, p. 1- 37, doi: 10.1029/2002GC000470.

DEPAOLO, D.J., STOLPER, E.M., and THOMAS, D.M., 1996, Hawaii Scientific Drilling Project: Summary of preliminary results: GSA Today, v. 6, no. 8, p. 1–8.

DEPAOLO, D.J., THOMAS, D.M., STOLPER, E.J., and GARCIA, M.O., 2000, Scientific Drilling Project: Core logs and summarizing data report: California Institute of Technology, Pasadena, 471 p.

DROSER, M.L., and BOTTJER, D.J., 1986, A semiquantitative field classification of ichnofabric: Journal of Sedimentary Petrology, v. 56, p. 558–559.

DROSER, M.L., and BOTTJER, D.J., 1989, Ichnofabric of sandstones deposited in highenergy nearshore environments: Measurement and utilization: PALAIOS, v. 4, p. 598–604.

FISK, M.R., GIOVANNONI, S.J., and THORSETH, I.H., 1998, Alteration of oceanic volcanic glass: Textural evidence of microbial activity: Science, v. 281, p. 978–980.

FISK, M.R., STORRIE-LOMBARDI, M.C., DOUGLAS, S., POPA, R., MCDONALD, G., and DIMEO-SAVOIE, C., 2003, Evidence of biological activity in Hawaiian subsurface basalts: Geochemistry, Geophysics, Geosystems, v. 4, no. 12, p. 1103, doi:10.1029/ 2002GC000387.

FURNES, H., and STAUDIGEL, H., 1999, Biological mediation in ocean crust alteration: How deep is the deep biosphere?: Earth and Planetary Science Letters, v. 166, p. 97–103.

FURNES, H., THORSETH, I.H., TUMYR, O., TORSVIK, T., and FISK, M.R., 1996, Microbial activity in the alteration of glass from pillow lavas from Hole 896A, in Alt, J.C., Kinoshita, H., Stokking, L.B., and Michael, P.J., eds., Proceedings of the Ocean Drilling Program, Scientific Results, v. 148, p. 191–206.

FURNES, H., MUEHLENBACHS, K., TORSVIK, T., TUMYR, O., and SHI, L., 2002, Biosignatures in metabasaltic glass of a Caledonian ophiolite, west Norway: Geological Magazine, v. 139, p. 601–608.

FURNES, H., BANERJEE, N.R., MUEHLENBACHS, K., and KONTINEN, A., 2005, Preservation of biosignatures in metaglassy volcanic rocks from the Jormua ophiolite complex, Finland: Precambrian Research, v. 136, p. 125–137.

FURNES, H., DILEK, Y., MUEHLENBACHS, K., AND BANERJEE, N.R., 2006, Tectonic control of bioalteration in modern and ancient oceanic crust as evidenced by carbon isotopes: Island Arc, v. 15, p. 143–155.

GIOVANNONI, S.J., FISK, M.R., MULLINS, T.D., and FURNES, H., 1996, Genetic evidence for endolithic microbial life colonizing basaltic glass/sea water interfaces, in Alt, J.C., Kinoshita, H., Stokking, L.B., and Michael, P.J., eds., Proceedings of the Ocean Drilling Program, Scientific Results, v. 148, p. 207–213.

GOLUBIC, S., FRIEDMANN, I., and SCHNEIDER, J., 1981, The lithobiontic ecological niche, with special reference to microorganisms: Journal of Sedimentary Research, v. 51, p. 475–478.

GOLUBIC, S., RADTKE, G., and LE CAMPION-A , T., 2005, Endolithic fungi in marine

ecosystems: Trends in Microbiology, v. 13, p. 229–235.

HASIOTIS, S.T., 2008, Reply to the comments by Bromley et al. of the paper, ‘‘Reconnaissance of Upper Jurassic Morrison Formation ichnofossils, Rocky Mountain region, USA: Paleoenvironmental, stratigraphic, and paleoclimatic significance of terrestrial and freshwater ichnocoenoses’’ by Stephen T. Hasiotis: Sedimentary Geology, v. 208, p. 61–68.

HASIOTIS, S.T., ROGERS, J.R., and GOLDSTEIN, R.H., 2002. Traces of life: Macro- and microscopic evidence of past and present biogenic activity potentially preserved in extraterrestrial sediments and rocks: 33rd Annual Lunar and Planetary Science Conference (March 11–15, Houston, Texas), Abstract 2054, http://adsabs.harvard. edu/abs/2002LPI….33.2054H. Checked January 2006.

HEMBREE, D.I., and HASIOTIS, S.T., 2006, The identification and interpretation of reptile ichnofossils in paleosols through modern studies: Journal of Sedimentary Research, v. 76, p. 575–588.

HEMBREE, D.I., and HASIOTIS, S.T., 2008, Miocene vertebrate and invertebrate burrows defining compound paleosols in the Pawnee Creek Formation, Colorado, U.S.A.: Palaeogeography, Palaeoclimatology, Palaeoecology, v. 270, p. 349–365, doi: 10.1016/j.palaeo.2008.07.019.

LOCKLEY, M.G., LIRES, J., GARCIA-RAMOS, J.C., PINUELA, L., and AVANZINI, M., 2007, Shrinking the world’s largest dinosaur tracks: Observations on the ichnotaxonomy of Gigantosauropus asturiensis and Hispanosauropus hauboldi from the Upper Jurassic of Asturias, Spain: Ichnos, v. 14, p. 247–255.

MCLOUGHLIN, N., BRASIER, M.D., WACEY, D., GREEN, O.R., and PERRY, R.S., 2007, On biogenicity criteria for endolithic microborings on early Earth and beyond:

Astrobiology, v. 7, p. 10–26.

MCLOUGHLIN, N., FURNES, H., BANERJEE, N.R., STAUDIGEL, H.,MUEHLENBACHS, K., DEWIT, M., and VAN KRANENDONK, M.J., 2008, Micro-bioerosion in volcanic glass: Extending the ichnofossil record to Archaean basaltic crust, in Wisshak, M., and Tapanila, L., eds., Current Developments in Bioerosion: Springer, Berlin, p. 372–396.

MCLOUGHLIN, N., FURNES, H., BANERJEE, N.R., MUEHLENBACHS, K., and STAUDIGEL, H., 2009, Ichnotaxonomy of microbial trace fossils in volcanic glass: Journal of the Geological Society, London, v. 166, p. 1–11.

MEADOWS, P.S., 1991, The environmental impact of burrows and burrowing animals—Conclusions and a model, in Meadows, P.S., and Meadows, A., eds., The Environmental Impact of Burrowing Animals and Animal Burrows: Zoological Society of London Symposia 63, Clarendon Press, Oxford, p. 327–338.

MILLER, M.F., and SMAIL, S.E., 1997, A semiquantitative field method for evaluating bioturbation on bedding planes: PALAIOS, v. 12, p. 391–396.

MILLER, W., III, ED., 2007, Trace Fossils: Concepts, Problems, Prospects: Elsevier Press, Amsterdam, 611 p.

OptiAnalysis Package, Soft Imaging Systems, Denver, Colorado.

PLATT, B.F., and HASIOTIS, S.T., 2006, Newly discovered sauropod dinosaur tracks with skin and foot-pad impressions from the Upper Jurassic Morrison Formation, Bighorn Basin, Wyoming, U.S.A.: PALAIOS, v. 21, p. 249–261.

RETRUM, J.B., HASIOTIS, S.T., and KAESLER, R.L., 2005, Neoichnological experiments with freshwater ostracodes: Geological Society of America Abstracts with Programs, v. 37, p. 443.

SHARP, W.D., and RENNE, P.R., 2005, The 40Ar/39Ar dating of core recovered by the

Hawaii Scientific Drilling Project (phase 2), Hilo, Hawaii: Geochemistry, Geophysics, Geosystems, v. 6, no. 4, p. 1–18, doi: 10.1029/2004GC000846.

STAUDIGEL, H., FURNES, H., BANERJEE, N.R., DILEK, Y., and MUEHLENBACHS, K., 2006, Microbes and volcanoes: A tale from the oceans, ophiolites, and greenstone belts: GSA Today, v. 16, no. 10, p. 4–10.

STOLPER, E., SHERMAN, S., GARCIA, M., BAKER, M., and SEAMAN, C., 2004, Glass in the submarine section of the HSDP2 drill core, Hilo, Hawaii: Geochemistry, Geophysics, Geosystems, v. 5, no. 7, p. 1–67, doi: 10.1029/2003GC000553.

STORRIE-LOMBARDI, M.C., and FISK, M.R., 2004, Evidence of biogenic alteration in sub-oceanic basalt glass: Complexity image analysis, elemental abundance distributions, and Bayesian probabilistic classification, in Hoover, R.B., Levin, G.V., and Rozanov, A.Y., eds., Instruments, Methods, and Missions for Astrobiology VIII: The International Society for Optical Engineering-SPIE, Bellingham, Washington, p. 47–58.

THORSETH, I.H., FURNES, H., and HELDAL, M., 1992, The importance of microbiological activity in the alteration of natural basaltic glass: Geochimica et Cosmochimica Acta, v. 56, p. 845–850.

THORSETH, I.H., TORSVIK, T., FURNES, H., and MUEHLENBACHS, K., 1995, Microbes play an important role in the alteration of oceanic crust: Chemical Geology, v. 126, p. 137–146.

TORSVIK, T., 1998, Evidence for microbial activity at the glass-alteration interface in oceanic basalts: Earth and Planetary Science Letters, v. 162, p. 165–176.

WALTON, A.W., 2008, Microtubules in basalt glass from Hawaii Scientific Drilling Project #2 phase 1 core and Hilina slope, Hawaii: Evidence of the occurrence and

behavior of endolithic microorganisms: Geobiology, v. 6, p. 351–364.

WALTON, A.W., and SCHIFFMAN, P., 2003, Alteration of hyaloclastites in the HSDP 2 Phase 1 Drill Core 1. Description and paragenesis: Geochemistry, Geophysics, Geosystems, v. 4, no. 5, p. 8709, doi: 10.1029/2002GC000368.

WEISS, N.A., 2005, Introductory Statistics, 7th Edition, Addison Wesley, Reading, Massachusetts, p. 374.

Chapter 3

Introduction

The study of bioerosion has typically concentrated on microborings in sedimentary media. More recently microbial ichnofossils were documented in glassy basalt of the ocean basins (Thorseth et al., 1995a; Furnes et al., 1996; Giovannoni et al., 1996; Fisk et al., 1998; Torsvik et al., 1998; Furnes and Staudigel, 1999; Furnes et al., 1999). Early reports concentrated on occurrences in oceanic crust, but the structures are also common in ocean-island basalts from Hawaii (Fisk, 2003; Walton and Schiffman, 2003; Walton, 2008). A common form of such ichnofossils is hollow or mineral-filled tubules that extend into glass from surfaces of pillows or glass fragments, i.e. hyaloclasts, or from fractures and vesicles in them. The tubules are bioerosion and are considered to be euendolithic microborings or ichnofossils generated by boring microorganisms. These microborings correspond with sizes of modern microorganisms, display features that are inconsistent with known inorganic processes, exist in areas associated with low $\delta^{13}C$ values (Furnes et al., 1998; Banerjee and Muehlenbachs, 2003; Furnes et al., 2005) and elevated concentrations of vital elements such as C, N, P, K, and S (Furnes et al., 2001; Banerjee and Muehlenbachs, 2003), and display evidence of behavior (Walton, 2008).

Several studies have briefly documented alteration textures produced by microorganisms (Thorseth et al., 1995; Furnes et al., 1996, 1998, 2007; Torsvik, 1998; Furnes and Staudigel, 1999; Banerjee and Muehlenbachs, 2003; Fisk et al., 2003; Storrie-Lombardi and Fisk, 2004). McLoughlin et al. (2009) provided the first systematic description of microbial ichnofossils in volcanic glass, erecting two ichnogenera and five ichnospecies. Such morphological descriptions demonstrate that the microborings meet the criteria to be traces of life in that they

establish that the tubules are evidence of biological morphology and behavior, evidence in addition to that from petrographic observations, and geochemical composition.

The purpose of this paper is to document and quantify some morphological and abundance characteristics of euendolithic microborings found in cores from the Hawaii Scientific Drilling Project. In this paper, we first describe some morphological characteristics of euendolithic microborings found within hyaloclastites. We then present quantitative data on the bioerosion using the microendolithic ichnofabric index (MII; Montague et al., 2010). This paper does not comment on the taxonomy of any microorganism(s) responsible for producing the euendolithic microborings, but quantitative description of the traces may be a basis for determining if different organisms have adopted the same lifestyle in different environments or through geologic time. The paper considers the controls on the distribution of microborings with depth in the core and compares this ocean-island system to similar microborings found in oceanic crust.

Geologic Setting

Samples used in this study come from the phase one core of the Hawaii Scientific Drilling Project (HSDP) #2, which was taken near Hilo, Hawaii (Fig. 1). The lower two-thirds of the core (Fig. 2), from 1,079 meters below sea level (mbsl) to total depth at 3,109.4 mbsl, contains submarine lavas, both massive and pillowed, hyaloclastites, and intrusions all with compositions showing they are from Mauna Kea (DePaolo et al. 2000). Rocks in this portion of the core range in age from ~413 to ~635 kyr (Sharp and Renne 2005). Rocks from the phase 2 core, drilled in 2004–5 are generally similar in lithology and alteration, both inorganic and organic, to the bottom of the core at 3,519.5 mbsl. Most samples studied here were from thick hyaloclastite beds, some of which were laminated and probably resedimented from their original

emplacement in lava deltas. A few were from pillow lavas, both from the margins of the pillows and inter-pillow hyaloclast breccias.

Hyaloclasts form in two ways: when basalt enters water or ice, quenches, and shatters, or by the spalling of of fragments from the vitreous margins of basalt pillows (Stroncik and Schmincke, 2001). Such fragments are composed of basaltic glass, or sideromelane; phenocrysts; microlites; and quench crystals. Basaltic glass has undergone successive alteration to smectite and palagonite, with precipitation of smectites, zeolites and Ca-silicates in pores, apparently through a combination of biogenic and inorganic processes (Furnes and Staudigel, 1999; Furnes et al., 2001; Walton and Schiffman, 2003).

In HSDP hyaloclastites the sequence of alteration begins with fracturing of the glass and formation of smectite pore linings (Fig. 3). After this event is when the euendolithic microborings initiated. At this same time, smectite replaced glass in irregular patches that extend inward from shard margins (Walton, 2008). This smectite is commonly reddened, probably with ferric oxihydroxides, and contains small spherules of titanium silicate, perhaps a precursor to titanite (Walton and Schiffman, 2003). The next step in the alteration sequence is the formation of a second pore-lining smectite coating. This second form of pore-lining smectite also replaces vitreous grains in few samples. Along with this smectite pore filling and replacement is the formation of phillipsite and Ca-silicates. The final step of alteration involves the formation of palagonite and chabazite. Palagonite is a gel-like material; in the Hawaiian samples, it appears yellow-orange in plane-polarized light, contrasting with the pale tannish yellow of the unaltered glass (Walton and Schiffman, 2003). It forms as marginal bands that are 0.01 to 0.5 mm thick on otherwise vitrious hyaloclasts. Chabazite forms blocky, equant to slightly elongate pore-filing crystals and, in the HSDP core, is seen only in samples that also contain palagonite. Most authors

consider palagonite to be an inorganic replacement of glass (Furnes and Staudigel, 1999; Furnes et al., 2001; Stronick and Schmincke, 2001).

The euendolithic microborings observed in thin sections of HSDP #2 samples extend into glass from the edges of vesicles, margins of shards, or along fractures in the glass fragments of the hyaloclastites (Fig. 4), some of which are replaced by smectite. These areas were open to the pore waters and, indirectly at least, to the ocean floor at one time. The borings are present from 1,080 mbsl to 3,100 mbsl in the phase 1 core and present in the phase 2 core as well (Walton, 2008). Fisk et al. (2003) and Walton and Schiffman (2003) concluded that these borings are the result of biotic activity. They resemble those boring described and interpreted as biogenic by Banerjee and Muehlenbachs (2003) and Furnes et al. (2004). The present-day subsurface temperature in the borehole is about 10˚C at 600 mbsl, rising to about 18˚ at 1,600 mbsl, and from there increases to about 43°C at 3,100 m (Fig. 2; D.M. Thomas, personal communication, 2003). These temperatures are suitable to support microorganisms (Fisk et al., 2003).

Methods

This study used standard thin sections that were impregnated with blue-dyed epoxy to make pore space more visible. Petrographic description had already been completed (Walton and Schiffman, 2003; Walton et al., 2005). The tools used to analyze the HSDP #2 samples were a Nikon Eclipse E600 optical microscope; an image analysis program, analySIS Opti 3.1; scanning electron microscope; and MII schematic diagrams (Montague et al., 2010).

An overview of alteration and microboring was obtained on each slide by making lengthwise and cross-wise traverses. The first step in analyzing the euendolithic microborings in

thin section was to select points randomly for characterization and locating them reproducibly. The slide was fixed to the stage of the optical microscope in a repeatable fashion because stage was outfitted with axis lines, and the thin section was secured on the stage so that the major axis line was on the top and the minor axis line was along the right. In order to avoid sampling bias, a random number generator was used to obtain random coordinates on the thin section to analyze for borings. The random number generator determined numbered pairs on the stage of the microscope. The field of view defined by the numbered pair was then located, photographed, analyzed, recorded, and plotted on a photomicrograph of the thin section. The microscope power used for this step was most commonly 60x, however, 100x was sometimes used.

Enlargements of the MII schematic diagrams one through five (Montague et al., 2010) were used in petrographic studies of hyaloclastite thin sections to quantify bioerosion on all 71 available slides. The six categories used in this study, and specific to dissolution of glass in hyaloclastites are (Fig. 5):

1) No dissolution of glass, no bioerosion.

2) Discrete, isolated borings, up to 10% dissolution of glass.

3) 10% to 40% dissolution of glass, borings are generally isolated.

4) 40% to 60% dissolution of glass, borings begin to overlap.

5) Greater than 60% dissolution of glass, borings are hard to distinguish one from another.

6) Complete dissolution of glass (not shown on the MII diagrams).

Sixty random locations were analyzed on each thin section and the assigned MII category was recorded. Each location was a 30 µm square. Only random locations that lay along free margins of glass fragments were used, not those in pores or in the interior of large fragments, beyond the reach of the boring organisms. The average MII was calculated for each thin section using a weighted average: Average microendolithic ichnofabric index = [number of observations of MII 1(1) + number of observation of MII 2 (2) +…+ number of observation of MII 5 (5)]/60.

The next step was to measure length, tortuosity, and complexity of euendolithic microborings on six thin sections. All microborings in a particular field of view were measured, if they could be unequivocally traced from origin to termination, and they lay entirely within the thickness of the thin section. Actual measurement of length and tortuosity was conducted on digital images of randomly chosen fields that were analyzed using analySIS Opti 3.1, an image-analysis program. This program allows for the direct measurement of total length and straight length from beginning to end of the microborings on digital images. The actual measurements are of apparent length and apparent tortuosity (x-y distance), owing to the difficulty of measuring the z-direction (vertical distances) on images of thin sections.

To obtain a more complete picture of the microborings scanning electron microscopy observations were performed on a LEO 1550 Field Emission Scanning Electron Microscope. The analyses were performed at an acceleration voltage of 10 kV and a working distance of 16 mm. Thin sections were sputter coated with a thin film of gold, approximately 100 Å-thick (Fig. 6).

Results

Bioerosion specific to hyaloclastites is defined by euendolithic microborings found extendng from surfaces where water was able to permeate. These surfaces are margins of shards, edges of vesicles, and along fractures in the sideromelane or smectite-replaced areas of the hyaloclasts. Euendolithic microborings are linear or curvilinear with varying diameters. The overall shape of the microborings is tubular; however, they are distinctly not smooth-walled tubes. The microborings may occur as clusters or as isolated individuals. When observing microborings originating from a fracture in the sideromelane or smectite, the abundance of microborings is not symmetrical with respect to the fractures (Fig. 7A). Staudigel et al. (2008) suggested that the lack of symmetry across fractures indicates that the borings postdate the fracture and are not inorganic or cooling-related features. Some of the borings are obviously filled with smectite.

Abundance.

The abundance of euendolithic microborings varies throughout the core. Figure 2, plots the mean of the readings for each sample against depth; the outline represents our judgement of the upper limit of the distribution. Five zones were recognized: 1) low abundance (average MII ~ 1) from 1,079 to 1,320 mbsl, 2) a zone of variable readings with a maximum average of 2.3 at 1,398, 3) low abundance in all samples between 1,799 and 1,900 mbsl, 4) another zone with variable amounts, but a maximum average MII of 2.5 at 2,117 mbsl, and 5) very sparse borings below 2,500 mbsl. The two intervals with high average values (>2) are closely interstratified with samples with low average MII (1.0 to 1.2), so the intervals centering on 1,398 and 2,117 mbsl are zones of variable amounts of borings, rather than uniformly high amounts of borings. Whereas, zone five with sparse borings was consistent at an average level of MII = 1.01.

Length.

Microboring length ranges from <1 μm to over 100 μm (Fig. 8). The shortest microboring measured from the HSDP #2 samples is from a depth of 2,040.1 mbsl and is 0.907 μm (Fig. 8A). The longest microboring measured from the HSDP #2 samples comes from a depth of 1,478.8 mbsl and is 129.22 μm (Fig. 8B). The length of microborings in six samples was approximately log-normally distributed (Figure 9, Table 1), with four of the samples satisfying the Anderson-Darling test for log normality and two failing it. The geometric mean length of all borings examined was 18.9 μm.

Longer microborings where common as dense clusters, whereas shorter microborings were more commonly found as individuals or sparse clusters. The majorities of euendolithic microborings originating from a fracture are short, < 3 μm, and appear to follow an irregular path. These borings appear to be more delicate than borings originating from vesicles (Fig. 7B). Compared to those originating from fractures, euendolithic microborings originating from vesicles are on average longer, more robust, and more numerous at the site (Table 2). The spacing interval between borings from a fracture or a vesicle is unequal and differs from location to location along the glass surface.

Diameter of microborings ranges from 0.5 μm to 2 μm. After microborings form, however, later processes convert them from their initial shape into steep cones with flared entrances (Walton, 2008). This alteration through time, whether it be the result of microbial or inorganic processes, makes significance of measurements of diameter unclear, so we do not report systematic results.

Tortuosity and Complexity.

Two additional quantitative descriptors of microboring morphology were measured: tortuosity and complexity. Tortuosity and complexity are independent of scale and can be applied to euendolithic microborings, although originally used to compare burrow systems produced by animals of different sizes (Meadows, 1991). Tortuosity is a measure of the deviation of the tunnels from a straight line (Fig. 10) (Hembree and Hasiotis, 2006), analogous to sinuosity in a river system. The tortuosity of a microboring is calculated by dividing the total length (u) by the straight-line distance (v) between the beginning and end of the microboring. A perfectly straight boring would have a tortuosity measurement of 1. The most tortuous microboring measured was 16.46 from a depth of 1,597.0 mbsl (Fig. 11A), whereas the least tortuous was 1.22 from a depth of 1,478.8 mbsl (Fig. 11B). The median tortuosity calculated for all samples analyzed was approximately 1.29 and the variation was small (Figure 12). Average tortuosity of the several samples ranged from 1.227 to 1.37, neglecting three points (two from one sample, one from another) that were judged to be anomalous.

As defined, burrow complexity counts the number of segments, openings to the sediment or soil surface, blind endings below the surface, branches, closed loops, and chambers (Meadows, 1991). The calculation of complexity needed modification for use with euendolithic microborings in basalt glass. Openings to the surface would mean openings to the sediment or soil surface for macroichnofossils in sedimentary rocks. For euendolithic microborings, openings to the surface might mean openings to the shard surface, fracture, or vesicle wall. No such multiple-entry borings were observed in the HSDP samples, however. This means that openings to the surface were not taken into consideration when calculating the complexity of a euendolithic microboring. Analyzing the microborings with an optical microscope coupled with the size range of the euendolithic microborings made calculating the complexity difficult. Thus,

complexity is divided into two categories: simple, meaning a roughly cylindrical, nonbranching form, and complex, where branching occurs or some sort of finial in present at the termination (Fig. 13). Five hundred eighty-two (84%) of the borings were classified as simple, while only 115 (16%) were classified as complex.

Discussion

Abundance of Microborings

The MII allows for the quantification of bioerosion in each sample (Fig. 2). Several samples in the interval from about 1,365.9 mbsl to 1,478.8 mbsl and the interval of the core centering at approximately 2,117 mbsl contain high average values of MII, ranging from 2 to 2.5, with individual sites having values as high as 5, or >60% disruption. These samples with high MII are closely interbedded with samples with much lower MII. While these two sections of the core are the most densely bored, borings are present throughout the core although average MII readings are generally 1.2 or less, or well under 10% disruption on average, and few individual samples points had MII of 3 (10 to 40% disruption). Of course, the cited abundance applies only to areas within range of the margins of the shards. Interiors of large shards, certainly those with diameter greater than 0.2 mm, and more generally those with diameter greater than 0.1 mm, lie beyond the reach of the boring process.

The only other studies of abundance of microbial and inorganic alteration with depth in basalt from ocean basins observed that the abundance of microbial alteration, i.e. formation of both tubular and granular textures, followed a particular pattern of decrease with depth in oceanic crust in several different locations and tectonic settings. In addition, those studies reported that the abundance of bioalteration decreased as a fraction of total alteration as a

function of depth: In the upper 300 m of the crust, micorbial features amount to between 20 and 90% of all alteration, whereas fraction of palagonite, formed inorganically, in the total alteration rises to over 90% at a depth of 500 m and amounts to 15 to 40% of the glassy fraction of the rock (Furnes and Staudigel, 1999; Furnes et al., 2001).

Ichnotaxonomy

The vast majorities of microborings are linear to curvilinear with no ornamentation and display simple complexity (Fig. 13A). They are appropriately classified as *Tubulohyalichnus simplus* (McLoughlin et al., 2009). Borings of this ichnotaxon predominate in all or virtually all samples that contain microborings. The very few microborings that exhibit branching-bud ornamentation are classified as *T. stipes* (McLoughlin et al. 2009). Such complex borings are typically found originating from fractures. Complex microborings that display branching budlike structures (Fig. 13B), those that have terminations similar to that of a nail head (Fig. 13C), and the variety of other types illustrated in Walton (2008) differ from any established ichnotaxon.

Features of T. Simplus.

The length of the *T. simplus* borings in these samples ranges from ~1 µm to >100 µm, with a geometric mean of 18.9 µm. The approximately log-normal distribution of length is consistent with biological origin (Holt, 1994). Tortuosity falls into a narrow range of values, with a very few anomalous outliers, and does not vary with length (slope of a linear regression line through all data is –0.0004). This result can be taken as characteristic of *T simplus* in HSDP samples. Of interest will be whether the length distribution and tortuosity of other occurrences of this ichnotaxon differ from these values.

The other characteristic feature of *T. simplus* in samples from HSDP and also those dredged from the Hilina Slope is peridophilia, apparent attraction to olivine (Walton, 2008). Where olivine pheoncrysts or microlites lie close to the margin of hyaloclasts, microtubules are concentrated near the olivine and bend toward the olivine crystals, even if they are not long enough to reach them. Those microtubules that do reach olivine crystals simply stop; they do not enter the olivine, bend or branch along its surface, or bend back into the glass. Conversely, microborings bend around plagioclase microlites.

Conclusion

Tubulohyalichnus simplus from the HSDP core consists of microborings that range from <1µm to >100 µm long and have an approximately log-normal distribution with a geometric mean length of 18.9 µm. Most individual microborings are simple in form: no branches, no nodes or chambers; they are irregular tubes, initially about 1 µm in diameter. Microborings are somewhat tortuous, with a mean tortuosity of 1.28, but there is virtually no correlation of tortuosity with length. Abundance of microboring varies down the core. The most abundant borings, with an average MII of 2 to 2.5—>10% of available volumes of hyaloclasts displaying boring in individual thin sections—were at depths centering at 1,398 mbsl and 2,117 mbsl. Individual 30 µm-square sampling areas of particluar thin sections displayed MII values up to 5—borings occupy >60% of the available area of the sample. Throughout the core, most studied thin sections had average MII of 1 to 1.2 (zero to a few % of the available area displaying borings), with values on individual 30 µm-square sample points ranging up to 3 (<40% of available area being bored) on 30 µm-square sampling points.

Walton (2008) concluded that the microboring took place after fracturing of the grains and formation of a first layer of smectite on their surfaces. As hyaloclastites from the top of the

submarine section of the core have smectite coatings of minimal thickness, the boring likely began after some burial of the sediments and occurred in total darkness. Boring took place at unexceptional temperature. Bored rocks are now at about 15˚ C and boring may have occurred at even lower temperatures. Bored rocks now at higher temperature have minute permeability and many borings in them appear to be filled with smectite and reshaped into steep cones. There is no need to suggest that the boring organisms are hyperthermophiles in this occurrence.

Results of this study contrast with earlier studies of the vertical distribution of boring activity in the oceanic crust, but do not refute them; instead this study expands the range of understanding of microbial borings in basaltic glass of the ocean basins.

Figures

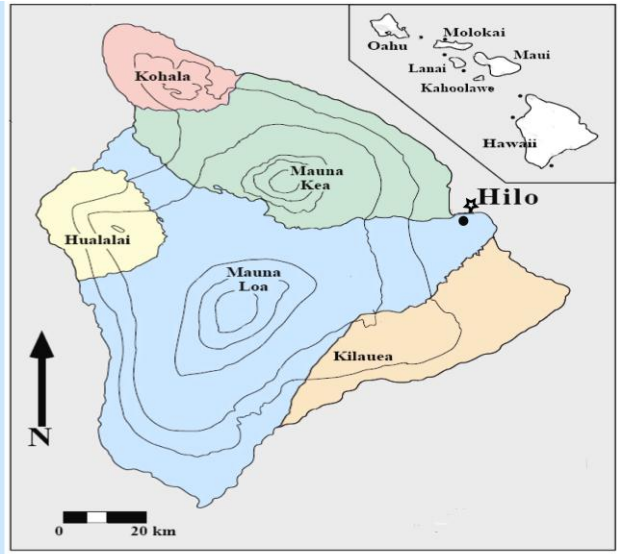

Figure 1

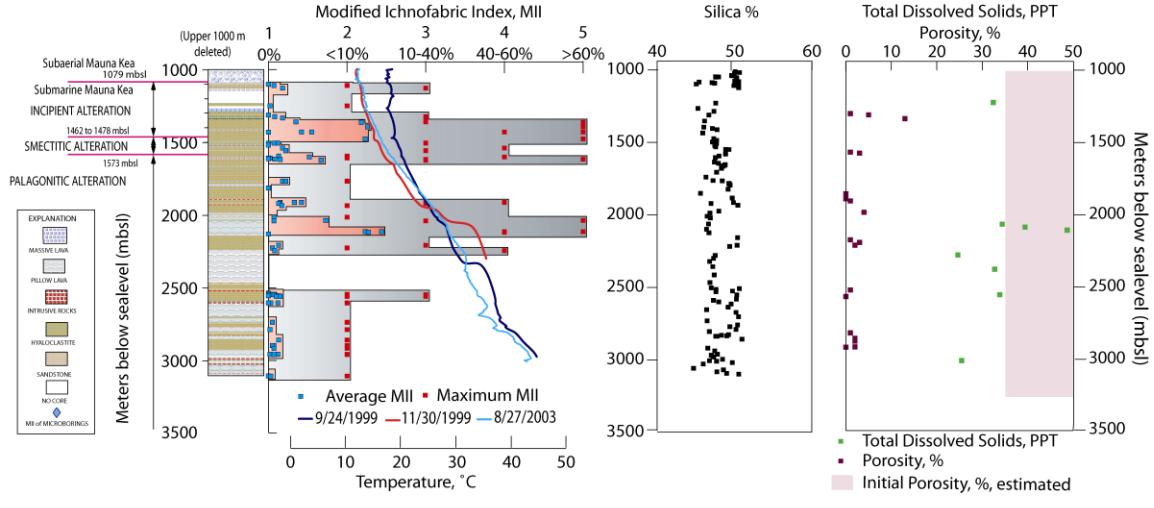

Figure 2

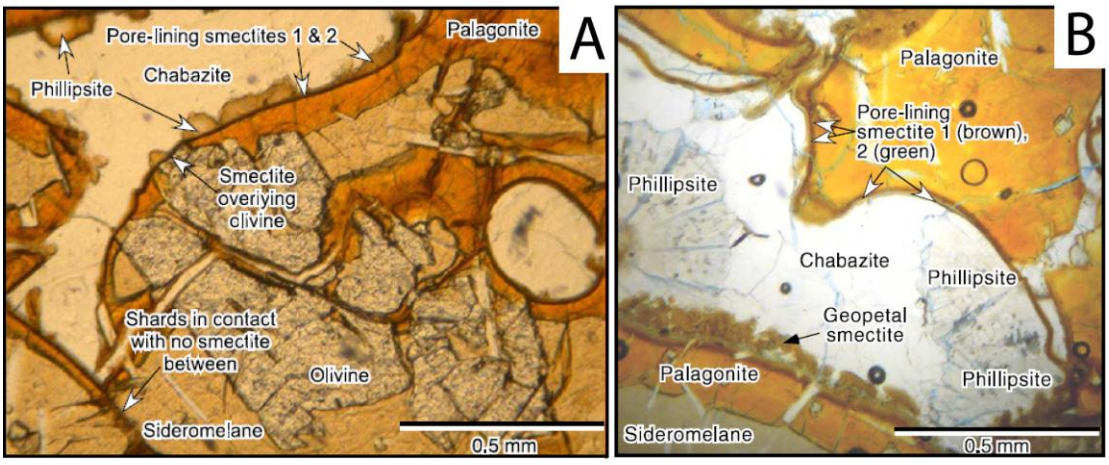

Figure 3

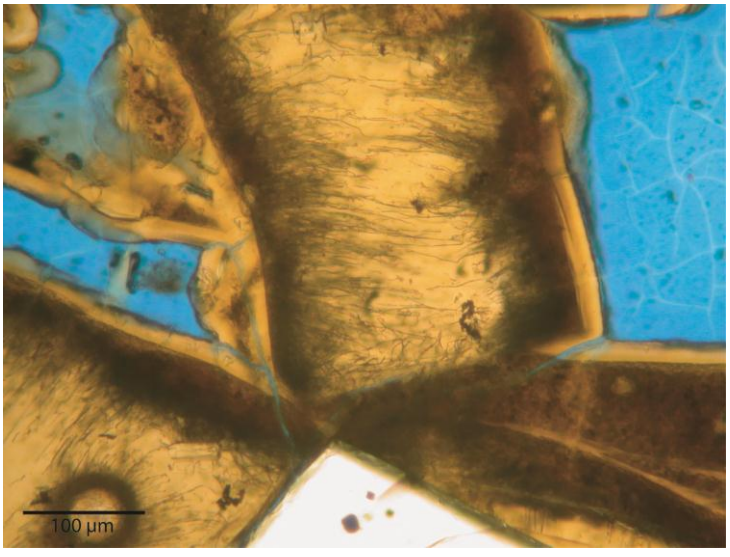

Figure 4

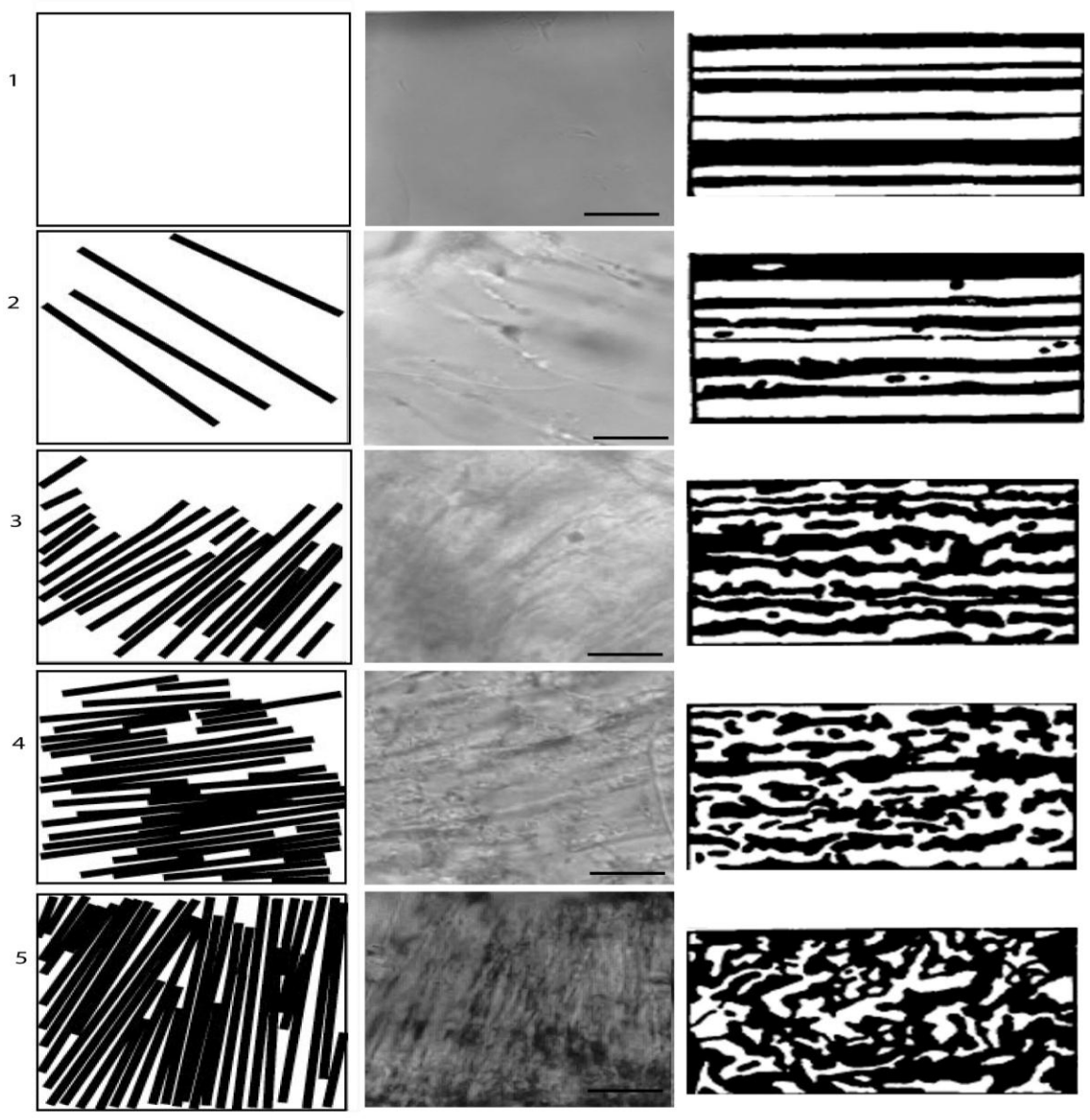

Figure 5

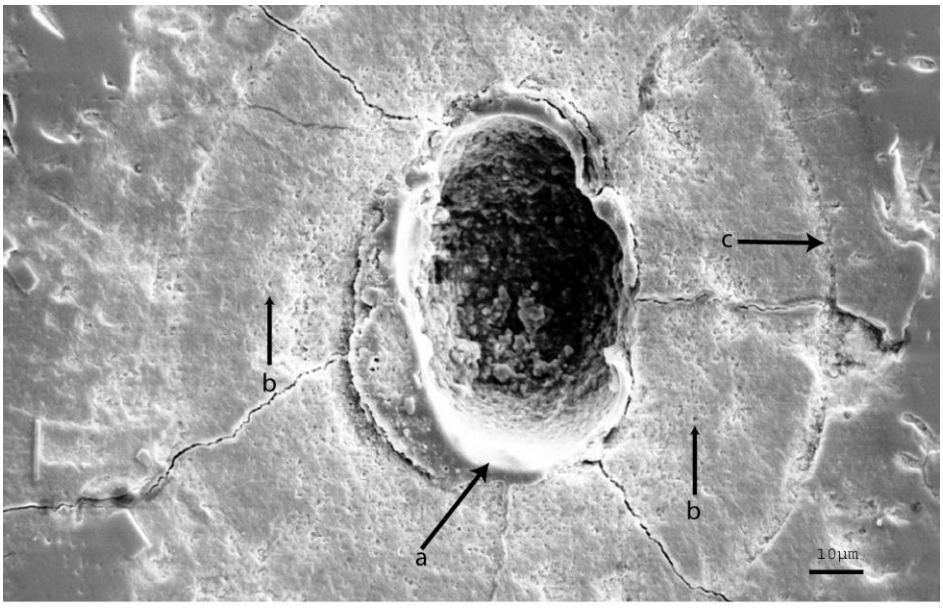

Figure 6

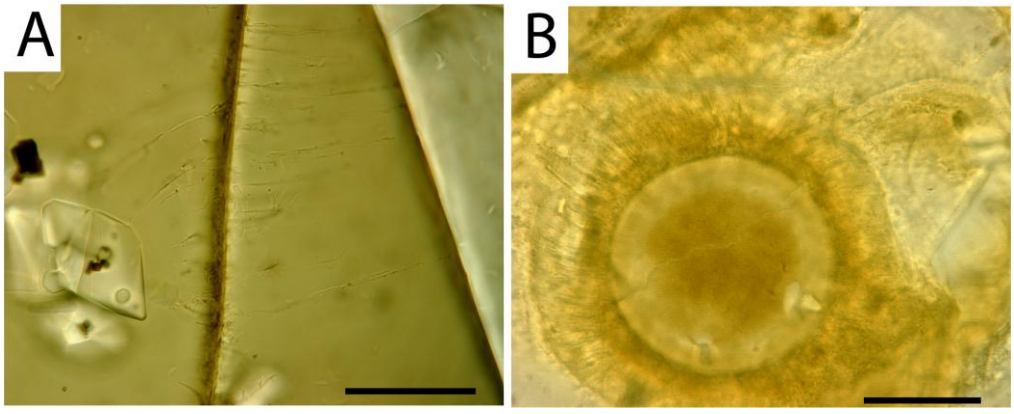

Figure 7

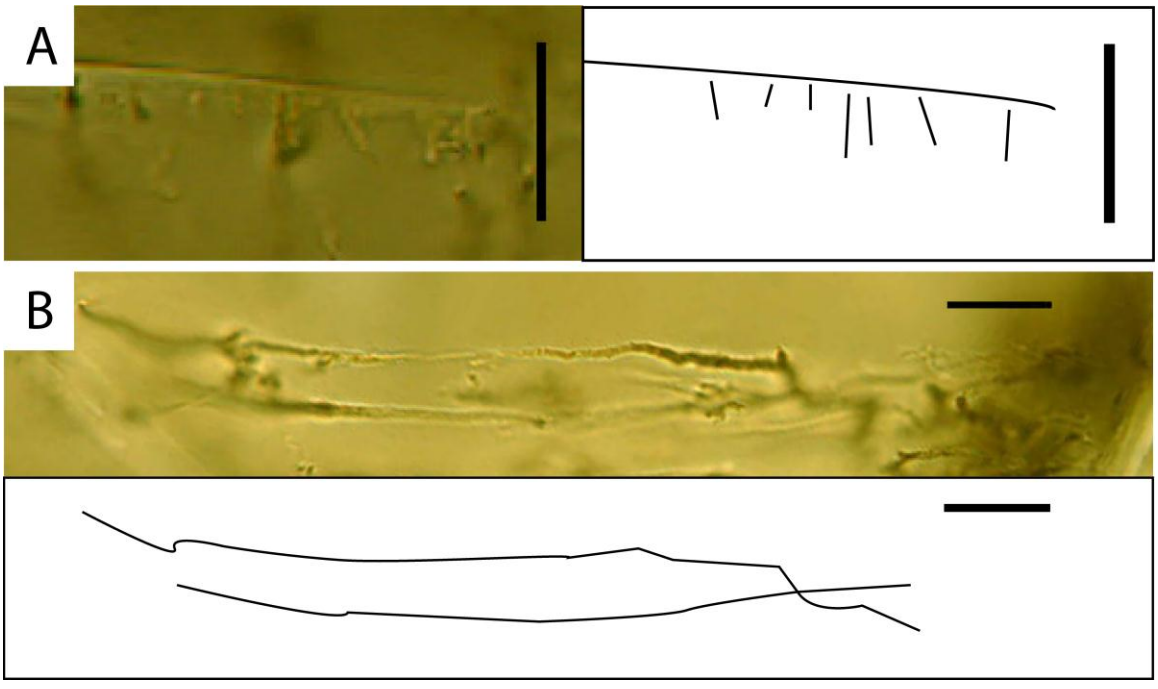

Figure 8

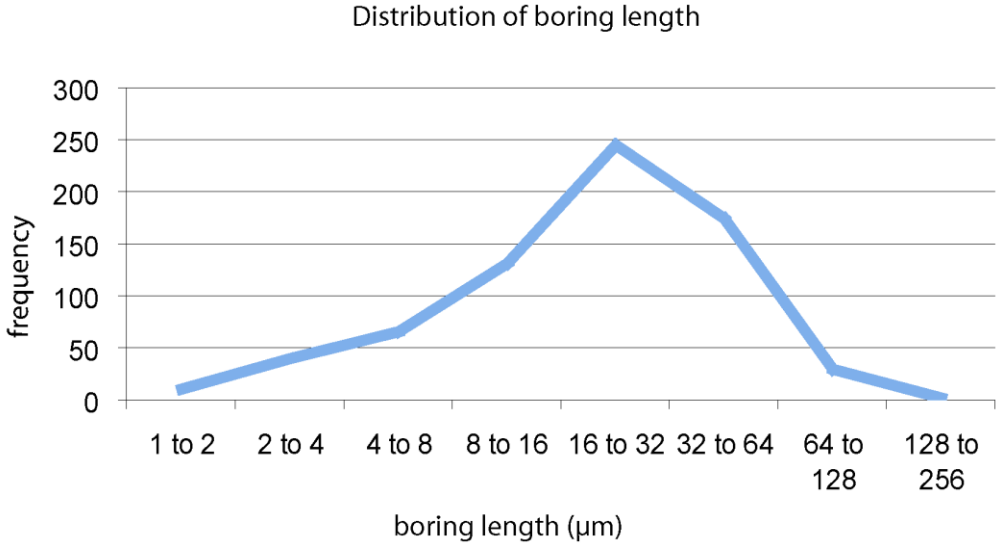

Figure 9

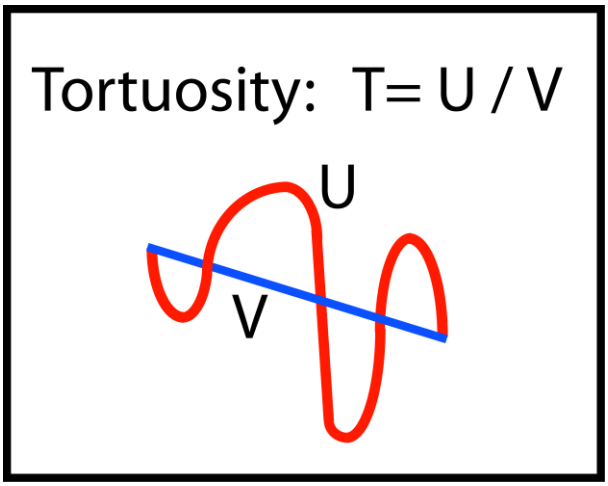

Figure 10

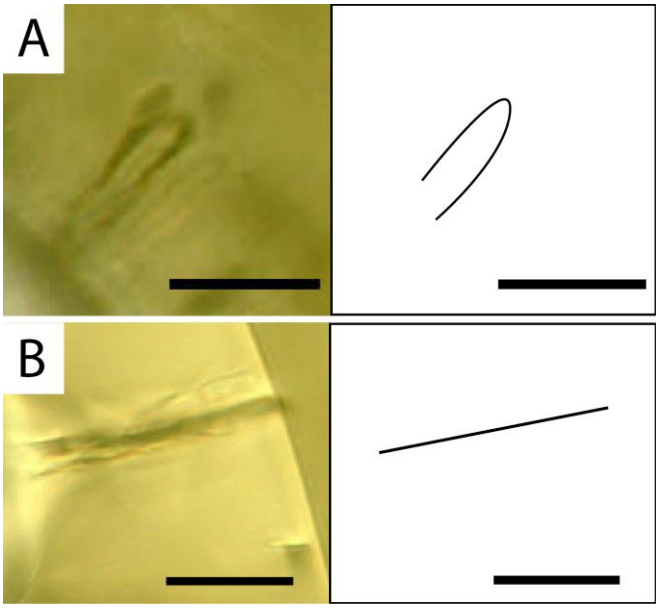

Figure 11

A

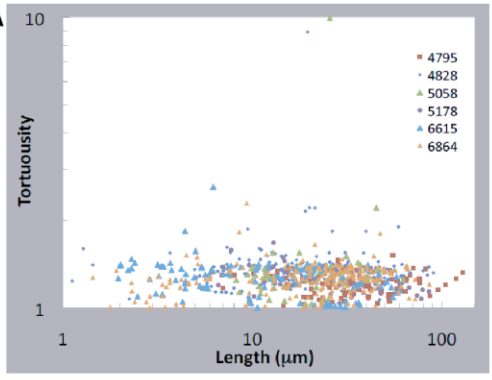

C

Sample #	Ave. overall length (μm)	Ave. Tortuosity
4428	25.5	1.42
4795	38.35	1.227
5058	21.9	1.686
5178	22.1	1.277
6615	17.2	1.271
6864	25.3	1.265
Overall averages	26.127	1.2849

B

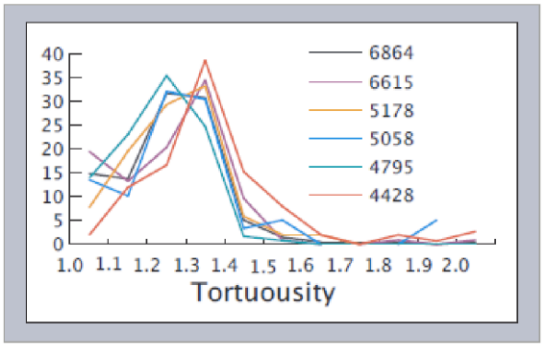

Figure 12

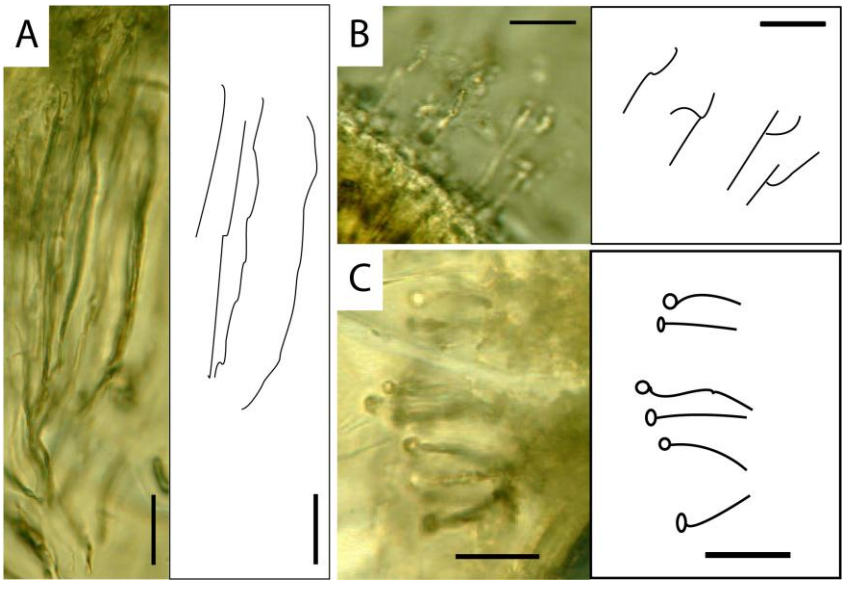

Figure 13

Slide #	P-value
1365.9	= .082
1478.8	= .330
1560.1	= .098
1597	= .403
2040.1	< .005
2117	< .005

Table 1

	Frequency	Min. Length	Max. Length	Ave Length	Ave Tortuosity	Ave Complexity
Fracture	324	0.80	129.22	22.88	1.25	1.31
Vesicle	87	6.16	84.10	27.08	1.32	1.23

Table 2

FIGURE 1—Map of the Hawaiian Islands (inset) and the island of Hawaii with the HSDP site near Hilo, Hawaii. Modified from DePaolo et al. (1996).

FIGURE 2—Lithologic description of the lower part of the HSDP #2 phase 1 core. Modified from (Walton 2008); Average MII and Temperature data; Silica %; Porosity and PPT all vs Depth.

FIGURE 3—Alteration history. A) Palagonite alteration in a hyaloclastite from HSDP #2 phase 1 core from a depth of 2565.7 mbsl. The sample is imaged in plane-polarized light. B) Later phase of alteration, pore-filling chabazite and radiated masses of bladed phillipsite. The sample is imaged in plane-polarized light. (Walton and Schiffman 2003).

FIGURE 4—Euendolithic microborings observed in the thin sections of HSDP #2 samples.

FIGURE 5—Schematic diagrams of micro-ichnofabric indices 1 through 5 with representative examples, left = schematic, right = example. 5 μm scale bar in 1B is for 1-5. 1; 0% dissolution; depth 2117 mbsl. 2; 8% dissolution; depth 2117 mbsl. 3; 30% dissolution; depth 2117 mbsl. 4; 50% dissolution; depth 2040.1 mbsl. 5; 61% dissolution; depth 2117 mbsl (after Montague et al., 2010)

FIGURE 6—Scanning Electron Microscope photomicrographs showing width of two different euendolithic microborings from a depth of 6902.4 mbsl. A) Tubular shaped boring, notice the texture on the inside of the boring is bumpy. Scale bar is 2 μm. B) Irregular shaped boring.

Scale bar is 1 μm.

FIGURE 7—A) Delicate borings originating from a fracture. B) More robust borings originating from a vesicle. Scale bars are 50 μm.

FIGURE 8—Extreme lengths of euendolithic microborings. A) Shortest borings, 0.96 μm from a depth of 6902.4 mbsl, these microborings originate from a fracture. B) Longest borings, 129.2 μm from a depth of 4833.1 mbsl. Scale bars are 10 μm.

FIGURE 9— Plot of length of borings vs. abundance in six samples.

FIGURE 10—Explanation of tortuosity: U= total length and V= straight-line distance between the beginning and end of the boring. Modified from (Hembree and Hasiotis 2006).

FIGURE 11—Comparison of a highly tortuous boring to a non-tortuous boring. A) High tortuosity, T= 25. 7 μm/ 2.59 μm = 9.93. Microboring is from a depth of 5096.6 mbsl. B) Low tortuosity, T= 20.5 μm/ 17.6 μm = 1.16. Microboring is from a depth of 4833.1 mbsl. Scale bars are 10 μm.

FIGURE 12— Descriptive features of euendolithic microborings: Tortuosity. A) Graph showing length (μm) versus tortuosity of all borings. B) Graph of tortuosity ranges of all six samples. C) Table of average length and tortousity from all six samples.

FIGURE 13—Comparison of simple and complex borings. A) Simple borings from a depth of

4466.8 mbsl. B) Complex borings, branching bud morphology from a depth of 6902.4 mbsl. C) Complex borings, nail head termination from a depth of 5096.6 mbsl. Scale bars are 10 μm.

TABLE 1—p-values of the six samples for the Anderson-Darling normality test.

TABLE 2—Descriptive statistics of borings found originating from a fracture or a vesicle.

References

BANERJEE, N.R., and MUEHLENBACHS, K., 2003, Tuff life: Bioalteration in volcaniclastic rocks from the Ontong Java Plateau: Geochemistry, Geophysics, Geosystems, v. 4, p. 1-22, doi: 10.1029/2002GC000470.

Bergey's Manual of Determinative Bacteriology, 9th ed. Edited by John G. Holt et al. Baltimore: Williams & Wilkins, 1994.

DEPAOLO, D., THOMAS, D., STOLPER, E., and GARCIA, M., 2000, Scientific Drilling Project: Core logs and summarizing data report: Pasadena, California Institute of Technology, p. 1-8.

FISK, M.R., GIOVANNONI, S.J., and THORSETH, I.H., 1998, Alteration of Oceanic Volcanic Glass: Textural Evidence of Microbial Activity: Science, v. 281, p. 978-980.

FISK, M.R., STORRIE-LOMBARDI, M.C., DOUGLAS, S., POPA, R., MCDONALD, G., and DI MEO-SAVOIE, C., 2003, Evidence of biological activity in Hawaiian subsurface basalts: Geochemistry, Geophysics, Geosystems, v. 4, p. 1-24, doi: 10.1029/2002GC000387.

FURNES, H., BANERJEE, N.R., MUEHLENBACHS, K., and KONTINEN, A., 2005, Preservation of biosignatures in metaglassy volcanic rocks from the Jormua ophiolite complex, Finland: Precambrian Research, v. 136, p. 125-137.

FURNES, H., BANERJEE, N.R., STAUDIGEL, H., MUEHLENBACHS, K., MCLOUGHLIN, N., DE WIT, M., and VAN KRANENDONK, M.J., 2007, Comparing petrographic signatures of bioalteration in recent to Mesoarchean pillow lavas: Tracicng subsurface life in oceanic igneous rocks: Precambrian Research, v. 158, p. 156-176.

FURNES, H., MUEHLENBACHS, K., TUMYR, O., TORSVIK, T., and THORSETH, I.H., 1999, Depth of active bio-alteration in the ocean crust: Costa Rica Rift (Hole 504B): Terra Nova, v. 11, p. 228-233.

FURNES, H., and STAUDIGEL, H., 1999, Biological mediation in ocean crust alteration: how deep is the deep biosphere? Earth and Planetary Science Letters, v. 166, p. 97-103.

Furnes, H., Staudigel, H., Thorseth, I., H., Torsvik, T., Muehlenbachs, K., and Tumyr, O., 2001, Bioalteration of basaltic glass in oceanic crust: Geochemistry, Geophysics, Geosystems, p. 1-30, doi: 2000GC000150.

FURNES, H., THORSETH, I.H., TUMYR, O., TORSVIK, T., and FISK, M.R., 1996, Microbial Activity in the Alteration of Glass From Pillow Lavas From Hole 896A, *in* Alt, J.C., Knoshita, H., Stokking, L.B., and Michael, P.J., eds., Proceedings of the Ocean Drilling Program, Scientific Results, vol. 148: College Station, TX, p. 191-206.

HEMBREE, D.I., and HASIOTIS, S.T., 2006, The identification and interpretation of reptile ichnofossils in paleosols through modern studies: Journal of Sedimentary Research, v. 76, p. 575-588.

MCLOUGHLIN, N., BRASIER, M.D., WACEY, D., GREEN, O.R., and PERRY, R.S., 2007, On Biogenicity Criteria for Endolithic Microborings on Early Earth and Beyond: Astrobiology, v. 7, p. 10-26.

MCLOUGHLIN, N., FURNES, H., BANERJEE, N.R., MUEHLENBACHS, K., and STAUDIGEL, H., 2009, Ichnotaxonomy of microbial trace fossils in volcanic glass: Journal of Geological Society, London, v. 166, n. 1, p. 159-169.

MEADOWS, P.S., 1991, The environmental impact of burrows and burrowing animals-conclusions and a model, *in* Meadows, P.S., and Meadows, A., eds., The Environmental Impact of Burrowing Animals and Animal Burrows, Zoological Society of London Symposia 63, Clarendon Press, Oxford, p. 327-338.

Stroncik, N. A., and Schmincke, H.U., 2001, Evolution of palagonite: Crystallization, chemical changes, element budget: Geochemistry, Geophysics, Geosystems, p. 1-43, Paper number 2000GC000102.

SHARP, W.D., and RENNE, P.R., 2005, The 40Ar/39Ar dating of core recovered by the Hawaii Scientific Drilling Project (phase 2), Hilo, Hawaii: Geochemistry, Geophysics, Geosystems, v. 6, p. 1-18, doi: 10.1029/2004GC000846.

STORRIE-LOMBARDI, M.C., and FISK, M.R., 2004, Evidence of Biogenic Alteration in Sub-oceanic Basalt Glass: Complexity Image Analysis, Elemental Abundance Distributions, and Bayesian Probabilistic Classification, *in* Hoover, R.B., Levin, G.V., and Rozanov, A.Y., eds., Instruments, Methods, and Missions for Astrobiology VIII: Bellingham, SPIE, p. 47-58.

THORSETH, I.H., TORSVIK, T., FURNES, H., and MUEHLENBACHS, K., 1995, Microbes play an important role in the alteration of oceanic crust: Chemical Geology, v. 126, p. 137-146.

TORSVIK, T., 1998, Evidence for microbial activity at the glass-alteration interface in oceanic basalts: Earth and Planetary Science Letters, v. 162, p. 165-176.

WALTON, A.W., 2008, Microtubules in basalt glass from Hawaii Scientific Drilling Project #2 phase 1 core and Hilina slope, Hawaii: evidence of the occurrence and behavior of endolithic microorganisms: Geobiology, v. 6, n. 4, p. 351-364.

WALTON, A.W., and SCHIFFMAN, P., 2005, Alteration of hyaloclastites in the HSDP 2 Phase 1 Drill Core 1: 2. Mass balance of the conversion of sideromelane to palagonite and chabazite: Geochemistry, Geophysics, Geosystems, v. 6, no. 9, p. 1-27, doi: 10.1029/2004GC000903.

WALTON, A.W., and SCHIFFMAN, P., 2003, Alteration of hyaloclastites in the HSDP 2 Phase 1 Drill Core 1. Description and paragenesis: Geochemistry, Geophysics, Geosystems, v. 4, p. 1-31, doi: 10.1029/2002GC000368.

Chapter 4

Conclusion

Most individual microborings studied (84%) were simple in form: no branches, no nodes or chambers; they were irregular tubes, initially about 1 μm in diameter and were classified as *Tubulohyalichnus simplus*. The length of the microborings ranged from <1 μm to over 100 μm. In the six samples analyzed the lengths were approximately log-normally distributed with a geometric mean length of 18.9 μm. Microborings are somewhat tortuous, with a mean tortuosity of 1.28, but virtually no correlation of tortuosity with length or complexity. Of the 16% of the borings studied which were labeled as complex, very few of these borings were classified as *T. stipes*. The *T. stipes* observed exhibited similar branching bud ornamentation. Most often *T. stipes* was found originating from fractures. Other complex borings included those that terminated in a form similar to a nail head and a variety of other types illustrated in Walton (2008), which differed from the established ichnotaxon.

The lower two thirds of the core, from 1,079 mbsl to total depth at over 3,109 mbsl, contained submarine lavas, hyaloclastites, and intrusions from Mauna Kea (DePaolo et al., 2000). The MII showed the abundance of microboring varied down the core. The most abundant areas of bioerosion, with an average MII of 2 to 2.5 (>10% of avilable volumes of hyaloclasts displaying boring in individual thin sections) were at depths centering in 1,398 mbsl and 2,117 mbsl, zones 2 and 5. Individual 30 μm-square sampling areas of particluar thin sections from these zones displayed MII values up to 5 (borings occupy >60% of the available area of the sample), however, no individual sample was assigned MII > 3. The areas of low bioerosion, zones 1, 3, and 4, had average MII of 1 to 1.2 (zero to a few % of the available area displaying borings), with values on individual 30 μm-square sample points from these zones ranging up to 3 (<40% of available area being bored).

Applying the MII schematic diagrams to the HSDP #2 samples provided a semi-quantitative estimate of the abundance of bioerosion of the HSDP core and for the comparison of bioerosion abundances from different samples of basaltic glass and facilitates the comparison of euendolithic microborings with much larger borings and larger diameter trace fossils in a variety of media, as long as the scale ratio of area of measure to trace fossil size is maintained at ~30:1. Statistical analysis verifies that analyzing 60 random locations will give detectable differences between samples at a 95% confidence level. Like any other semi-quantitative classification, even though no two persons will necessarily assign the same category of disruption, the use of MII schematic diagrams reduce the range of variability between observers of euendolithic microbial borings.

The vertical distribution of boring activity in the oceanic crust of previous studies differs from the results of this study. The earlier results are not refuted; instead this study expands the range of understanding of microbial borings in basaltic glass of the ocean basins. Furthermore, this study extends the scale of bioerosion to the microscopic level.

Appendices

Appendix A

Appendix A1: Length, straight length, and tortuosity of sample 1365.9 mbsl

Location	Specimen #	Length (µm)	Straight length (µm)	Tortuosity
51, 111	1	36.88	30.80	1.20
	2	62.07	51.11	1.21
	3	50.08	41.71	1.20
25, 103	1	21.81	17.09	1.28
	2	11.59	9.19	1.26
	3	9.41	7.17	1.31
	4	6.42	5.65	1.14
	5	9.62	6.58	1.46
	6	6.90	6.09	1.13
	7	7.54	5.73	1.32
	8	6.26	4.52	1.38
	9	9.66	6.82	1.42
	10	10.22	7.29	1.40
	11	13.63	10.55	1.29
	12	12.74	9.21	1.38
	13	7.28	6.43	1.13
46, 101	1	38.96	28.12	1.39
	2	14.76	11.23	1.31
	3	20.05	9.07	2.21
	4	25.50	16.46	1.55
	5	61.74	43.72	1.41
	6	30.91	22.13	1.40
	7	56.09	40.26	1.39
	8	80.03	59.59	1.34
	9	49.45	36.23	1.37
	10	56.42	41.86	1.35
	11	33.91	24.99	1.36
	12	18.13	13.89	1.31
	13	28.29	21.25	1.33
	14	36.96	28.16	1.31
	15	15.05	11.33	1.33
	16	27.25	19.74	1.38
	17	23.94	17.91	1.34
	18	46.36	38.89	1.19
	19	51.30	37.66	1.36
	20	31.01	19.99	1.55
	21	22.40	17.89	1.25
	22	24.54	17.38	1.41
51, 113	1	26.47	14.42	1.84

	2	7.38	4.57	1.62
	3	27.83	20.46	1.36
	4	26.82	20.22	1.33
	5	21.16	15.56	1.36
	6	5.77	4.75	1.22
	7	2.25	2.09	1.07
	8	3.69	2.38	1.55
	9	3.37	2.41	1.40
32, 120	1	68.45	51.83	1.32
	2	62.26	48.27	1.29
	3	24.22	19.30	1.25
	4	49.86	39.32	1.27
	5	52.26	41.70	1.25
	6	60.84	47.33	1.29
	7	29.71	25.95	1.14
	8	66.62	49.43	1.35
	9	46.19	37.28	1.24
	10	63.08	49.42	1.28
	11	41.06	31.01	1.32
	12	84.10	64.81	1.30
	13	46.29	32.08	1.44
	14	50.58	38.25	1.32
	15	39.63	29.42	1.35
31, 118	1	15.96	13.77	1.16
	2	38.72	25.03	1.55
	3	44.51	36.91	1.21
	4	19.09	8.87	2.15
	5	45.97	39.45	1.17
	6	31.76	22.39	1.42
	7	59.17	31.11	1.90
	8	39.94	21.75	1.84
31, 104	1	14.28	9.47	1.51
	2	14.44	11.31	1.28
	3	15.05	9.93	1.52
32,93	1	16.26	11.43	1.42
	2	23.51	17.54	1.34
	3	19.64	2.21	8.90
	4	22.93	16.78	1.37
	5	26.63	18.81	1.42
	6	10.88	7.99	1.36
	7	36.35	26.77	1.36
	8	14.22	10.45	1.36
	9	9.48	5.08	1.87
	10	12.87	9.34	1.38
	11	9.14	6.97	1.31
32, 103	1	27.88	21.19	1.32
	2	11.94	8.67	1.38

	3	7.70	4.95	1.55
	4	8.57	5.81	1.47
	5	6.58	4.92	1.34
	6	17.14	12.84	1.33
	7	16.91	13.39	1.26
37,97	1	21.88	14.55	1.50
	2	13.21	8.60	1.54
	3	12.70	8.18	1.55
	4	11.18	7.06	1.58
	5	17.14	11.72	1.46
	6	12.36	8.61	1.44
	7	7.79	6.94	1.12
	8	15.92	13.34	1.19
37,101	1	13.35	9.44	1.42
	2	10.91	6.81	1.60
	3	23.91	17.01	1.41
	4	34.12	28.25	1.21
	5	8.82	7.74	1.14
	6	11.13	9.28	1.20
	7	7.06	5.25	1.34
39, 90	1	5.29	4.11	1.29
	2	10.49	7.61	1.38
	3	24.30	17.61	1.38
	4	11.07	7.54	1.47
	5	32.18	22.24	1.45
	6	17.16	12.19	1.41
	7	25.67	17.84	1.44
	8	24.58	17.69	1.39
	9	18.32	12.84	1.43
	10	21.21	15.57	1.36
	11	15.70	12.65	1.24
	12	12.03	7.97	1.51
	13	7.38	5.22	1.41
	14	24.86	18.59	1.34
	15	14.76	10.81	1.36
	16	21.49	9.73	2.21
	17	14.34	10.68	1.34
	18	20.05	14.64	1.37
	19	15.21	11.08	1.37
39, 117	1	6.90	4.98	1.38
	2	8.18	5.87	1.39
	3	8.02	6.85	1.17
46, 109	1	46.87	33.91	1.38
	2	36.64	26.21	1.40
	3	44.99	32.79	1.37
	4	19.09	16.43	1.16
	5	9.53	8.78	1.09

	6	6.10	5.14	1.19
	7	7.38	5.68	1.30
	8	4.97	3.66	1.36
	9	46.75	33.94	1.38
	10	27.01	21.96	1.23
	11	37.14	26.28	1.41
49, 112	1	47.04	44.13	1.07
	2	90.55	68.55	1.32
	3	31.45	26.34	1.19
	4	85.54	61.87	1.38
	5	17.20	14.28	1.20
	6	43.93	34.40	1.28
51,108	1	1.28	0.80	1.60
	2	1.12	0.91	1.24
	3	1.44	1.03	1.41
	4	5.74	4.85	1.18
	5	5.36	4.59	1.17

Appendix A2: Length, straight length, and tortuosity of sample 1478.8 mbsl

Location	**Specimen #**	**Length (µm)**	**Straight length (µm)**	**Tortuosity**
51,117	1	40.71	37.21	1.09
	2	95.79	83.11	1.15
	3	86.83	78.94	1.10
	4	18.39	17.81	1.03
	5	21.31	18.94	1.12
	6	18.74	17.20	1.09
	7	105.29	87.73	1.20
	8	25.60	21.71	1.18
	9	23.60	21.82	1.08
	10	25.21	20.99	1.20
30,109	1	45.80	34.22	1.34
	2	46.43	34.49	1.35
	3	38.96	30.85	1.26
	4	45.27	33.51	1.35
47,106,d	1	32.56	26.52	1.23
	2	29.51	27.36	1.08
	3	35.75	29.61	1.21
	4	44.93	35.93	1.25
	5	70.69	51.72	1.37
	6	42.89	32.30	1.33

	7	14.60	14.28	1.02
	8	19.22	17.68	1.09
	9	20.44	18.79	1.09
47,106,c	1	76.24	60.48	1.26
	2	58.16	49.98	1.16
	3	52.41	47.21	1.11
	4	53.48	48.16	1.11
	5	47.90	41.92	1.14
	6	58.84	51.44	1.14
	7	61.08	52.80	1.16
	8	46.88	36.78	1.27
	9	40.85	34.28	1.19
47,106,b	1	39.60	33.38	1.19
	2	36.86	31.93	1.15
	3	32.41	28.56	1.13
	4	33.47	30.33	1.10
	5	34.55	30.85	1.12
	6	30.51	28.88	1.06
	7	30.80	27.45	1.12
	8	26.28	25.07	1.05
47,106	1	76.78	62.87	1.22
	2	64.19	56.25	1.14
	3	56.63	50.59	1.12
	4	52.71	48.39	1.09
28,110	1	129.22	97.91	1.32
	2	118.84	94.27	1.26
	3	58.16	46.97	1.24
	4	62.72	49.15	1.28
	5	65.03	52.55	1.24
	6	63.58	50.94	1.25
	7	20.28	16.03	1.27
	8	54.82	43.65	1.26
	9	41.16	38.14	1.08
	10	53.06	50.30	1.05
	11	45.98	44.32	1.04
43,118	1	67.90	52.42	1.30
	2	36.80	28.77	1.28
	3	65.16	51.54	1.26
30,106	1	30.56	22.84	1.34
	2	26.69	21.95	1.22
	3	27.44	21.09	1.30
	4	20.52	16.82	1.22
	5	15.75	12.09	1.30
	6	16.13	11.79	1.37
	7	18.95	15.35	1.23
	8	28.33	19.42	1.46
	9	7.02	5.07	1.38

	10	6.91	5.32	1.30
	11	10.15	7.72	1.31
	12	8.05	6.20	1.30
	13	15.15	11.38	1.33
	14	11.97	8.89	1.35
40,118	1	34.26	30.70	1.12
	2	7.04	6.01	1.17
	3	33.96	27.79	1.22
	4	38.50	31.99	1.20
	5	32.88	27.18	1.21
27,108	1	35.00	30.05	1.16
	2	30.44	26.41	1.15
	3	29.03	24.05	1.21
	4	42.09	36.22	1.16
	5	30.99	28.02	1.11
39,108	1	33.73	27.39	1.23
	2	41.51	34.82	1.19
	3	41.20	37.63	1.09
	4	27.63	23.47	1.18
27,118	1	16.41	13.74	1.19
	2	13.59	10.13	1.34
	3	12.45	9.65	1.29
	4	13.56	10.48	1.29
	5	16.56	13.17	1.26
29,116	1	82.20	60.24	1.36
	2	41.97	30.60	1.37
	3	55.20	36.45	1.51
	4	54.16	41.16	1.32
	5	53.29	39.45	1.35
	6	58.61	47.20	1.24
	7	37.84	31.51	1.20
	8	40.69	33.23	1.22
52,115	1	19.61	15.60	1.26
	2	15.08	11.87	1.27
	3	15.30	12.68	1.21
	4	35.71	26.41	1.35
	5	31.07	22.81	1.36
	6	31.43	23.39	1.34
	7	20.50	17.65	1.16
	8	46.57	37.27	1.25
	9	49.30	40.37	1.22
	10	25.53	18.99	1.34
	11	22.38	17.48	1.28
	12	22.62	21.19	1.07
	13	23.58	19.42	1.21
	14	27.40	20.52	1.34
	15	30.88	25.45	1.21

16	29.42	23.89	1.23
17	33.20	25.03	1.33
18	30.30	22.45	1.35
19	29.08	21.77	1.34
20	28.84	20.56	1.40
21	24.13	18.33	1.32
22	26.28	19.49	1.35
23	20.45	15.24	1.34

Appendix A3: Length, straight length, and tortuosity of sample 1560.1 mbsl

Location	**Specimen #**	**Length (µm)**	**Straight length (µm)**	**Tortuosity**
22,109	1	20.67	15.63	1.32
	2	31.48	20.87	1.51
	3	22.75	17.11	1.33
	4	23.16	16.56	1.40
	5	13.06	11.14	1.17
30,110	1	11.78	9.09	1.30
	2	11.07	9.85	1.12
	3	13.06	10.67	1.22
	4	14.82	12.51	1.18
	5	12.32	11.55	1.07
	6	12.19	9.67	1.26
	7	9.62	9.15	1.05
31,109,b	1	19.11	18.49	1.03
	2	25.06	23.59	1.06
	3	14.84	14.04	1.06
	4	23.45	22.04	1.06
	5	25.35	24.07	1.05
	6	20.64	19.97	1.03
31,109	1	16.49	12.70	1.30
	2	11.79	8.82	1.34
33,109	1	30.10	1.83	16.46
	2	25.74	2.59	9.93
	3	11.65	8.53	1.37
	4	7.71	5.97	1.29
	5	15.53	11.32	1.37
38,111	1	45.27	20.46	2.21
	2	17.49	12.83	1.36
	3	15.46	11.01	1.41
	4	12.12	9.30	1.30
38.5,111	1	10.88	9.14	1.19
	2	25.46	20.07	1.27

	3	20.85	16.90	1.23
	4	21.81	18.49	1.18
	5	30.55	25.04	1.22
	6	25.96	20.76	1.25
31,101	1	11.56	9.23	1.25
	2	8.57	7.55	1.14
	3	9.94	7.24	1.37
	4	6.23	4.65	1.34
51,109	1	45.31	33.50	1.35
	2	37.35	26.66	1.40
	3	26.02	18.64	1.40
	4	29.39	23.11	1.27
	5	10.43	7.52	1.39
	6	12.90	8.32	1.55
	7	17.78	11.48	1.55
28,108,b	1	62.65	50.00	1.25
	2	40.61	32.67	1.24
	3	46.36	33.75	1.37
	4	36.75	27.38	1.34
	5	40.79	31.68	1.29
	6	38.97	30.56	1.28
	7	20.34	14.99	1.36
28,108,c	1	9.47	7.26	1.30
	2	10.39	8.01	1.30
	3	10.05	8.08	1.24
	4	8.24	6.60	1.25
28,108	1	36.22	25.24	1.43
	2	39.37	31.67	1.24
	3	26.38	20.26	1.30

Appendix A4: Length, straight length, and tortuosity of sample 1597.0 mbsl

Location	**Specimen #**	**Length (µm)**	**Straight length (µm)**	**Tortuosity**
21,109	1	18.34	14.53	1.26
	2	26.23	20.85	1.26
	3	25.47	20.65	1.23
	4	19.19	15.34	1.25
	5	21.10	16.82	1.25
21,110,c	1	79.50	68.88	1.15
	2	78.10	72.71	1.07
	3	47.90	42.76	1.12
	4	60.19	49.94	1.21
	5	85.69	75.11	1.14

	6	39.47	28.71	1.37
	7	74.05	67.05	1.10
	8	67.26	57.23	1.18
	9	28.75	24.08	1.19
21,110,b	1	16.73	12.37	1.35
	2	19.10	13.92	1.37
	3	20.06	14.91	1.35
	4	15.46	11.48	1.35
	5	15.32	11.10	1.38
	6	30.87	23.21	1.33
	7	22.86	16.82	1.36
	8	23.27	16.82	1.38
21,110	1	38.62	34.23	1.13
	2	28.90	27.85	1.04
	3	33.36	30.73	1.09
	4	25.95	23.33	1.11
	5	10.25	9.37	1.09
26,109	1	12.53	9.13	1.37
	2	14.02	11.17	1.26
	3	14.85	10.22	1.45
	4	14.09	11.67	1.21
	5	12.93	10.40	1.24
	6	12.97	9.34	1.39
	7	14.55	9.74	1.49
	8	6.63	5.54	1.20
	9	13.00	7.75	1.68
	10	36.68	27.29	1.34
25,108	1	15.65	11.99	1.31
	2	6.16	4.65	1.33
	3	7.77	4.91	1.58
	4	18.38	14.43	1.27
	5	11.56	9.45	1.22
26,110	1	5.05	3.97	1.27
	2	13.18	10.82	1.22
	3	23.65	17.92	1.32
	4	28.54	21.78	1.31
	5	30.36	22.76	1.33
	6	33.55	26.34	1.27
	7	9.63	6.85	1.41
	8	18.50	14.98	1.24

Appendix A5: Length, straight length, and tortuosity of sample 2040.1 mbsl

Location	Specimen #	Length (μm)	Straight length (μm)	Tortuosity
29, 101,b	1	7.63	5.82	1.31
	2	2.21	1.64	1.35
	3	2.31	1.68	1.37
	4	2.02	1.44	1.40
	5	4.43	3.65	1.22
	6	5.67	4.35	1.30
	7	8.71	6.30	1.38
	8	5.86	5.03	1.17
	9	3.41	2.46	1.39
	10	3.76	2.78	1.35
	11	2.41	1.68	1.43
	12	1.97	1.55	1.27
	13	4.47	3.42	1.31
	14	4.95	3.88	1.28
	15	3.95	3.17	1.25
	16	13.78	10.77	1.28
	17	17.23	14.29	1.21
	18	18.20	13.40	1.36
	19	19.80	15.18	1.31
	20	5.43	3.95	1.38
	21	3.10	2.77	1.12
	22	2.02	1.43	1.41
29, 101	1	10.83	7.65	1.42
	2	5.91	4.54	1.30
	3	2.31	1.57	1.47
	4	3.22	2.50	1.29
	5	4.43	2.41	1.84
	6	2.89	2.30	1.26
	7	3.70	2.59	1.43
	8	5.42	3.90	1.39
	9	4.24	3.11	1.36
	10	7.74	5.54	1.40
	11	7.05	5.39	1.31
	12	6.11	4.50	1.36
	13	5.03	3.21	1.57
	14	0.91	0.79	1.14
	15	3.18	2.26	1.41
	16	3.31	2.38	1.39
27.5, 101	1	22.57	16.01	1.41
	2	20.45	15.02	1.36
	3	20.69	15.04	1.38
	4	20.25	14.50	1.40
	5	18.95	14.88	1.27
	6	19.85	14.67	1.35
35,104	1	47.72	40.12	1.19
36.5,104	1	19.57	13.78	1.42

	2	17.68	13.23	1.34
	3	17.04	12.39	1.38
	4	20.48	15.13	1.35
	5	20.55	15.35	1.34
	6	23.46	17.53	1.34
	7	16.71	13.49	1.24
	8	12.99	10.31	1.26
	9	9.69	9.01	1.08
	10	9.85	9.46	1.04
	11	21.17	15.57	1.36
	12	20.48	15.71	1.30
	13	19.31	14.06	1.37
	14	20.34	14.88	1.37
	15	20.89	15.54	1.34
	16	18.67	13.76	1.36
	17	19.96	14.85	1.34
	18	21.50	15.59	1.38
	19	10.49	7.74	1.36
	20	14.50	11.52	1.26
	21	11.62	9.85	1.18
	22	12.74	10.12	1.26
	23	16.59	13.04	1.27
32,106	1	36.55	34.97	1.04
	2	35.32	34.05	1.04
	3	31.09	30.86	1.01
	4	10.68	10.64	1.00
	5	29.18	28.81	1.01
	6	26.05	25.42	1.02
	7	27.44	26.98	1.02
	8	25.72	24.96	1.03
	9	21.45	20.99	1.02
	10	23.34	22.91	1.02
	11	24.92	24.56	1.01
	12	36.93	35.95	1.03
	13	55.43	50.93	1.09
	14	17.94	17.25	1.04
	15	31.38	29.72	1.06
	16	24.66	23.85	1.03
	17	24.45	23.45	1.04
26.5,104	1	12.12	8.81	1.38
	2	13.24	10.29	1.29
27,113	1	37.86	31.18	1.21
	2	51.29	41.60	1.23
	3	37.45	30.32	1.23
	4	30.24	23.67	1.28
24,116	1	54.28	46.11	1.18
	2	60.00	52.08	1.15

	3	57.85	51.29	1.13
	4	46.59	35.62	1.31
	5	57.87	45.14	1.28
	6	21.76	17.62	1.24
	7	34.02	29.32	1.16
29,102	1	4.46	3.60	1.24
	2	5.31	4.46	1.19
	3	4.98	5.04	0.99
	4	3.36	3.01	1.12
	5	4.44	3.80	1.17
	6	10.87	9.98	1.09
	7	7.43	5.39	1.38
	8	3.26	3.37	0.97
	9	5.53	4.72	1.17
	10	4.29	4.09	1.05
	11	10.38	8.40	1.24
	12	2.48	2.27	1.09
	13	12.24	8.62	1.42
	14	6.23	2.38	2.61
	15	5.77	4.83	1.19
32,107	1	35.75	30.05	1.19
	2	40.86	29.11	1.40

Appendix A6: Length, straight length, and tortuosity of sample 2117.0 mbsl

Location	**Specimen #**	**Length (µm)**	**Straight length (µm)**	**Tortuosity**
26,103	1	30.26	25.83	1.17
	2	38.52	30.55	1.26
	3	36.72	29.01	1.27
	4	39.07	30.60	1.28
	5	46.54	33.72	1.38
	6	47.45	37.49	1.27
	7	40.24	29.05	1.39
	8	34.52	26.53	1.30
	9	26.22	19.76	1.33
	10	31.38	25.29	1.24
	11	27.99	21.40	1.31
	12	44.47	36.03	1.23
	13	34.74	30.10	1.15
	14	42.34	33.27	1.27
29,103	1	44.29	38.08	1.16
	2	31.98	26.83	1.19
	3	45.50	36.19	1.26

	4	46.28	38.51	1.20
	5	42.40	37.00	1.15
	6	43.43	34.95	1.24
32,103	1	12.75	10.99	1.16
	2	17.84	14.93	1.19
	3	39.63	30.91	1.28
	4	23.11	20.00	1.16
	5	15.41	12.99	1.19
	6	17.84	14.66	1.22
	7	29.68	24.36	1.22
	8	28.03	23.61	1.19
	9	23.71	20.14	1.18
	10	25.29	20.75	1.22
	11	27.29	22.08	1.24
	12	26.89	22.36	1.20
	13	24.54	19.73	1.24
28,103	1	22.82	22.62	1.01
	2	18.97	18.58	1.02
	3	11.71	11.57	1.01
	4	31.94	30.92	1.03
	5	44.57	44.13	1.01
	6	23.10	22.54	1.02
	7	18.66	18.58	1.00
32,110,d	1	5.99	4.70	1.28
	2	0.80	0.96	0.83
	3	12.08	9.12	1.32
	4	2.32	2.03	1.14
	5	1.78	1.77	1.01
	6	2.89	2.89	1.00
	7	2.89	2.94	0.98
	8	2.77	2.65	1.05
	9	2.90	2.65	1.09
	10	3.97	3.86	1.03
	11	4.34	4.28	1.01
	12	3.48	3.46	1.01
	13	5.18	3.66	1.42
32,110,c	1	8.95	6.49	1.38
	2	24.38	17.52	1.39
	3	21.47	12.99	1.65
	4	8.57	4.70	1.82
	5	11.88	7.78	1.53
	6	37.38	29.53	1.27
	7	21.88	17.82	1.23
	8	33.71	26.19	1.29
	9	24.89	19.89	1.25
	10	72.48	57.88	1.25
	11	34.52	27.28	1.27

	12	44.19	35.58	1.24
	13	40.04	32.14	1.25
	14	18.48	14.66	1.26
	15	23.36	18.13	1.29
	16	13.09	10.61	1.23
	17	4.62	3.78	1.22
	18	9.30	9.15	1.02
	19	11.13	9.64	1.16
	20	11.87	10.66	1.11
	21	23.76	22.69	1.05
	22	23.95	21.91	1.09
	23	2.09	2.11	0.99
	24	19.77	18.18	1.09
	25	18.35	14.61	1.26
32,110,b	1	86.14	71.54	1.20
	2	31.55	23.39	1.35
	3	37.10	29.01	1.28
	4	66.00	48.41	1.36
	5	23.16	22.18	1.04
	6	21.00	17.12	1.23
	7	26.86	20.88	1.29
	8	17.14	15.58	1.10
	9	61.25	51.55	1.19
	10	72.59	67.67	1.07
	11	67.33	62.43	1.08
	12	34.56	33.71	1.03
	13	59.48	52.78	1.13
	14	19.47	15.69	1.24
	15	16.70	13.08	1.28
	16	25.64	23.29	1.10
32,110	1	15.78	12.11	1.30
	2	13.01	10.27	1.27
	3	13.00	10.08	1.29
	4	5.10	4.18	1.22
	5	47.42	26.35	1.80
	6	4.24	3.38	1.25
	7	5.97	4.76	1.26
	8	5.68	4.51	1.26
	9	7.69	5.69	1.35
	10	2.31	1.89	1.22
	11	1.93	1.43	1.35
37,103	1	17.14	13.70	1.25
	2	24.22	18.35	1.32
	3	20.51	15.21	1.35
	4	25.72	20.29	1.27
	5	8.31	5.86	1.42
28,111	1	57.01	42.42	1.34

	2	36.88	27.65	1.33
	3	33.89	24.80	1.37
	4	25.90	19.26	1.34
	5	49.95	36.70	1.36
	6	17.33	13.03	1.33
	7	65.53	47.00	1.39
	8	29.28	21.72	1.35
	9	32.04	25.11	1.28
	10	53.53	40.68	1.32
	11	17.84	12.57	1.42
	12	33.21	23.50	1.41
	13	26.99	21.15	1.28
31, 107	1	3.37	2.80	1.20
	2	3.37	3.06	1.10
	3	3.66	3.74	0.98
	4	5.13	3.43	1.50
	5	1.44	1.13	1.27
	6	0.96	0.82	1.18
	7	9.37	4.09	2.29
	8	7.48	5.61	1.33
	9	4.65	3.86	1.21
	10	2.86	2.27	1.26
	11	4.17	3.55	1.17
	12	9.69	7.87	1.23
	13	2.41	2.30	1.05
	14	3.69	2.95	1.25
	15	3.21	2.51	1.28
55,118	1	19.97	15.14	1.32
	2	15.28	13.07	1.17
	3	22.72	16.59	1.37
	4	9.66	8.60	1.12
	5	14.57	12.34	1.18
	6	11.29	8.91	1.27
36, 120	1	29.71	22.52	1.32
	2	24.51	17.53	1.40
	3	24.54	18.24	1.35
	4	28.43	20.37	1.40
	5	29.90	20.34	1.47
45, 121	1	38.98	34.10	1.14
	2	22.27	16.24	1.37
	3	15.88	11.55	1.37
	4	20.21	15.79	1.28
	5	9.94	8.03	1.24
33,112	1	64.56	46.72	1.38
	2	53.79	40.31	1.33
	3	39.67	28.70	1.38
	4	38.88	28.97	1.34

	5	42.44	31.61	1.34
	6	27.00	20.29	1.33
	7	32.26	24.27	1.33
	8	27.48	19.56	1.41
	9	30.92	22.80	1.36
	10	14.98	10.89	1.38
	11	2.25	2.61	0.86
	12	3.69	3.03	1.22
	13	3.53	2.98	1.18
	14	4.49	2.96	1.52
44,102	1	26.31	22.92	1.15
	2	22.47	17.82	1.26
	3	15.60	12.89	1.21
	4	32.89	28.87	1.14
43,108	1	21.69	21.50	1.01
	2	21.90	19.63	1.12
	3	33.19	30.33	1.09
	4	28.93	23.44	1.23
	5	26.14	23.92	1.09
	6	15.79	14.63	1.08
21,113	1	43.88	29.05	1.51
	2	49.23	37.11	1.33
	3	36.62	26.38	1.39
	4	24.58	17.60	1.40
	5	50.20	37.89	1.32
	6	30.68	22.94	1.34
	7	49.62	36.37	1.36
	8	17.12	12.82	1.34
	9	17.01	12.65	1.34
	10	21.53	14.97	1.44
	11	32.21	23.27	1.38
	12	20.12	14.56	1.38
	13	32.98	24.98	1.32
	14	29.50	21.10	1.40
	15	20.70	14.73	1.41
	16	22.83	16.82	1.36
	17	32.99	23.73	1.39
	18	18.51	12.71	1.46
51,111	1	33.02	23.75	1.39
	2	28.87	21.62	1.33
	3	19.41	14.21	1.37
	4	33.11	23.68	1.40

Location:

51, 111

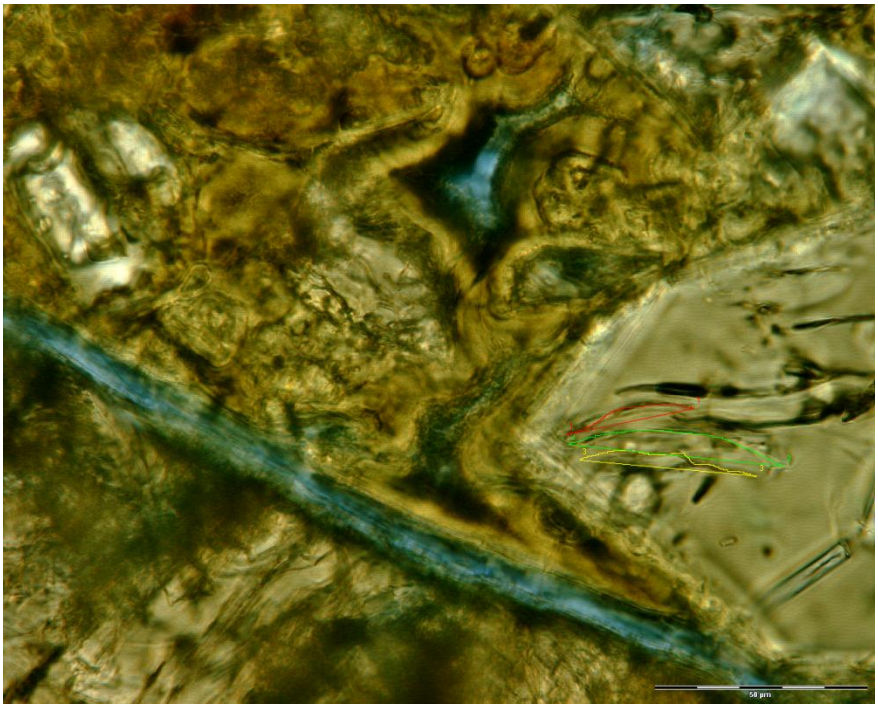

25, 103

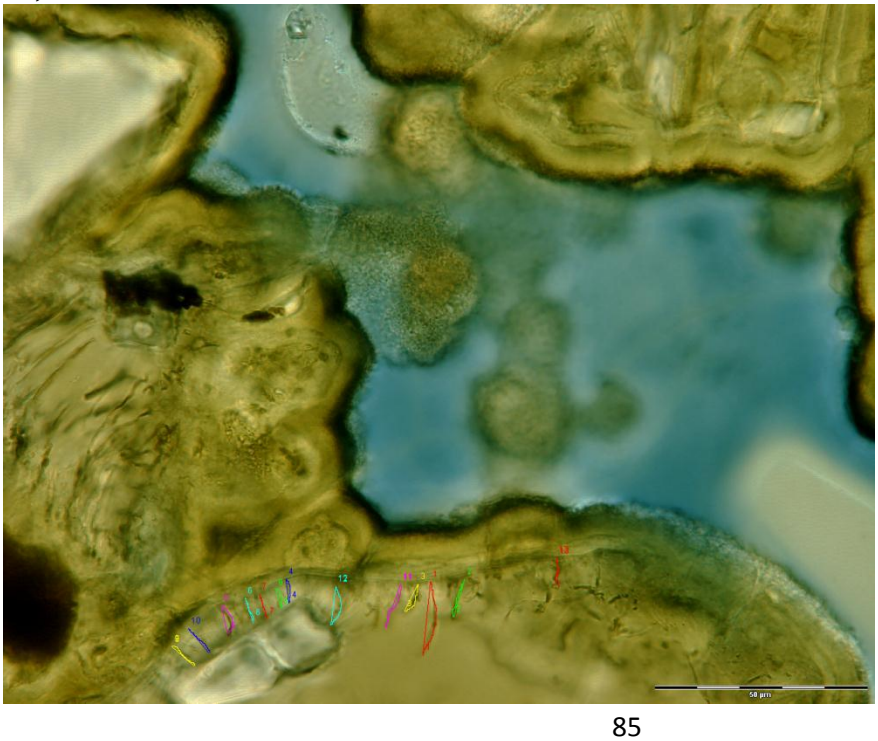

46, 101

51, 113

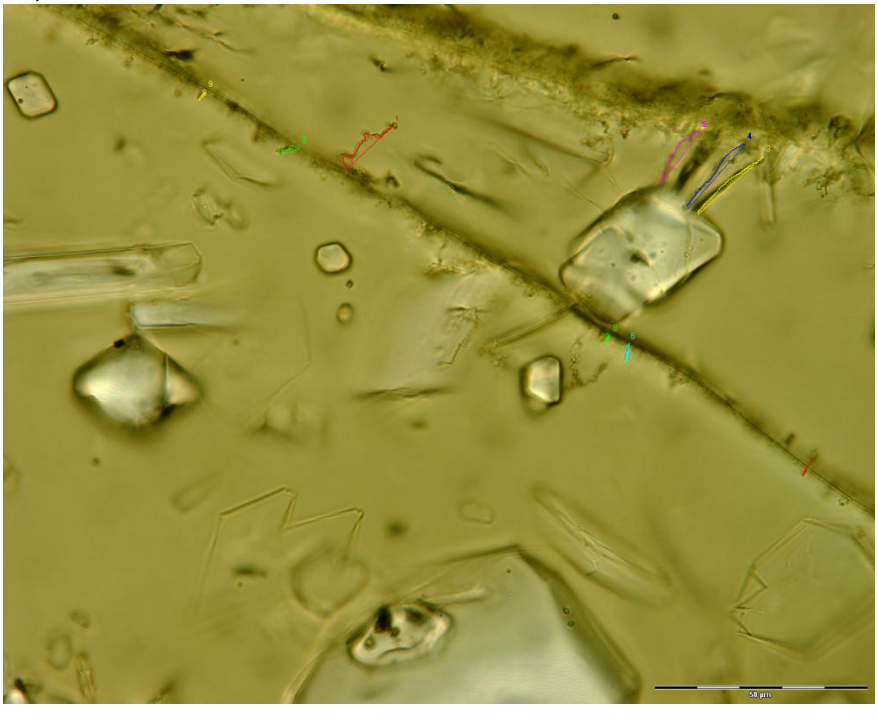

32, 120

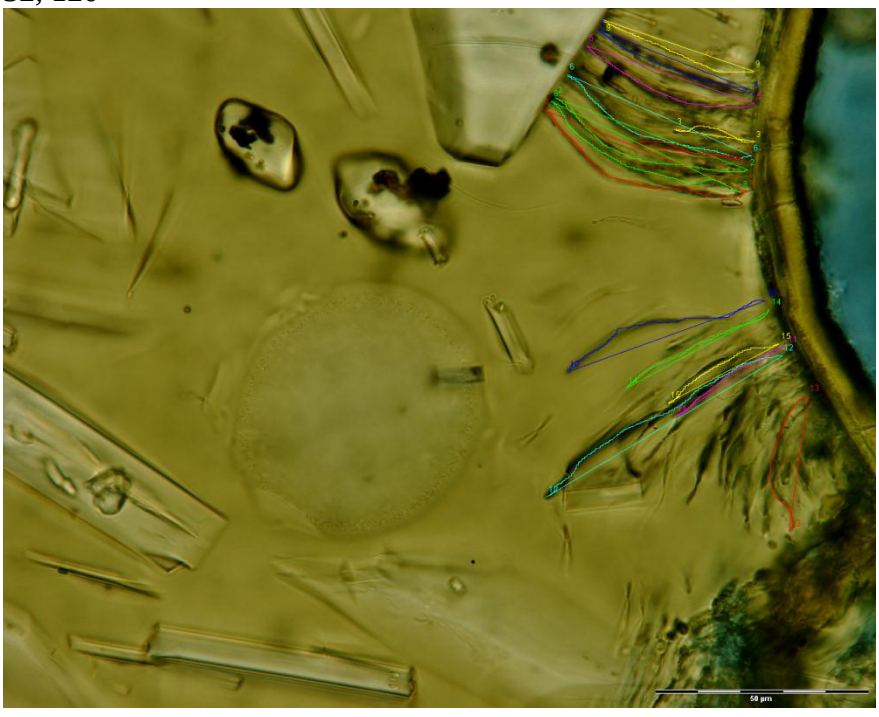

31, 118

31, 104

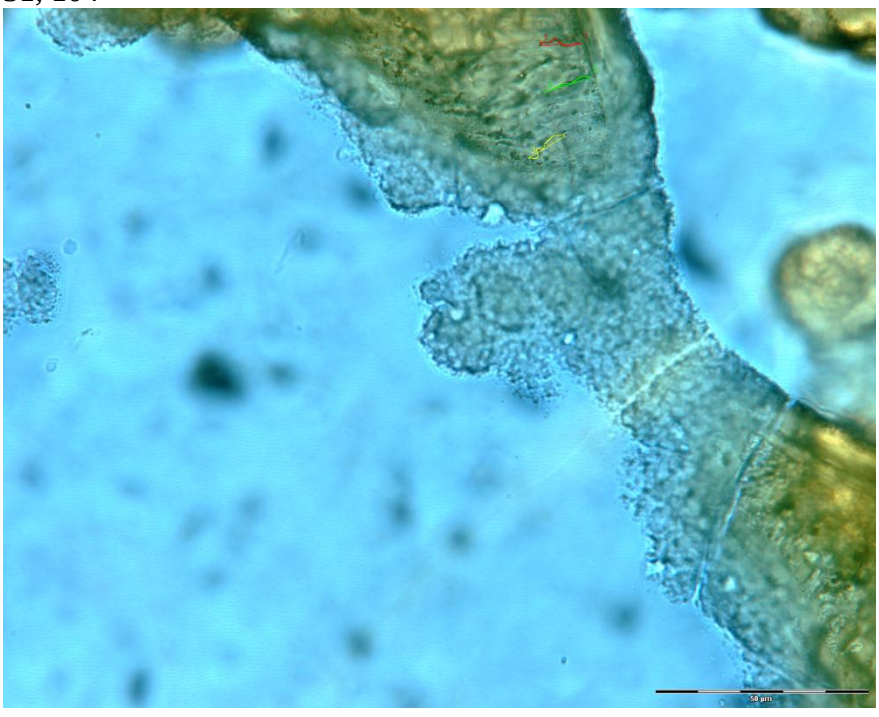

32,93

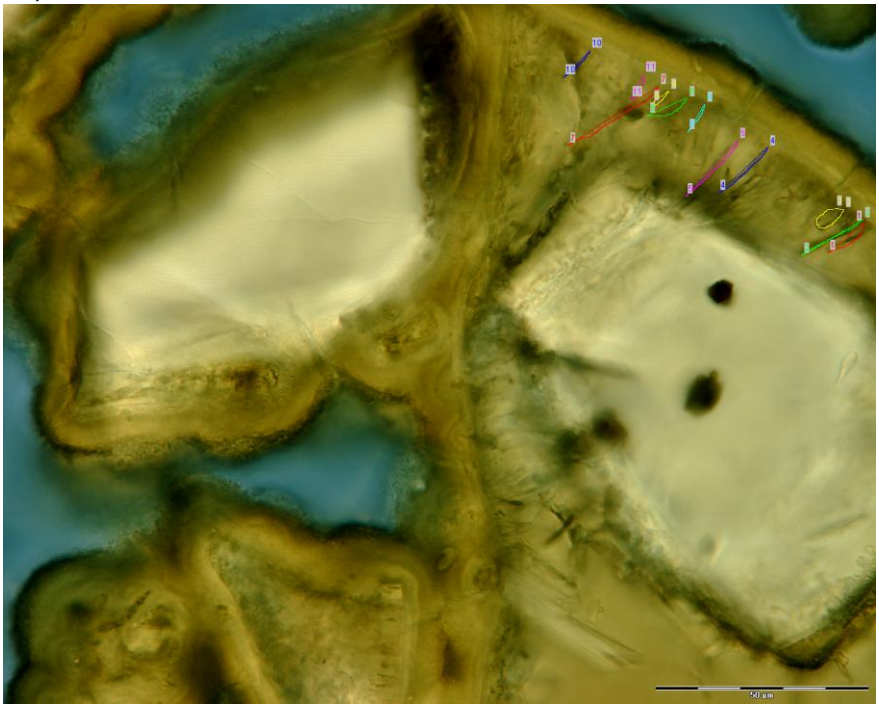

32, 103

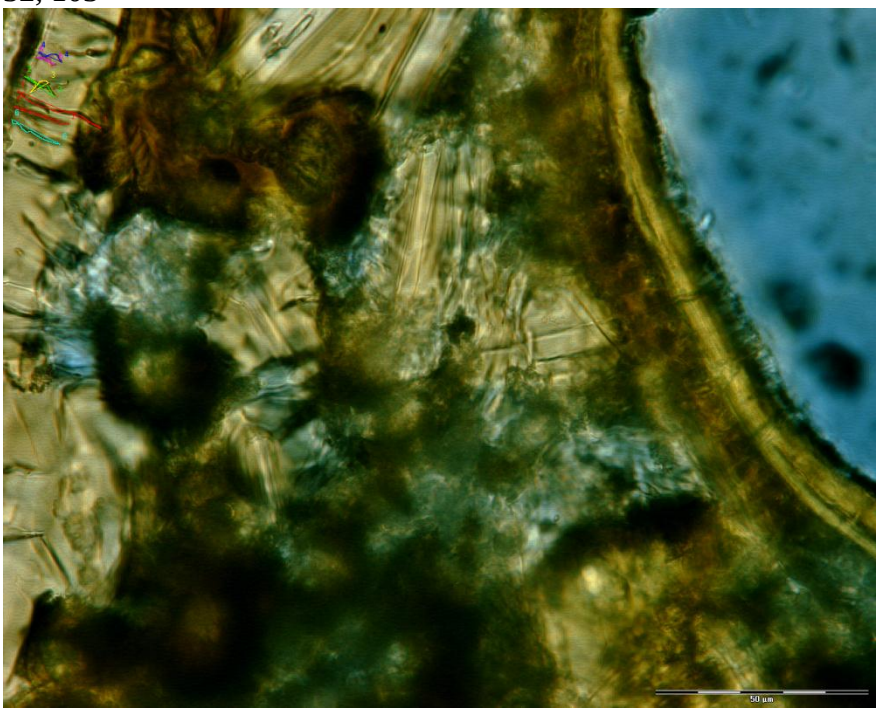

37,97

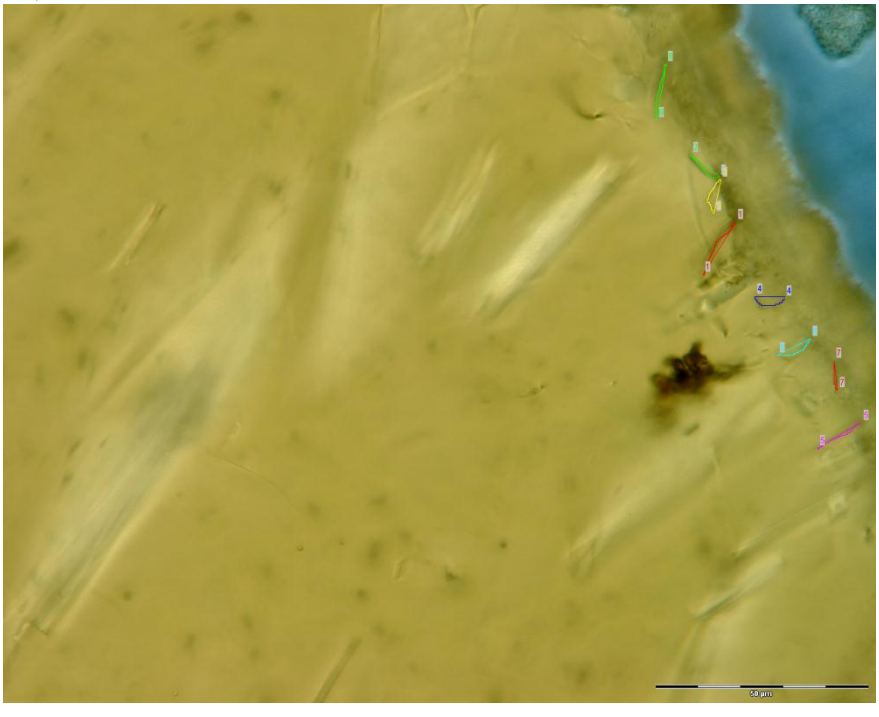

37,101

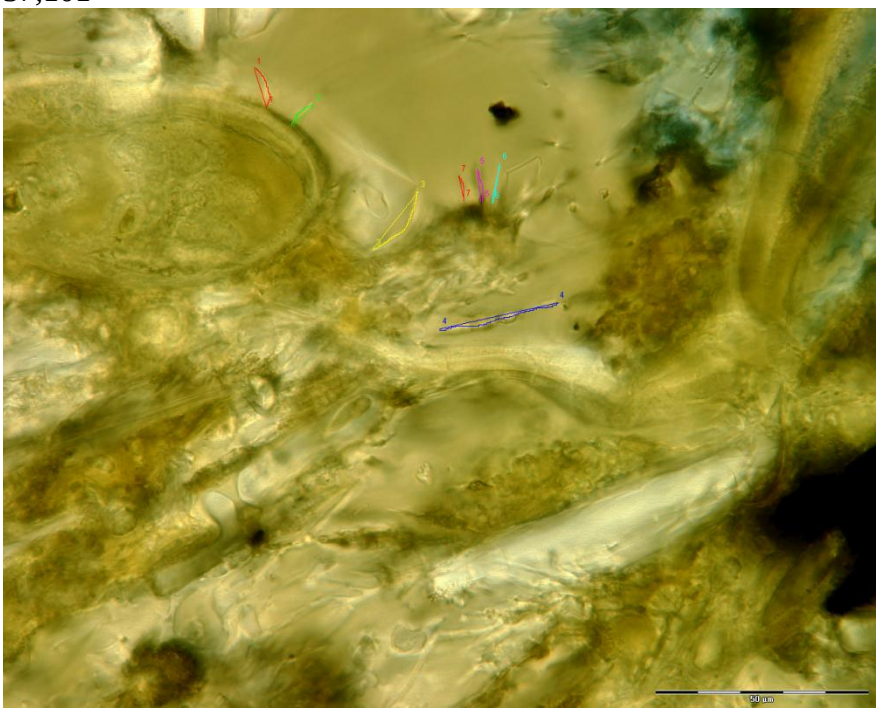

39, 90

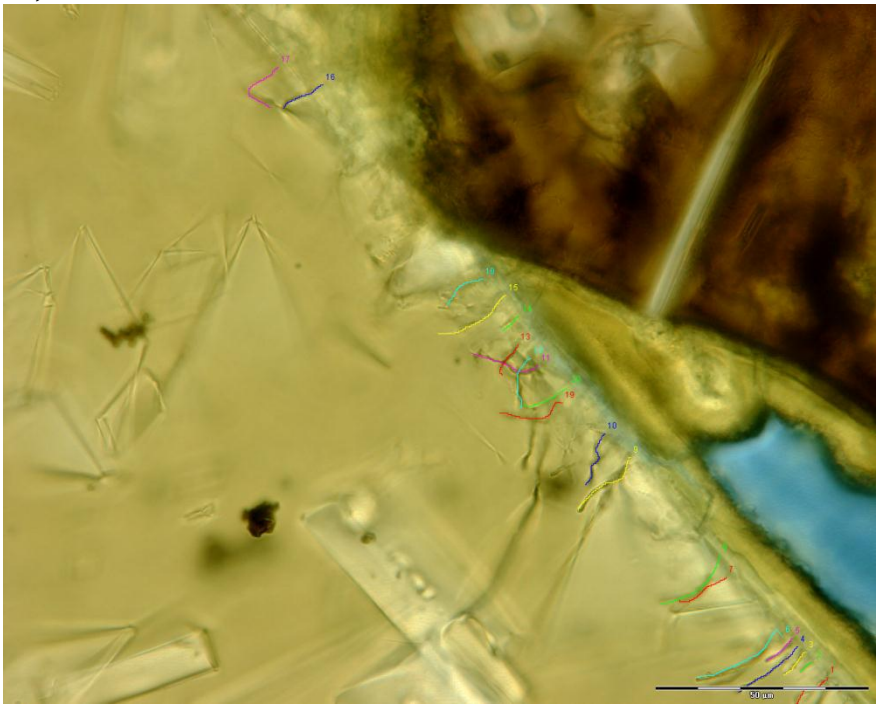

39, 117

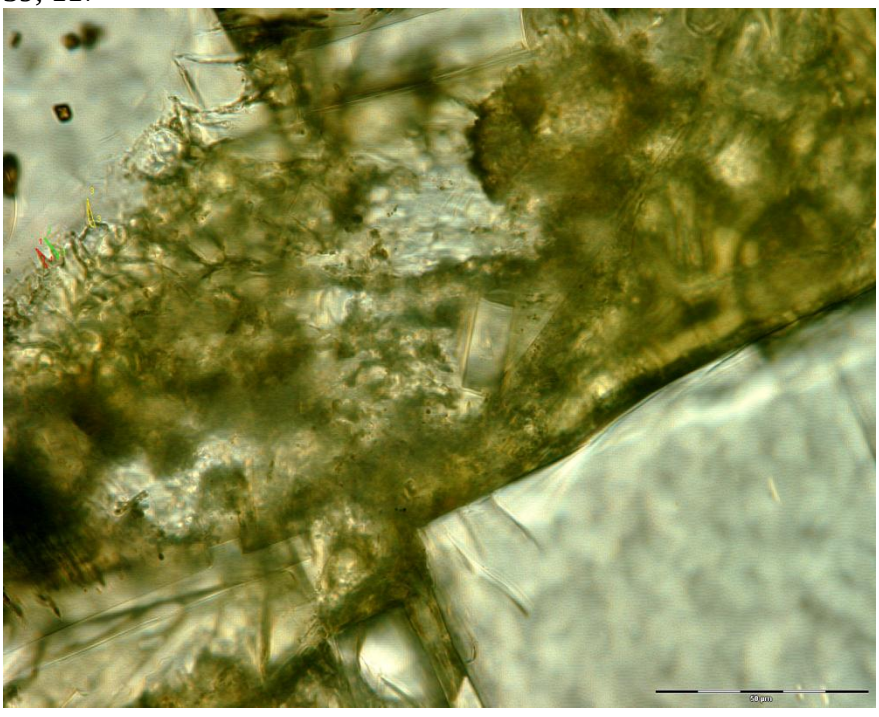

46, 109

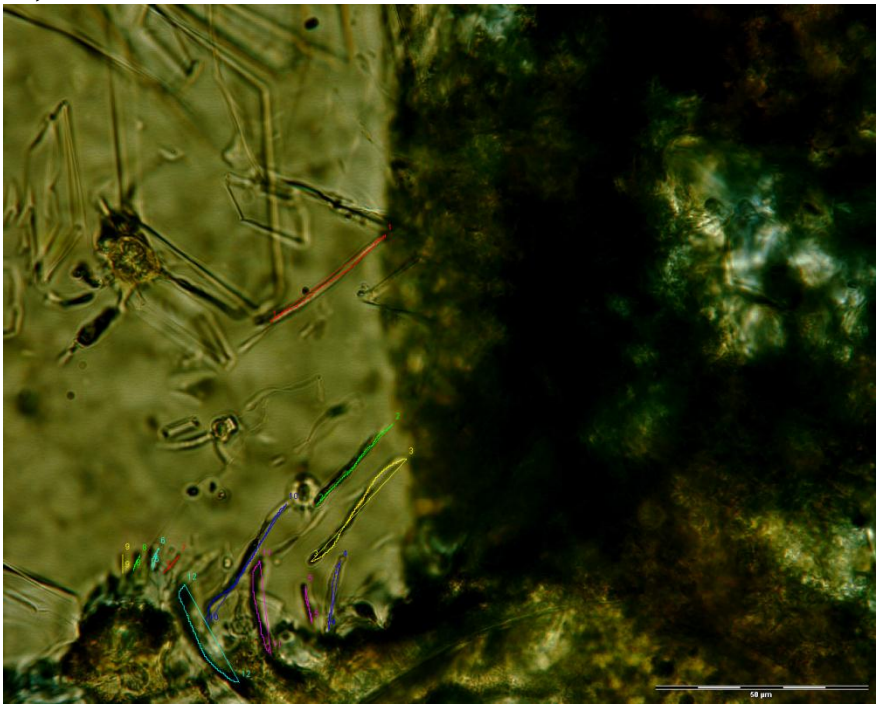

49, 112

51,108

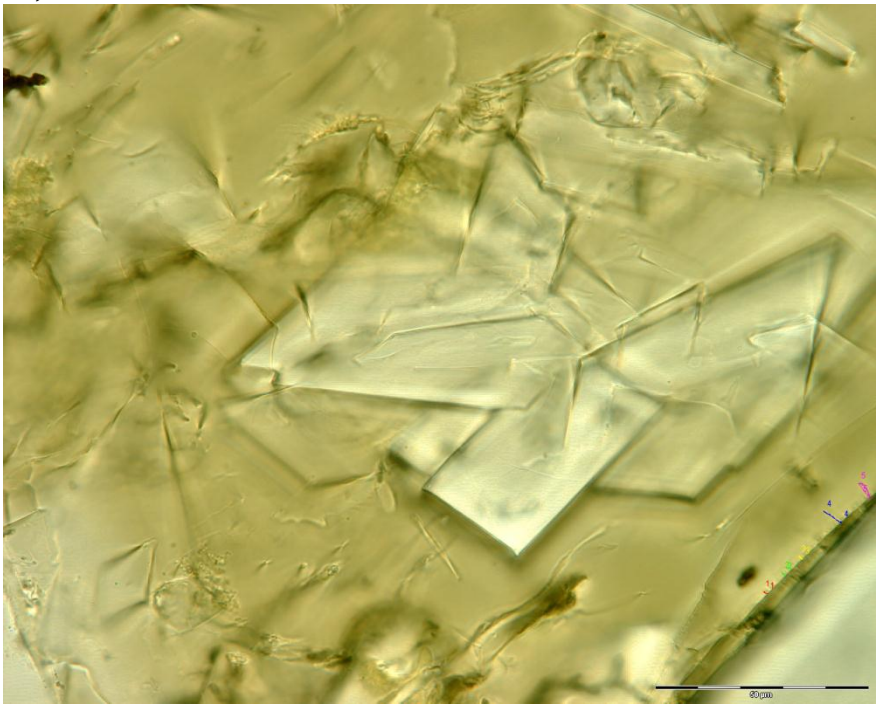

Location:

51,117

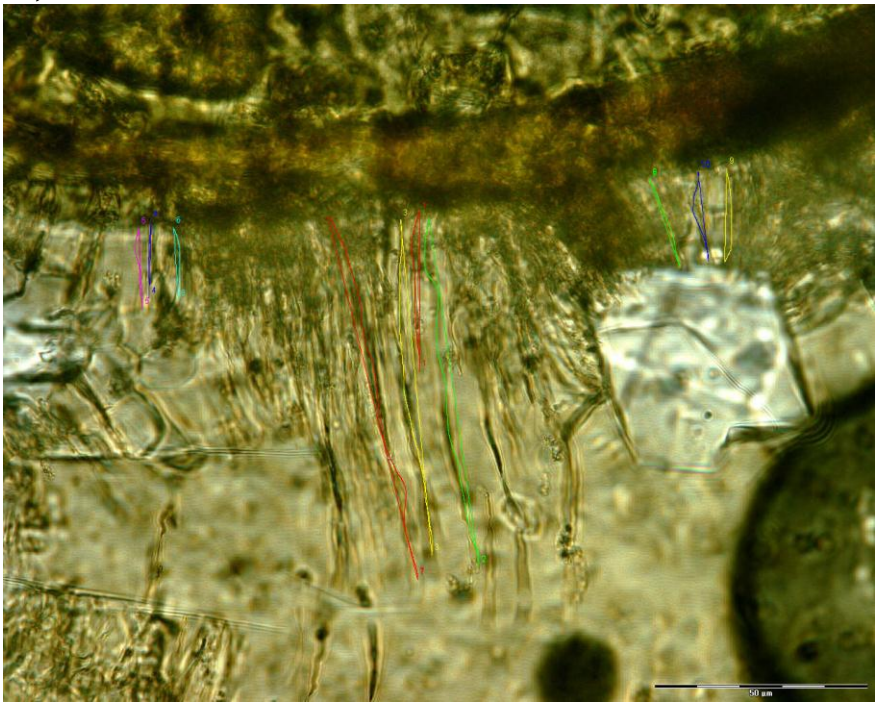

30,109

47,106,d

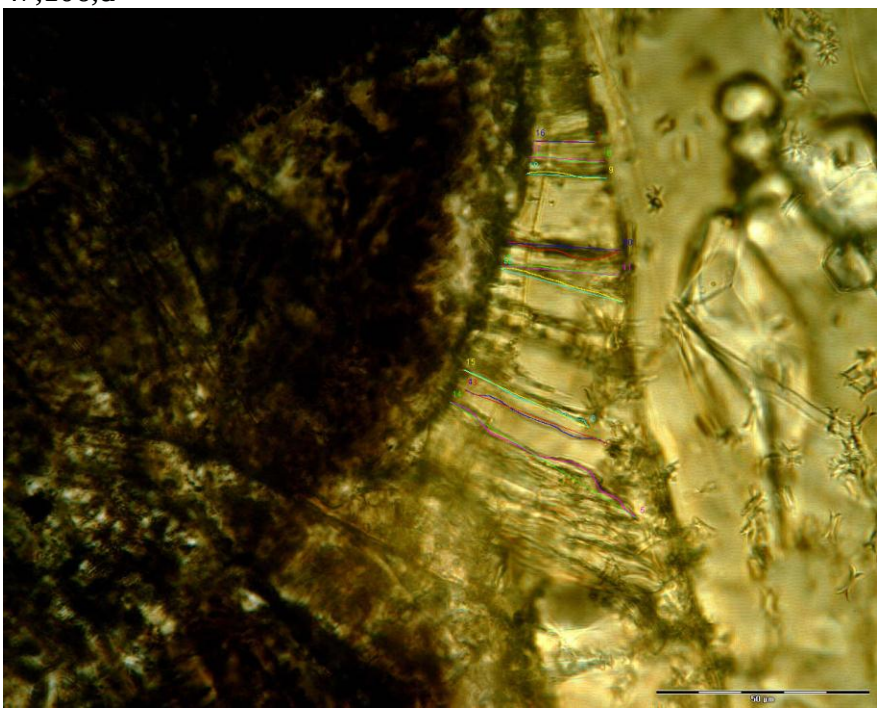

47,106,c

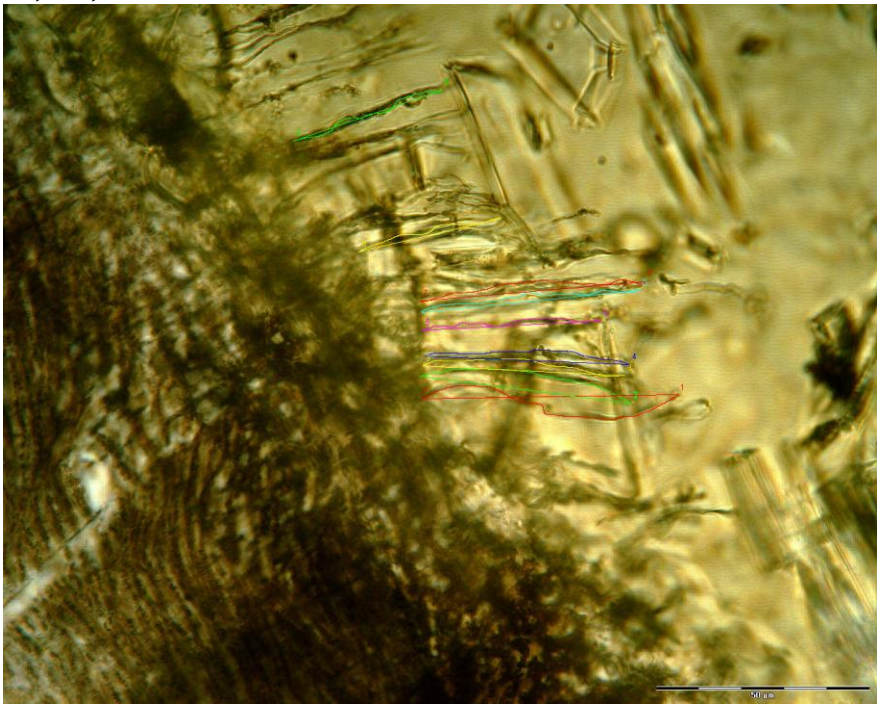

47,106,b

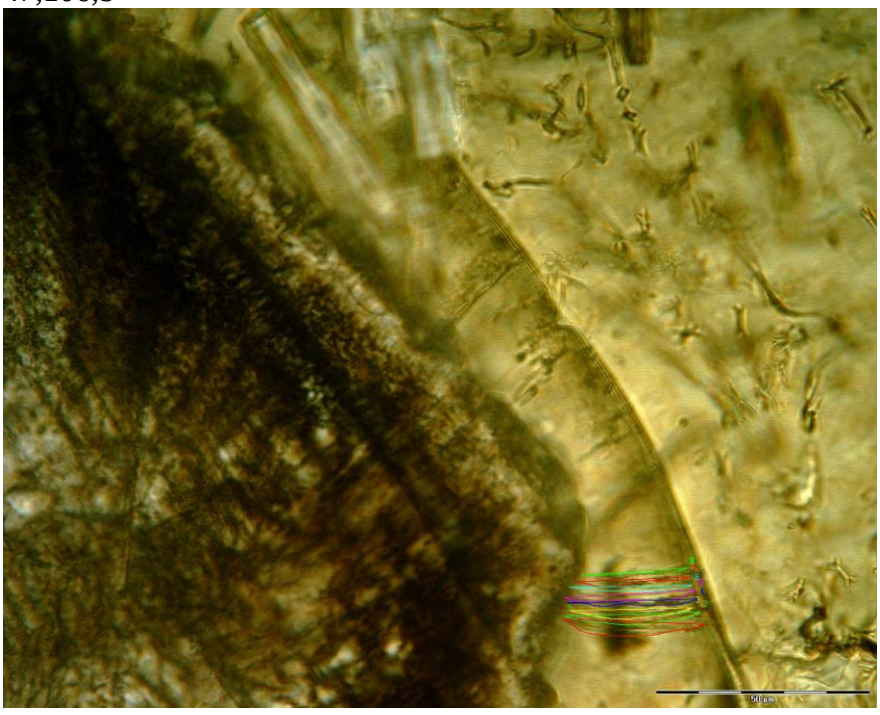

47,106

28,110

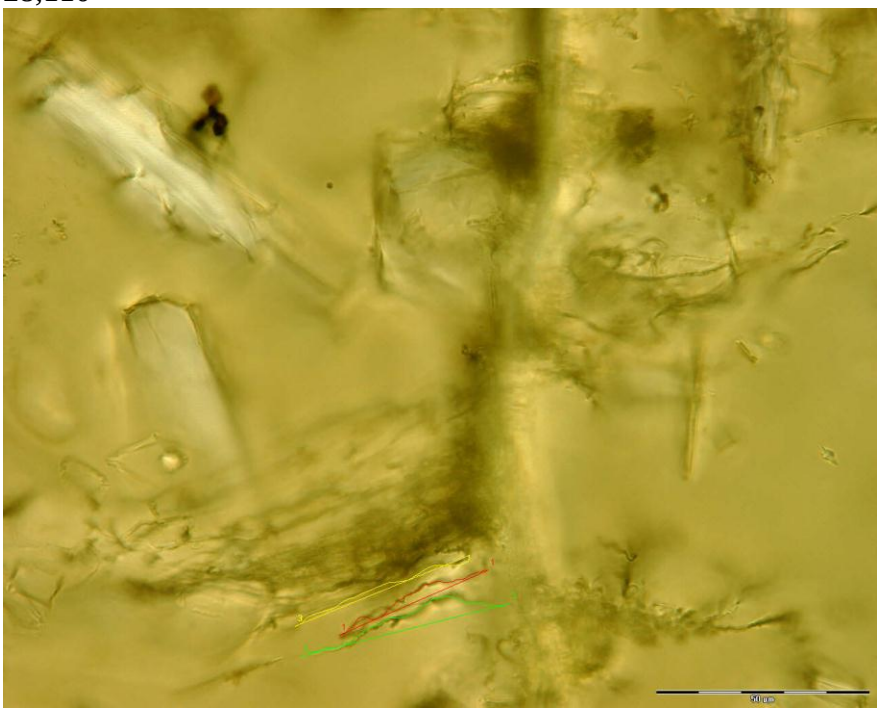

43,118

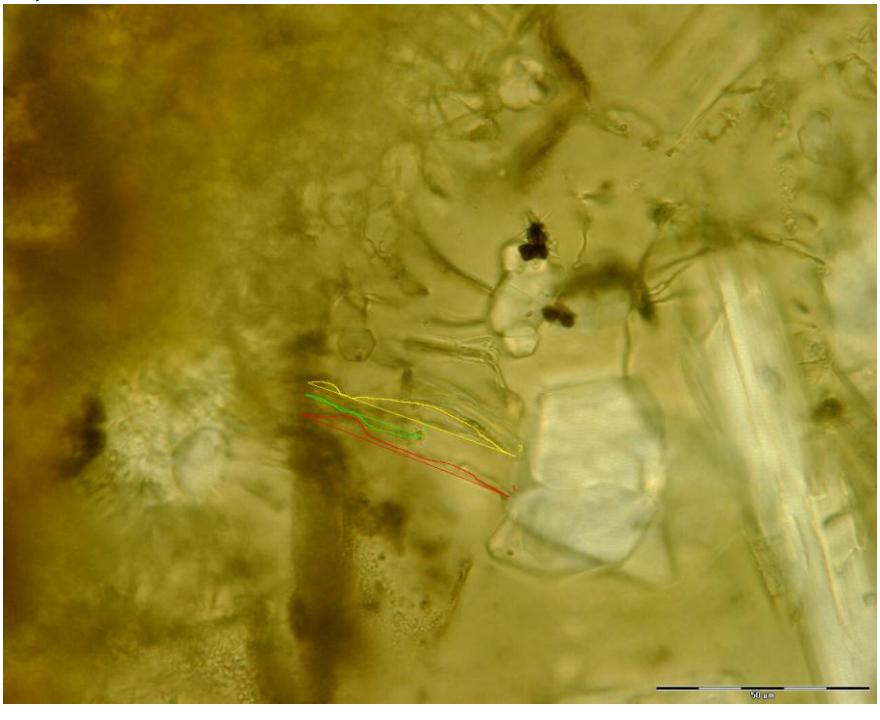

30,106

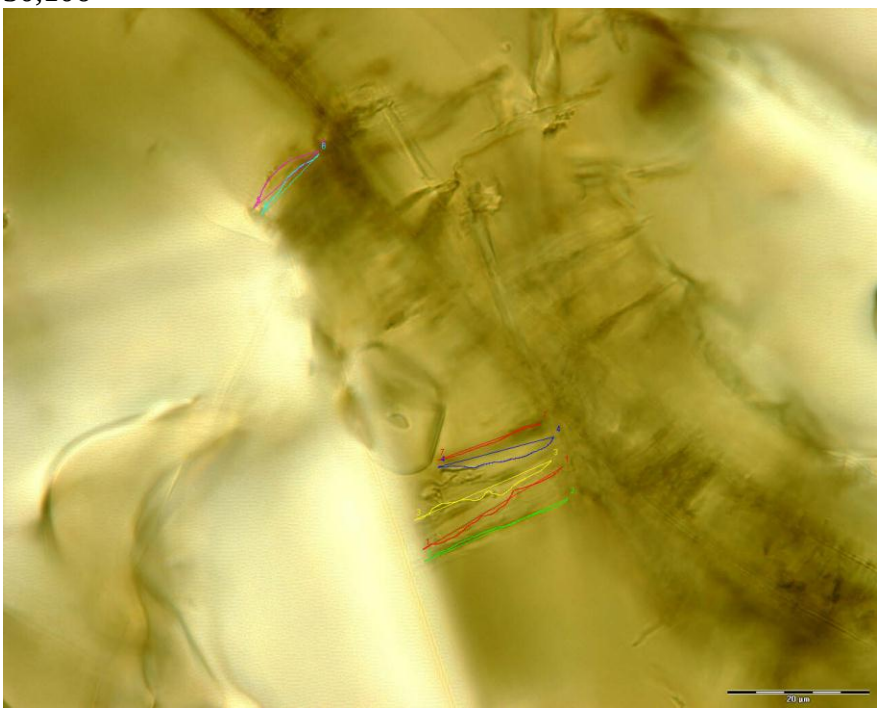

40,118

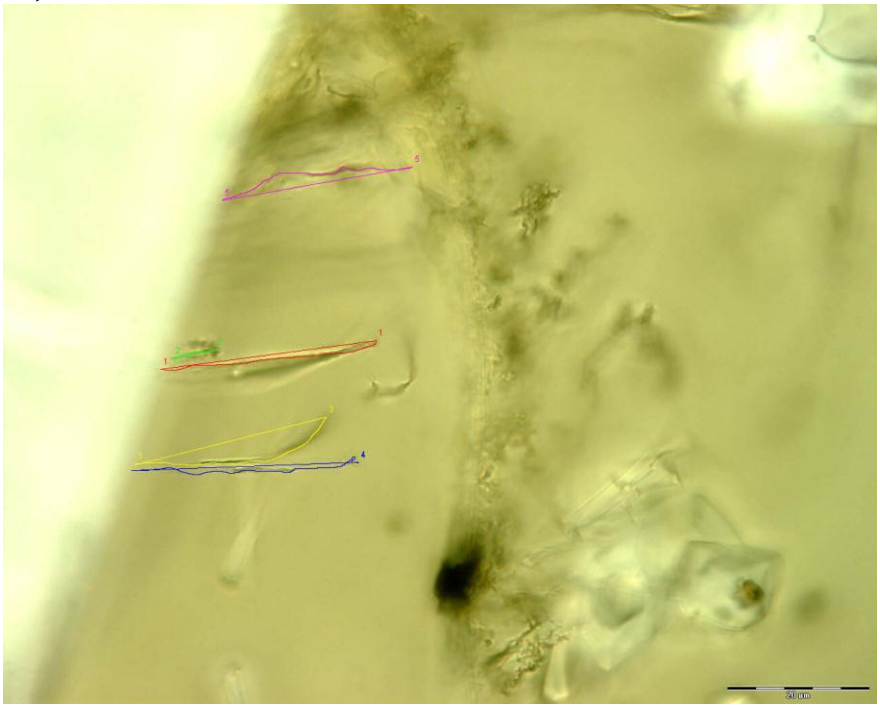

27,108

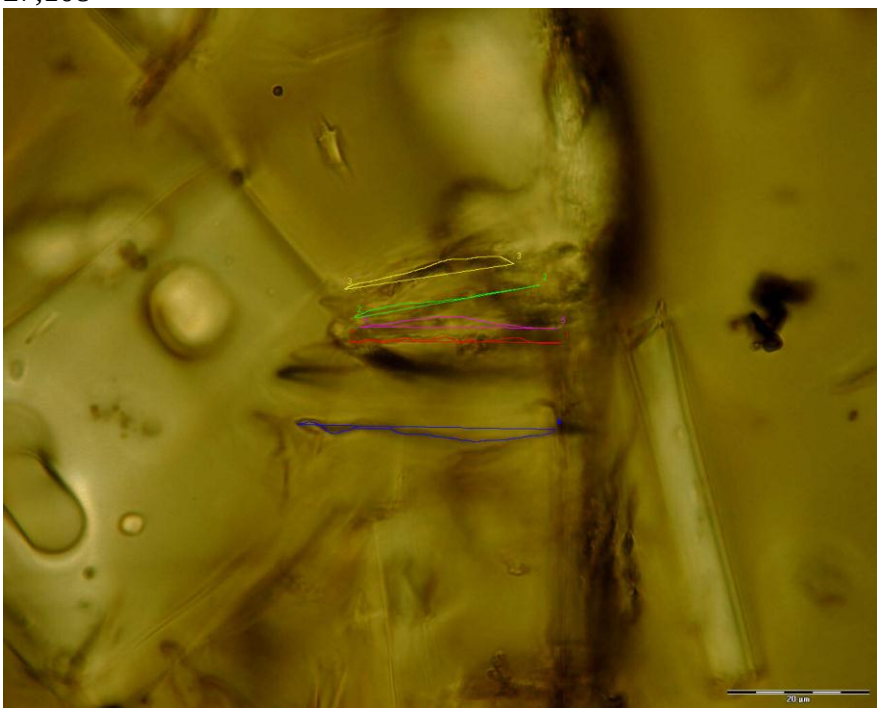

39,108

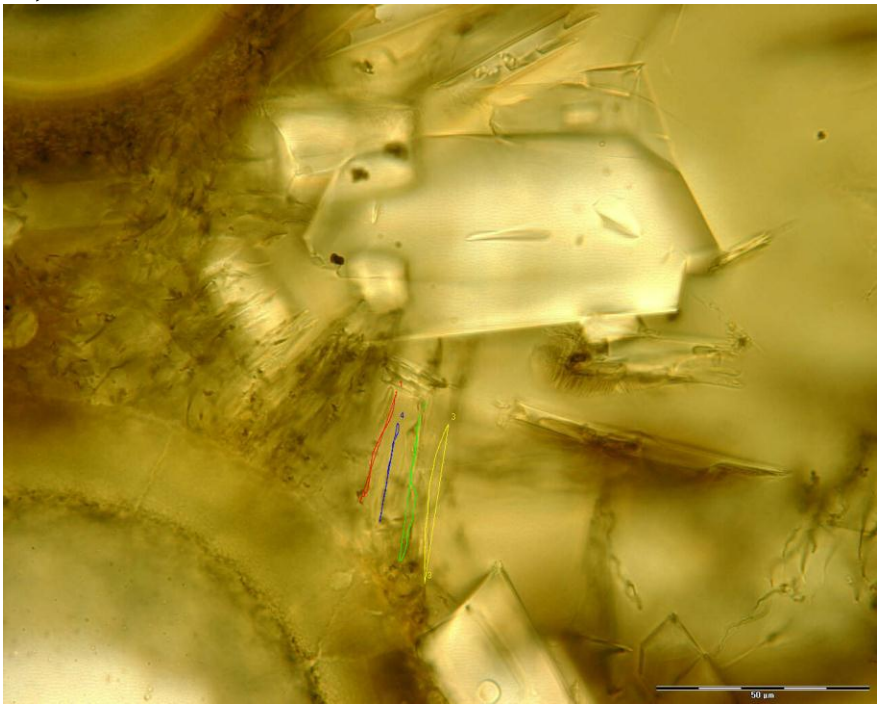

27,118

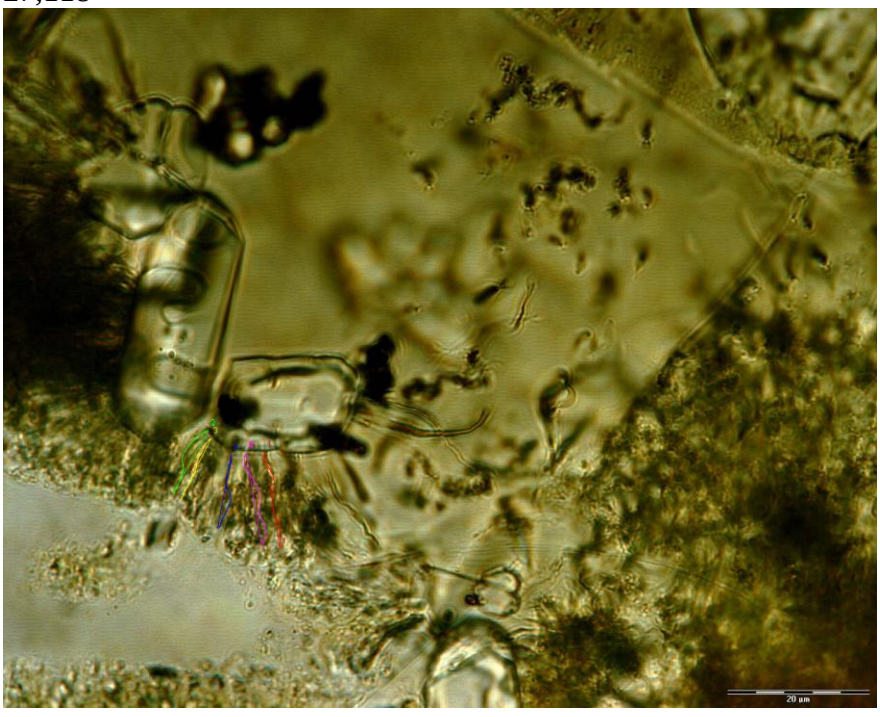

29,116

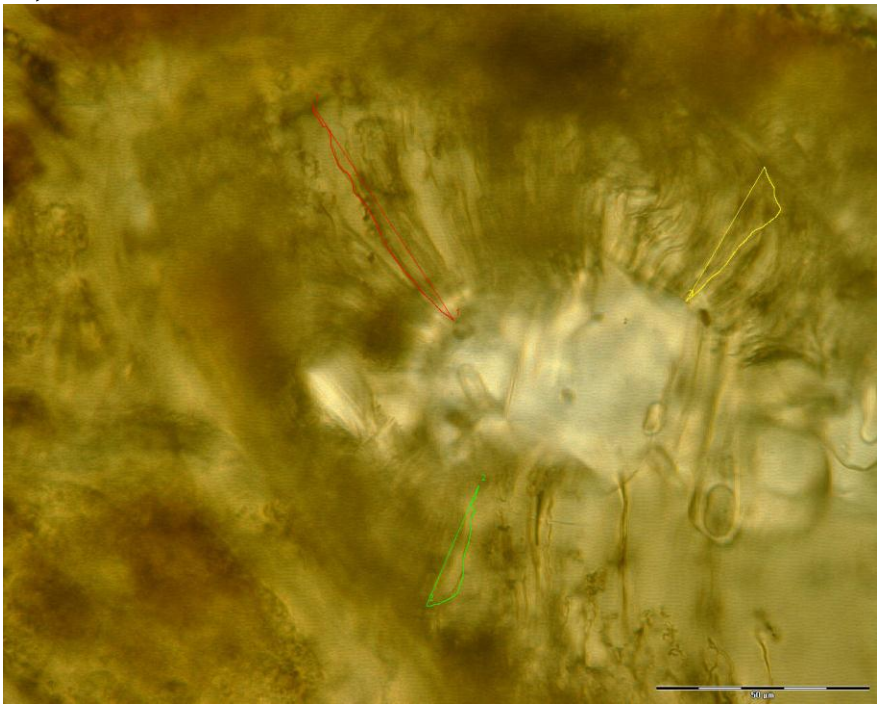

52,115

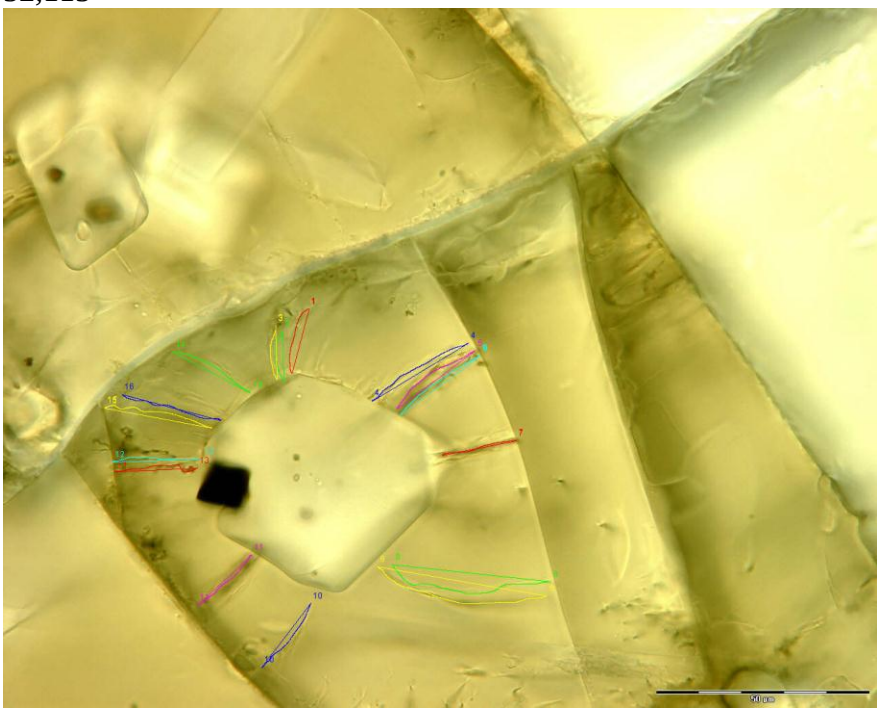

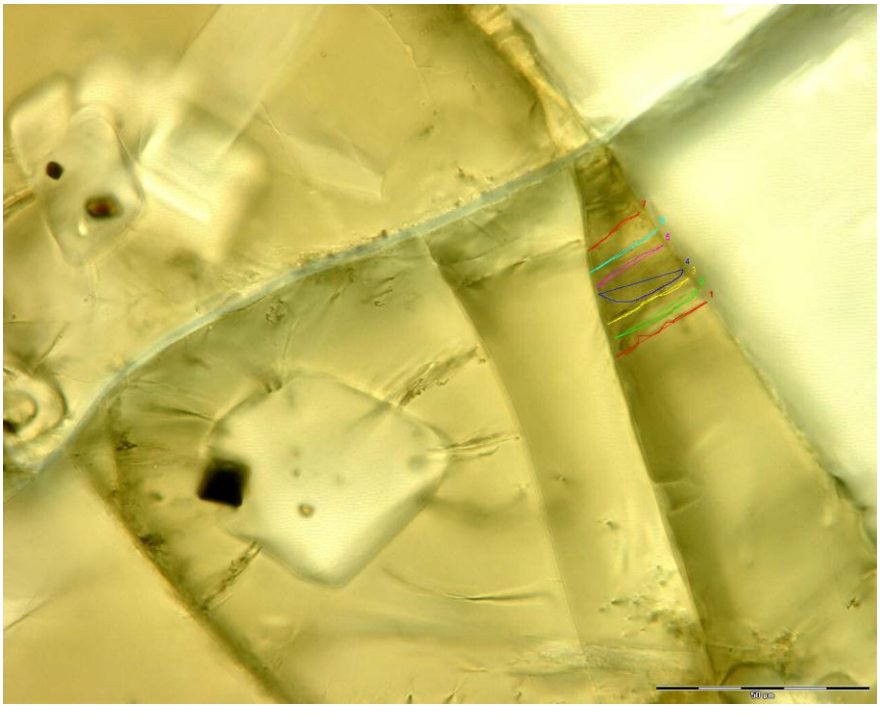

Location:

22,109

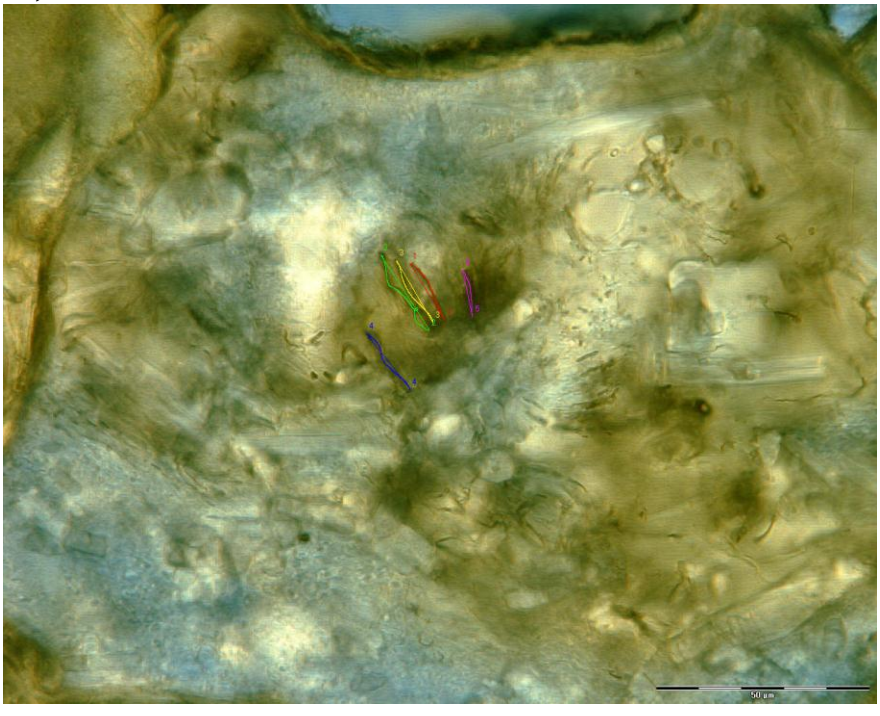

30,110

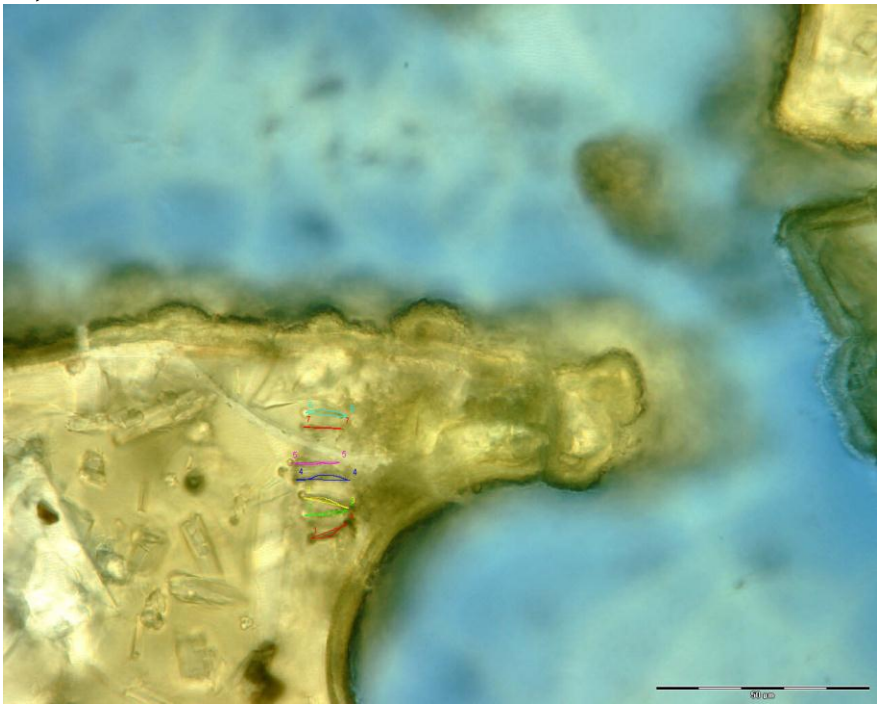

31,109,b

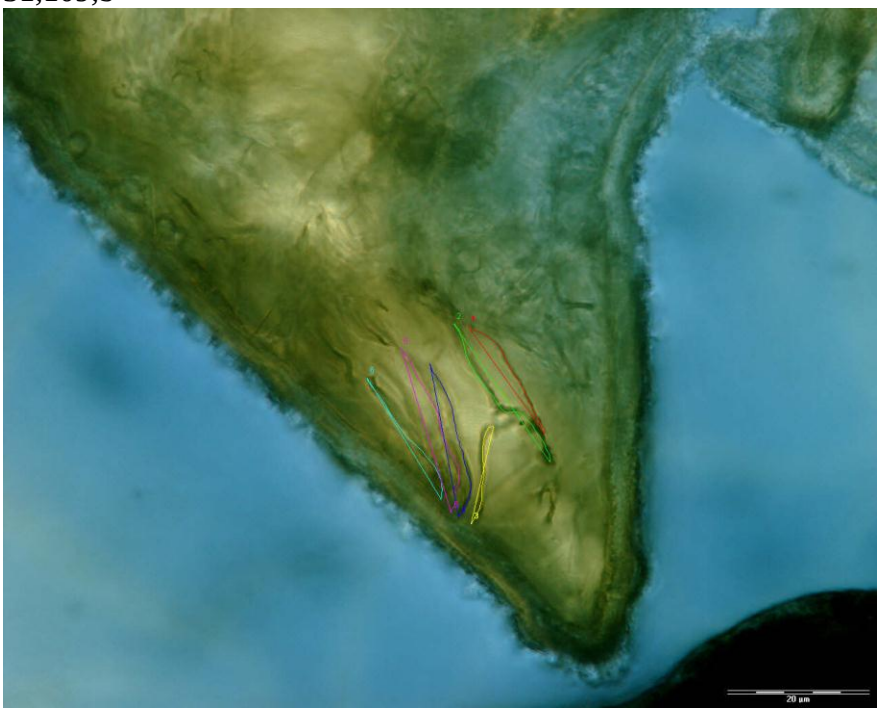

31,109

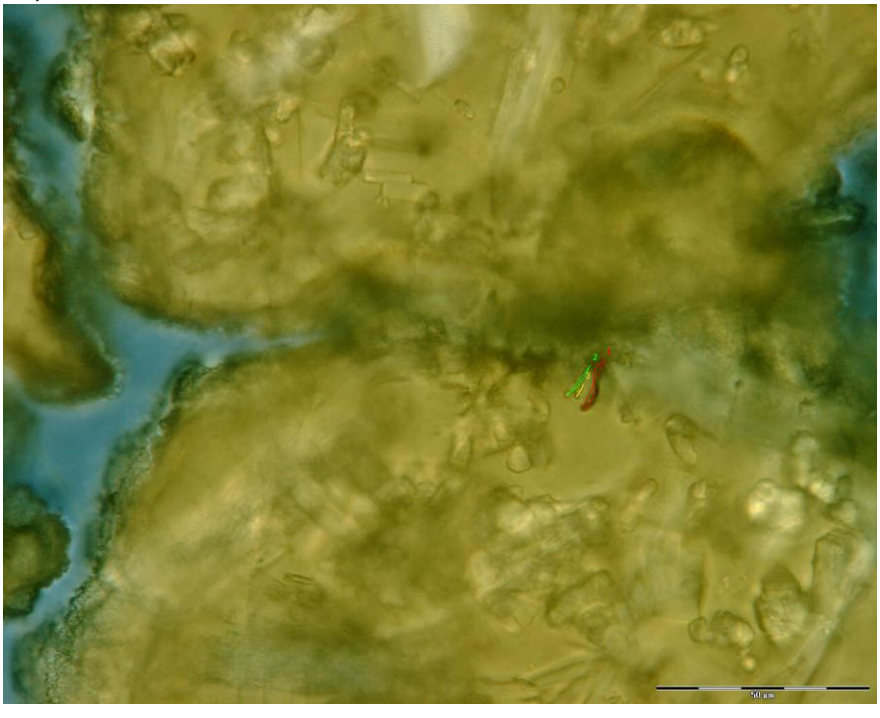

33,109

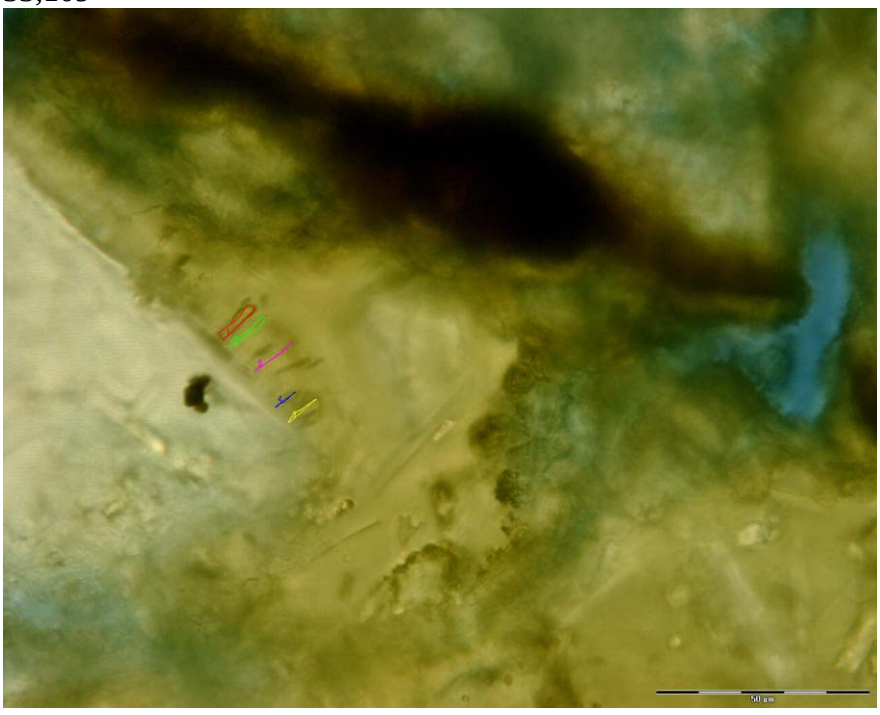

38,111

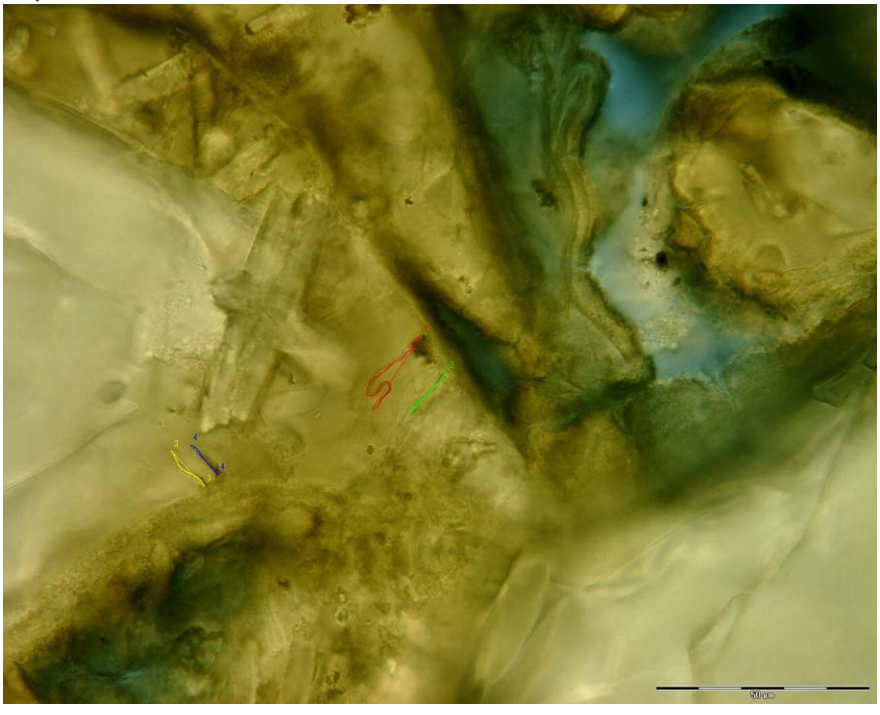

38.5,111

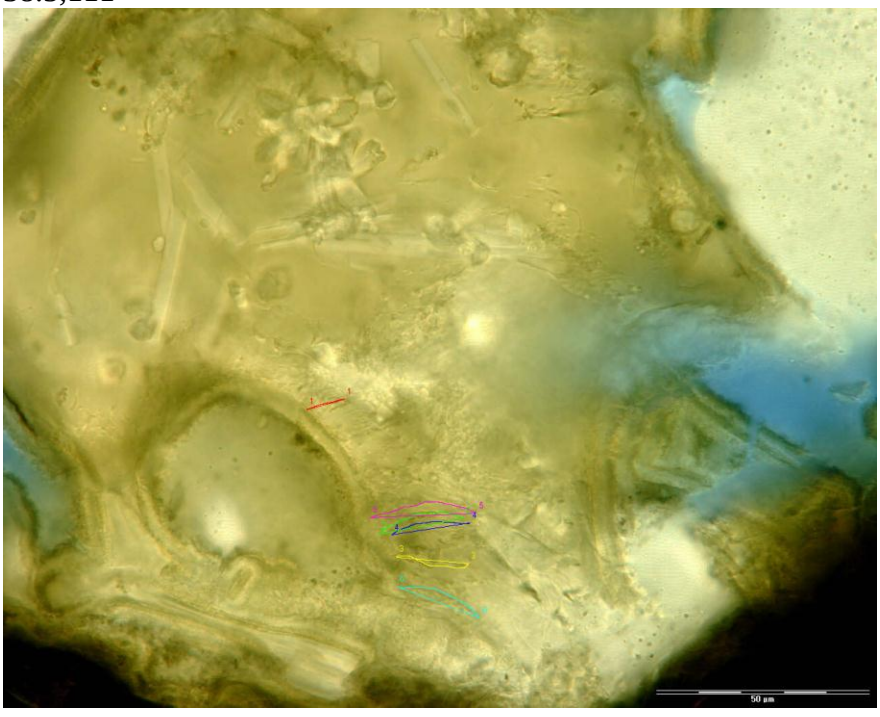

31,101

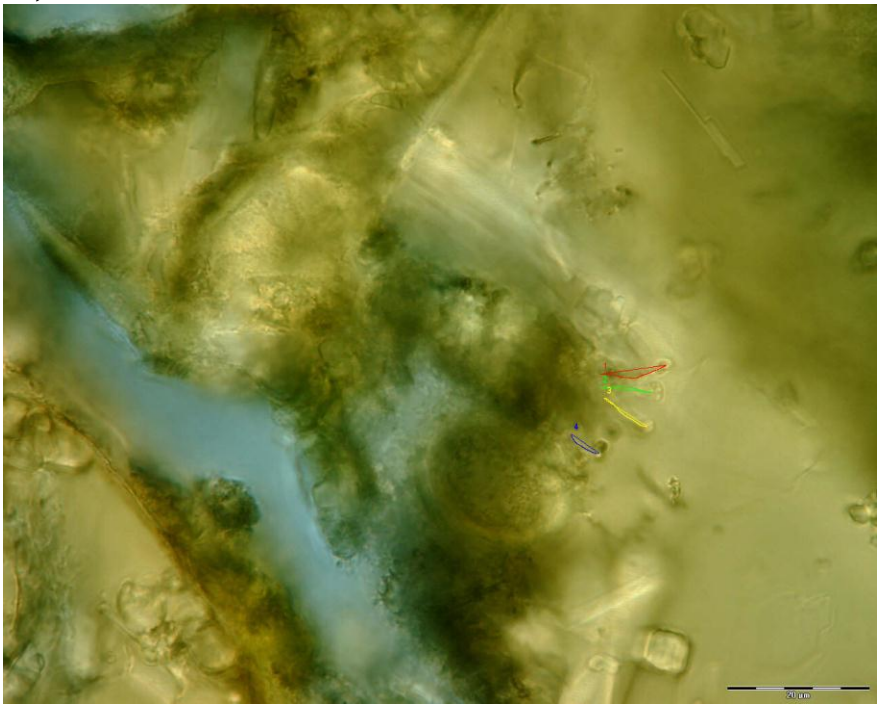

51,109

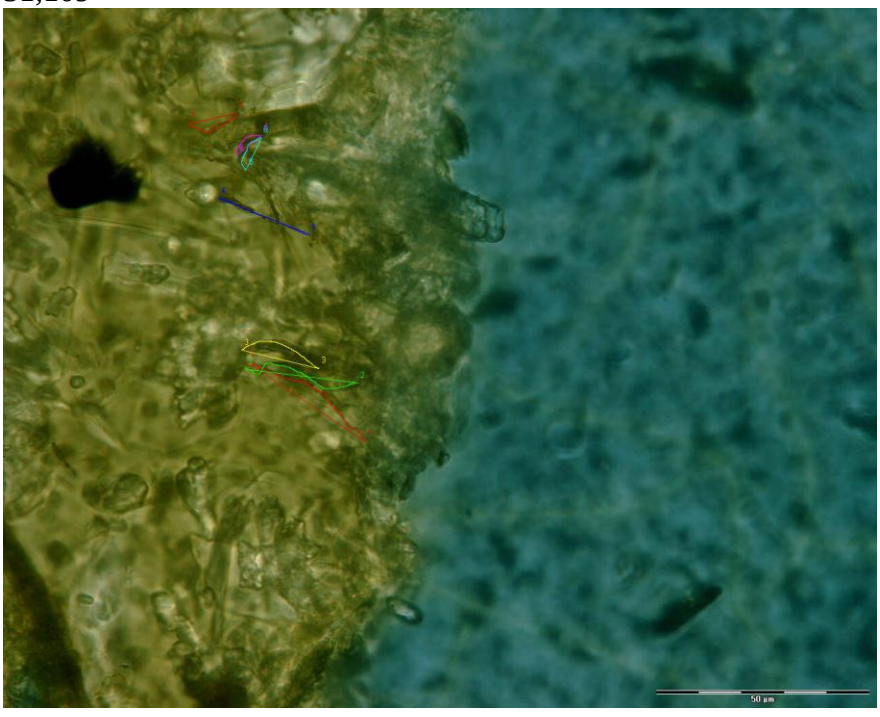

28,108,b

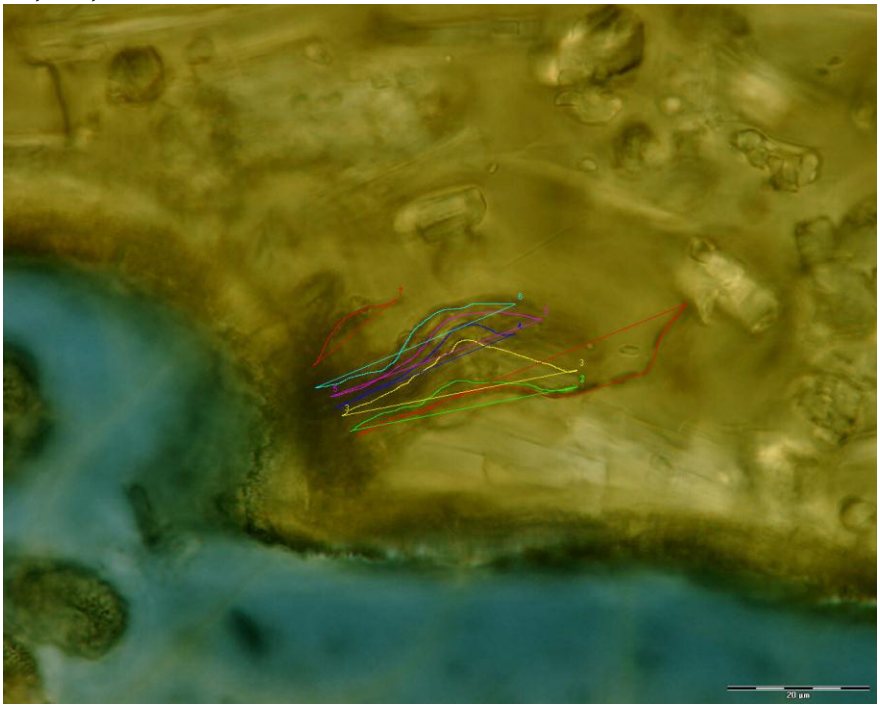

28,108,c

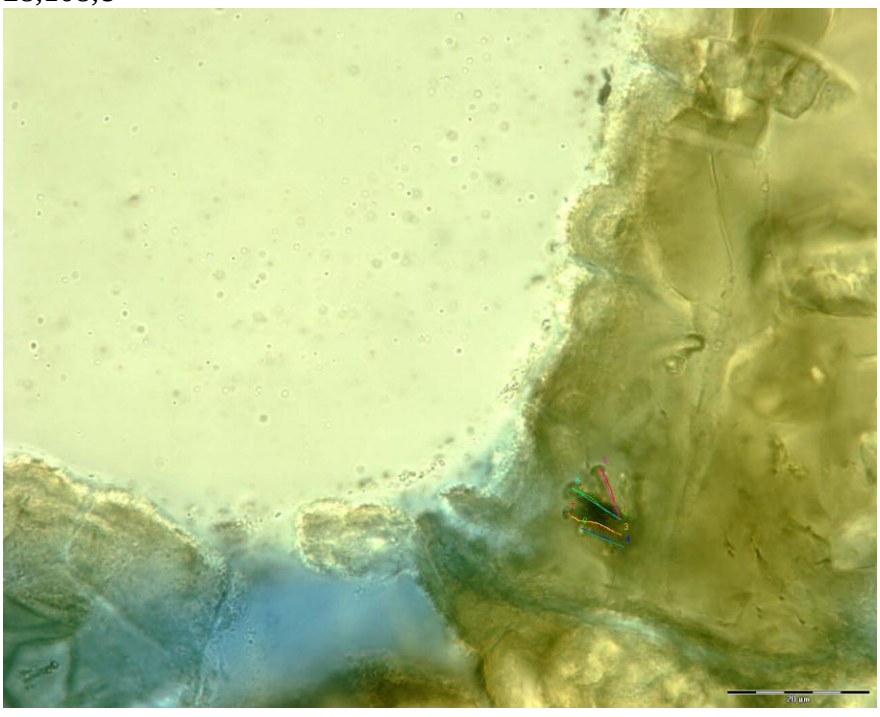

28,108

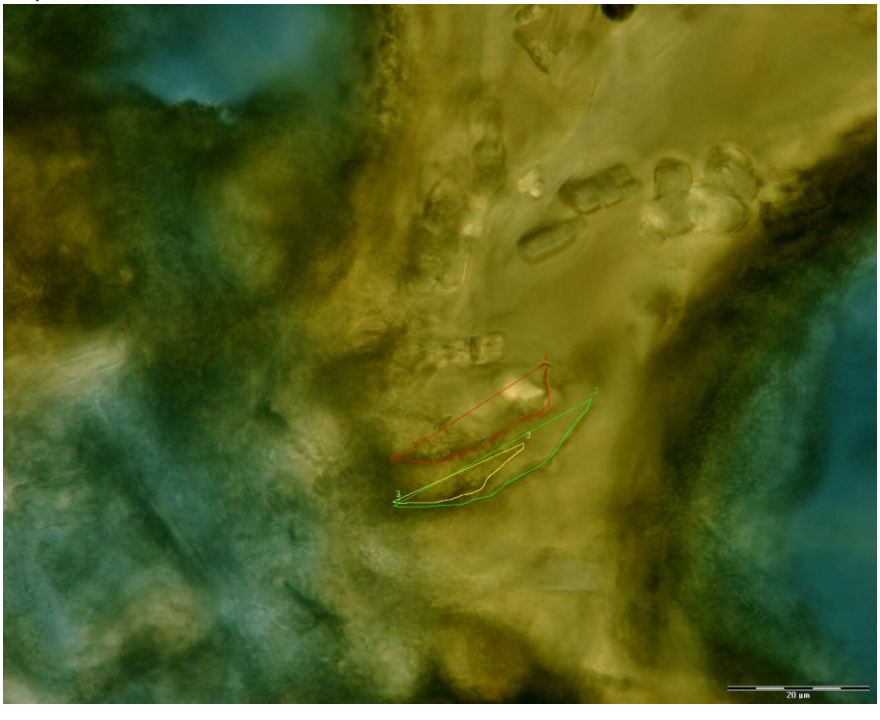

Location:

21,109

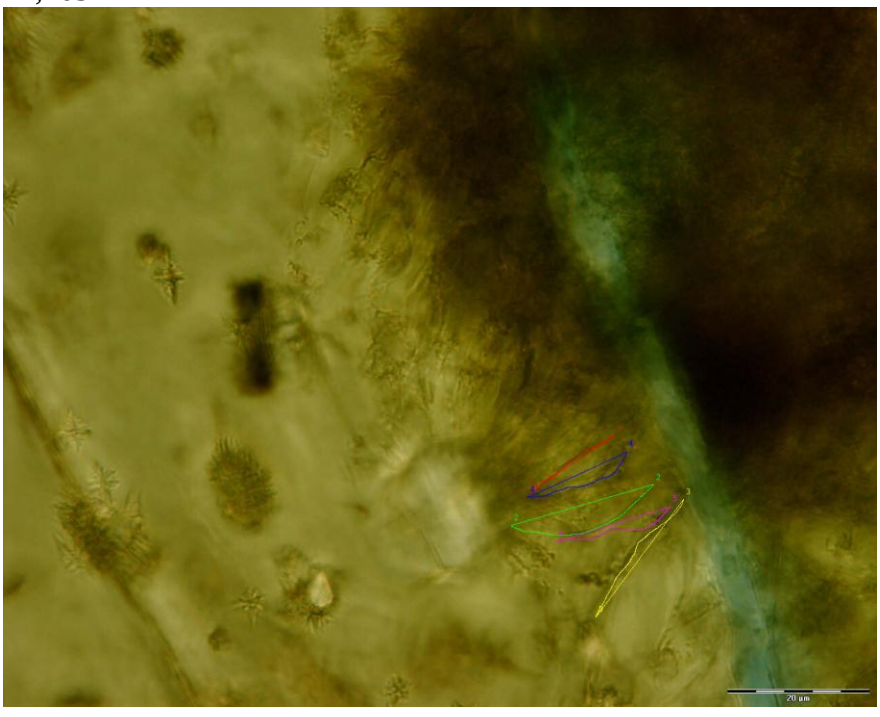

21,110,c

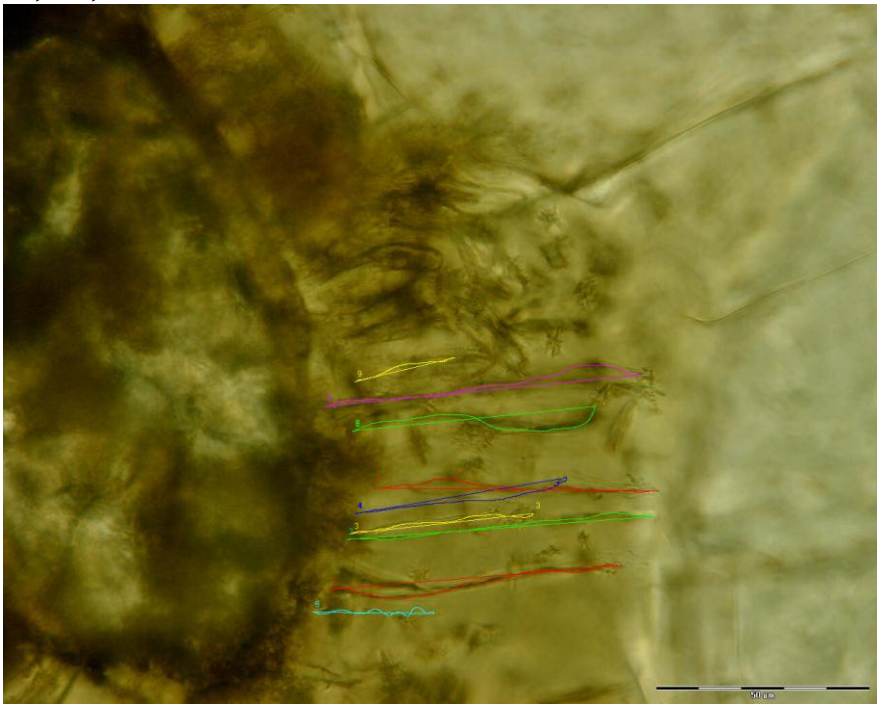

21,110,b

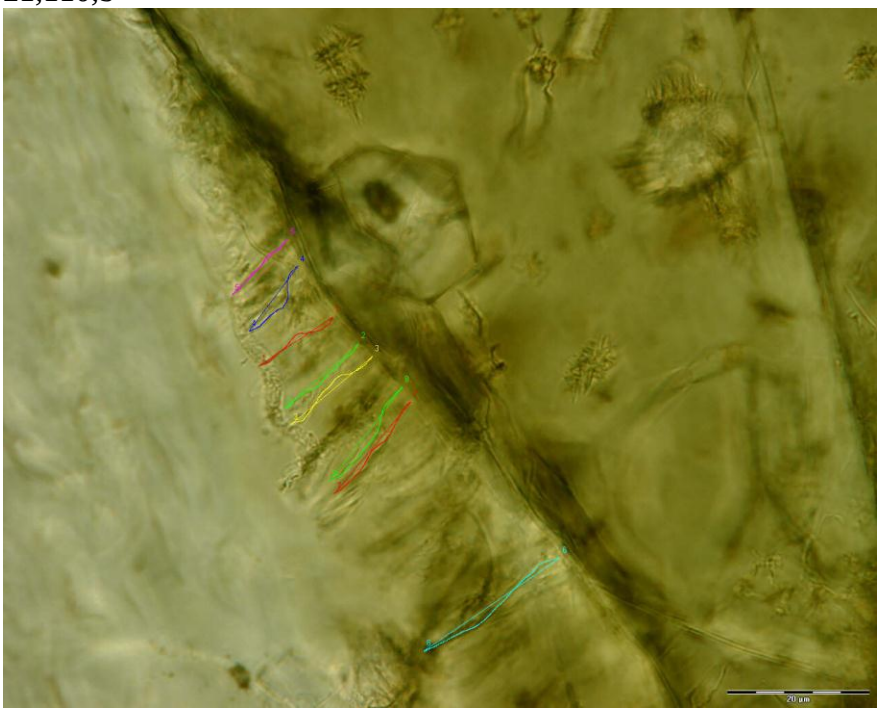

21,110

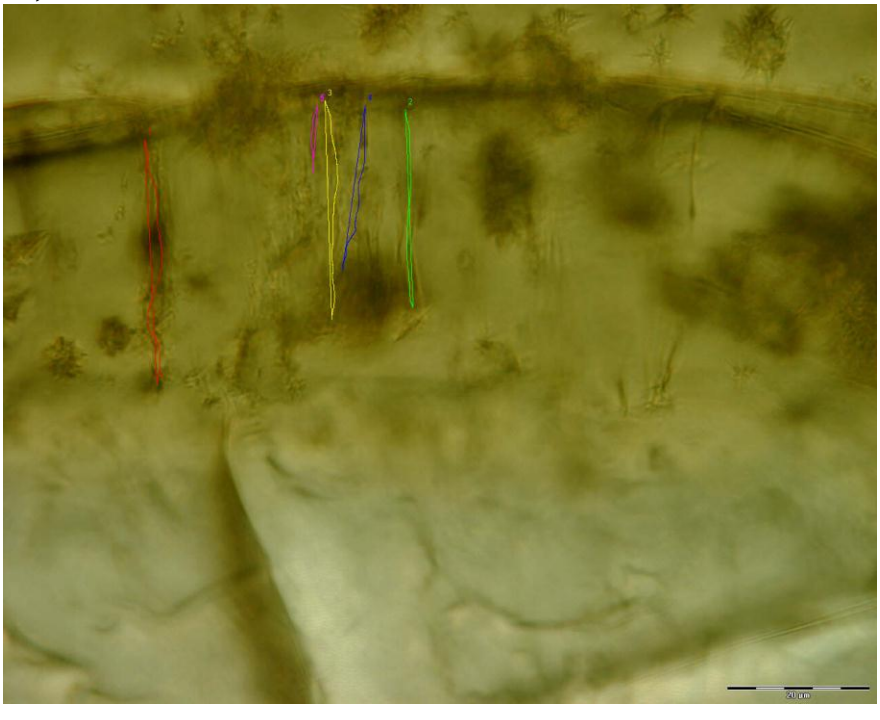

26,109

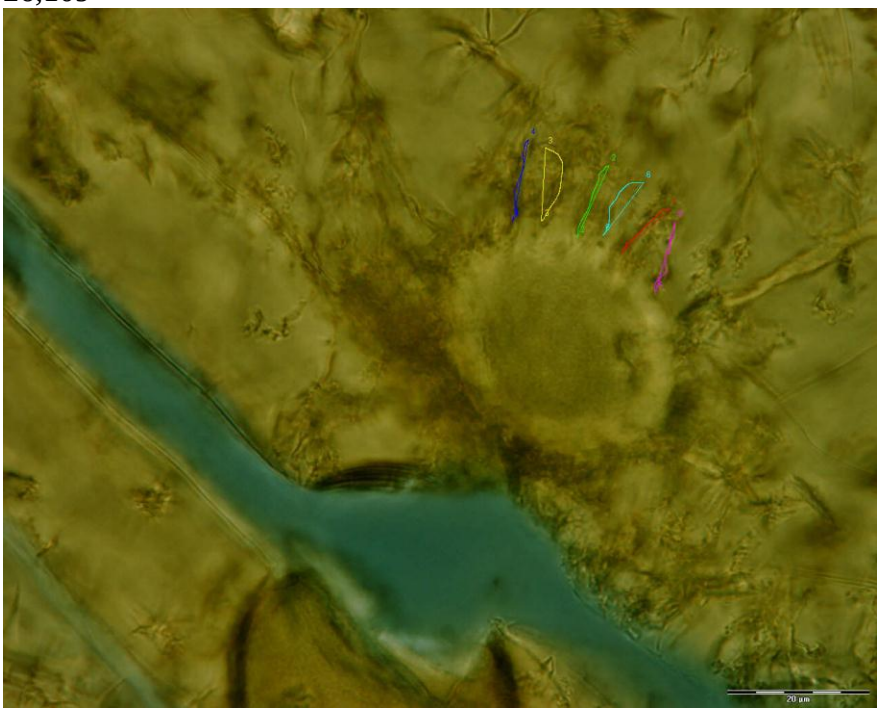

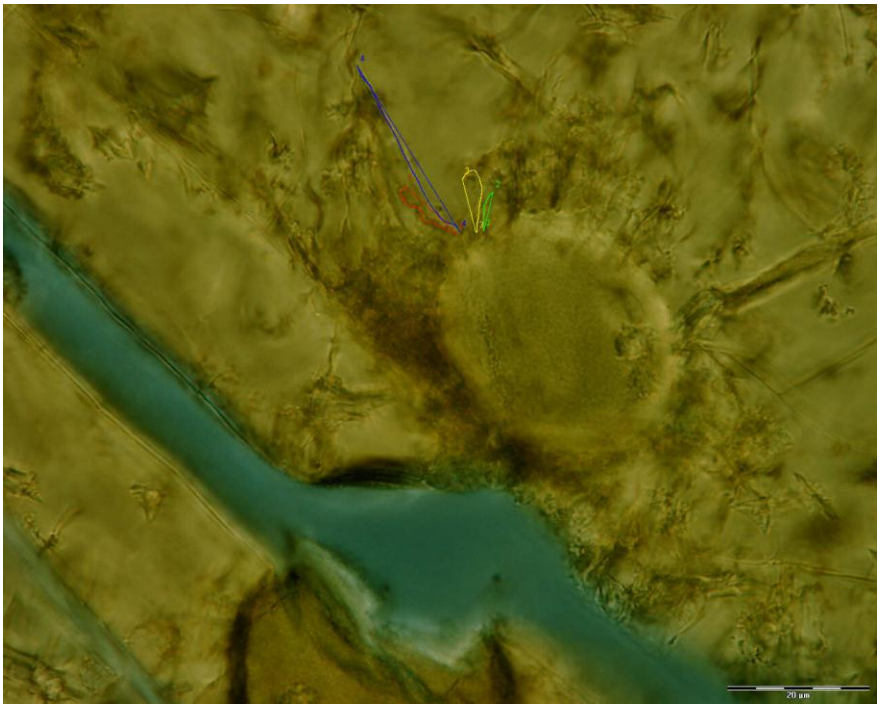

25,108

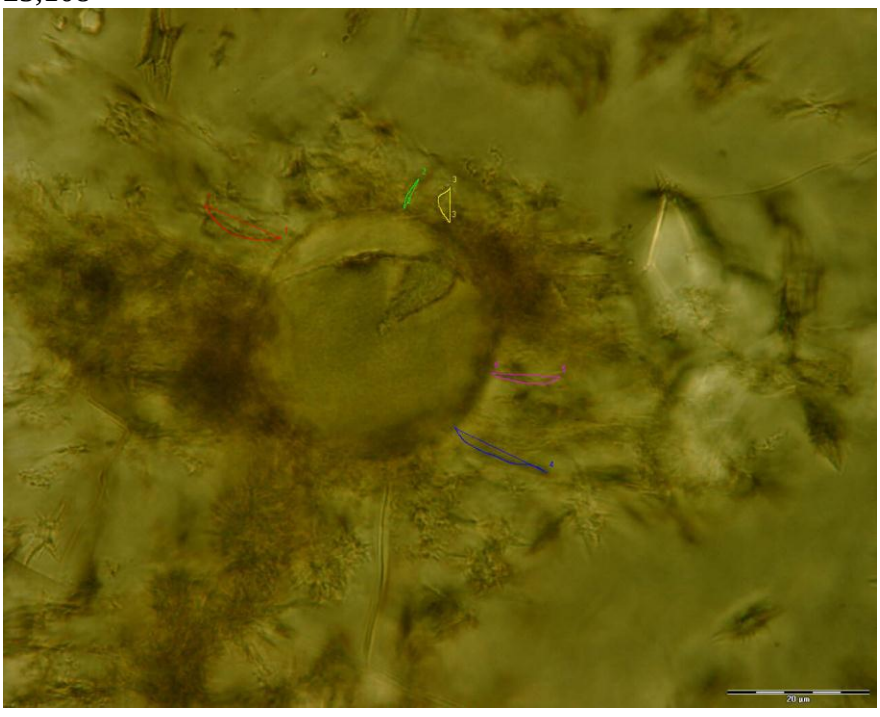

26,110

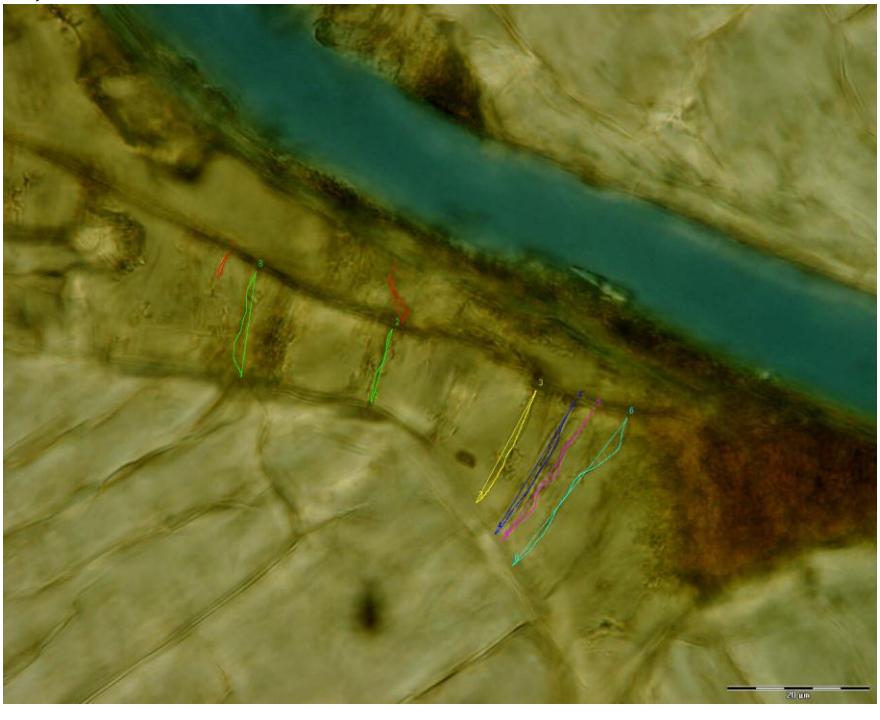

Location:

29, 101,b

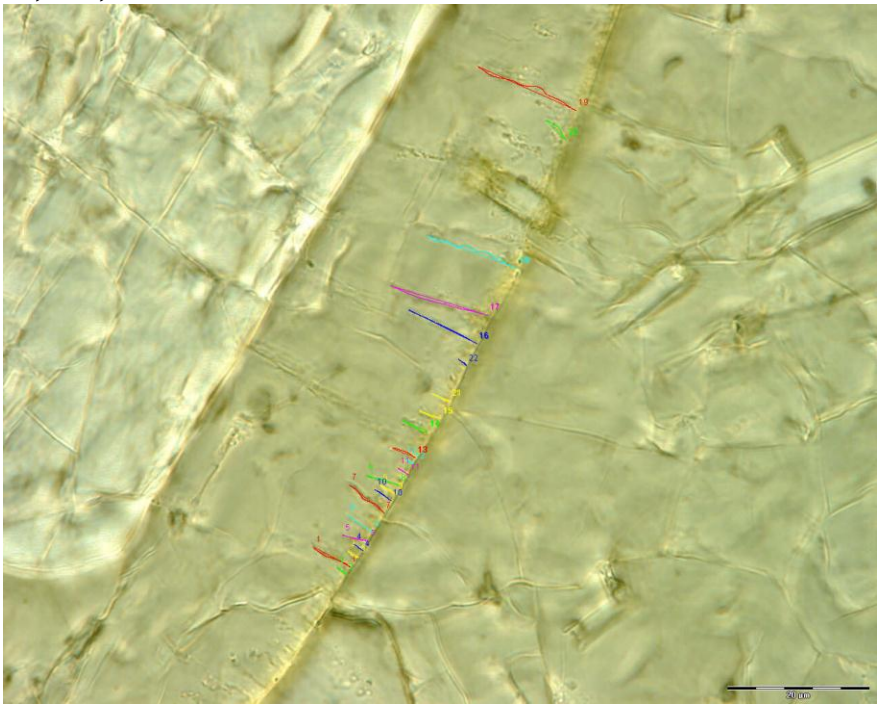

29, 101

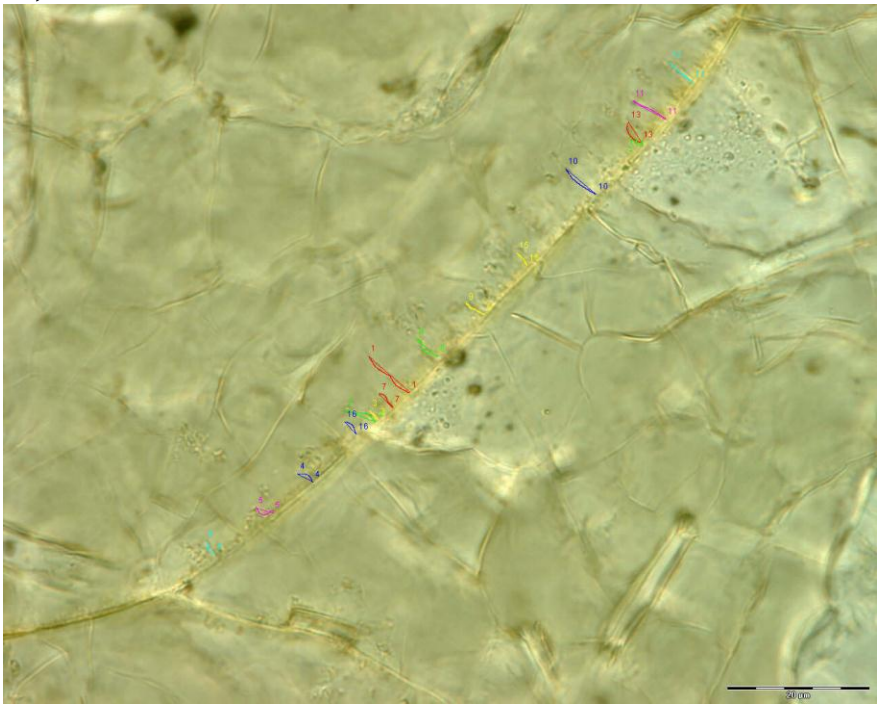

27.5, 101

35,104

36.5,104

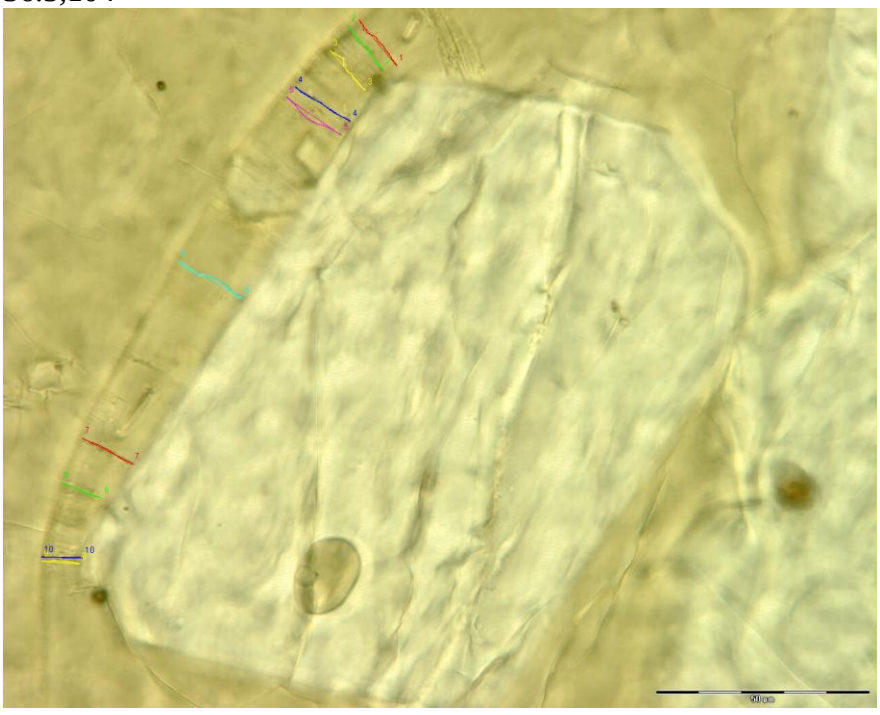

32,106

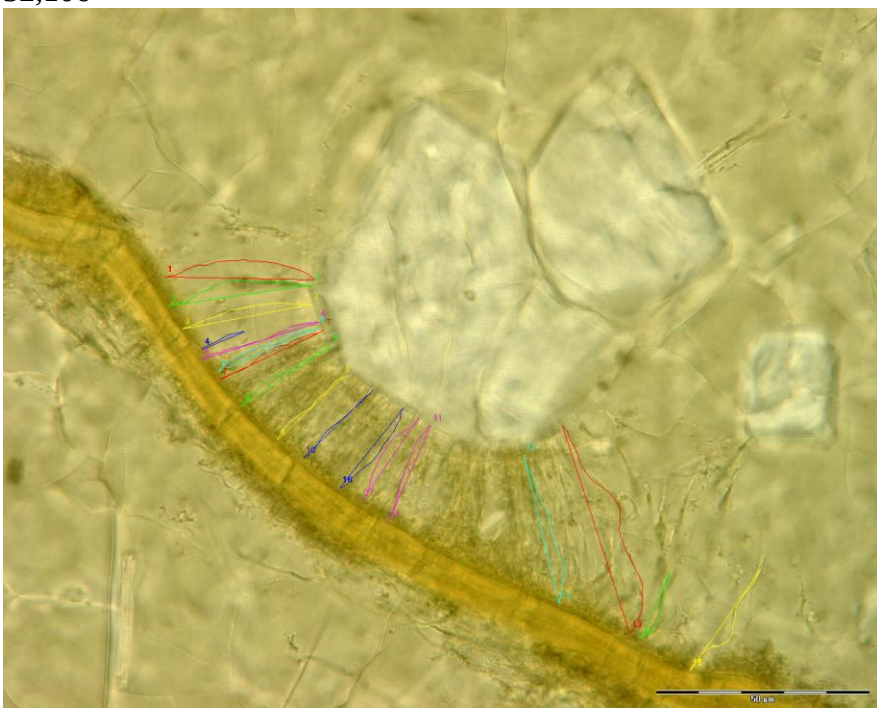

26.5,104

27,113

24,116

29,102

32,107

Location:

26,103

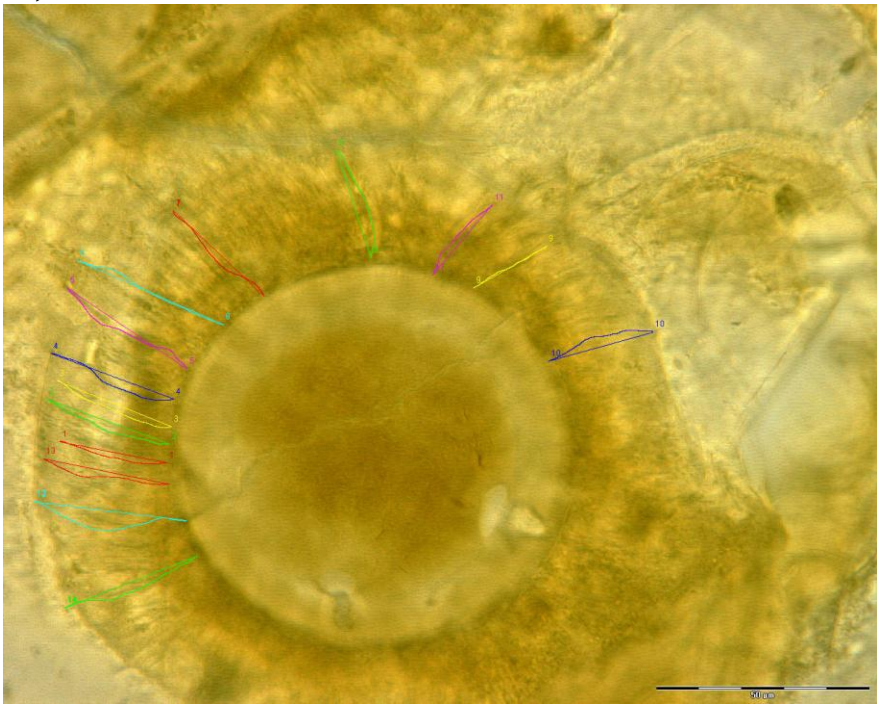

29,103

32,103

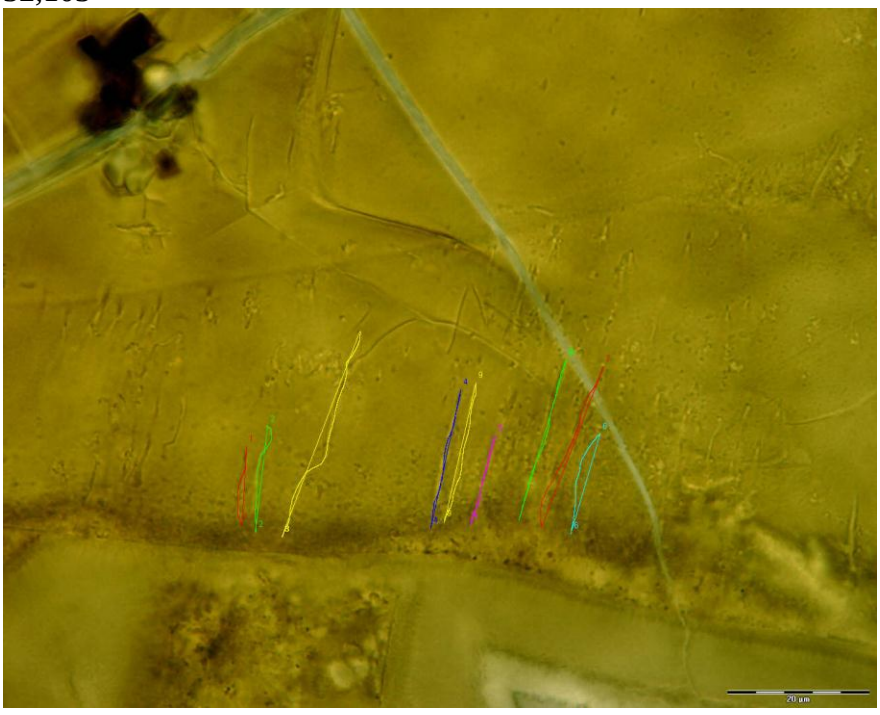

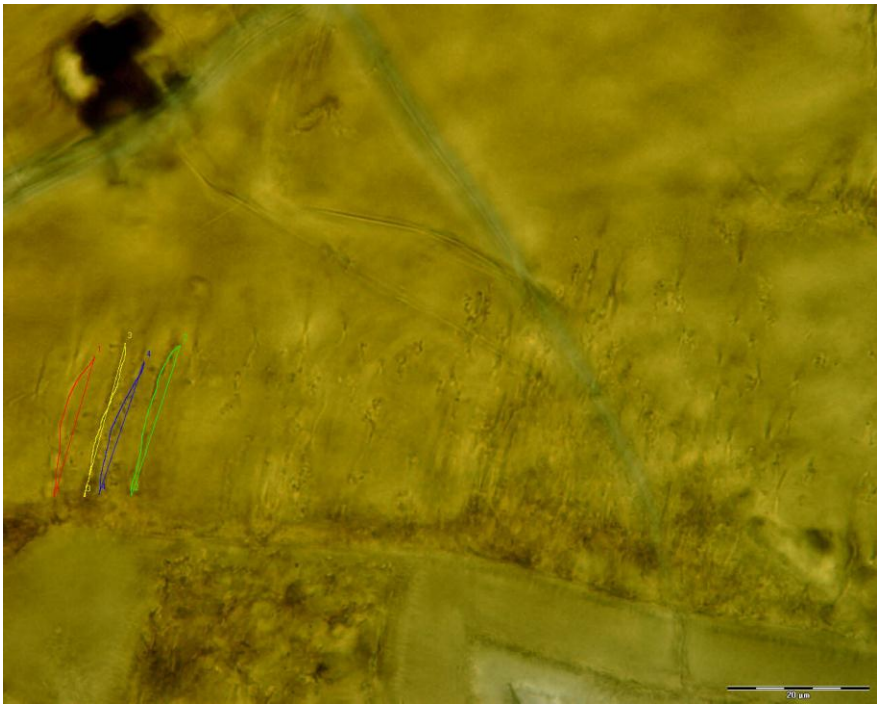

28,103

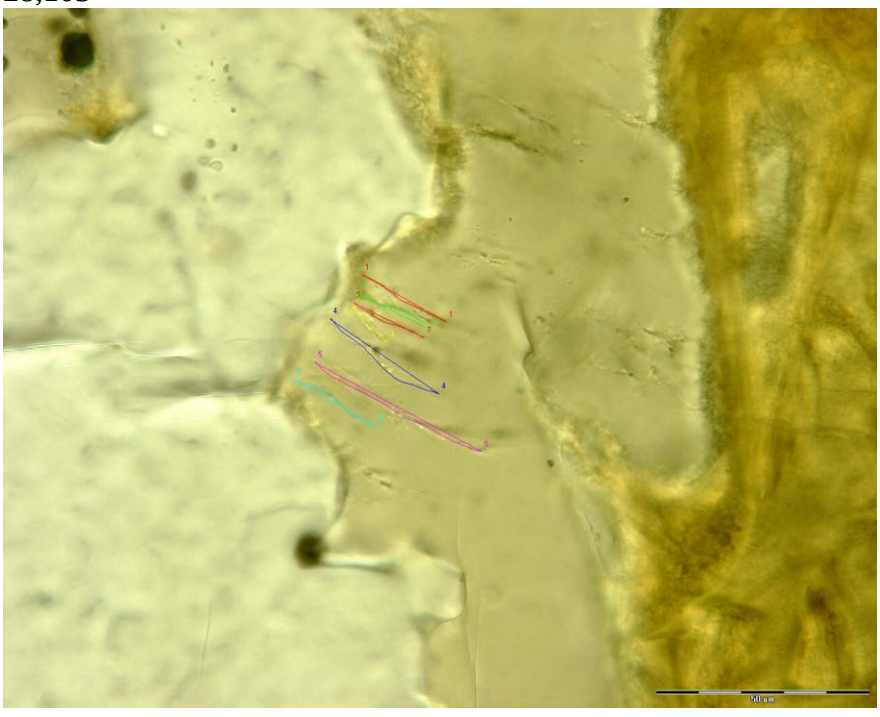

32,110,d

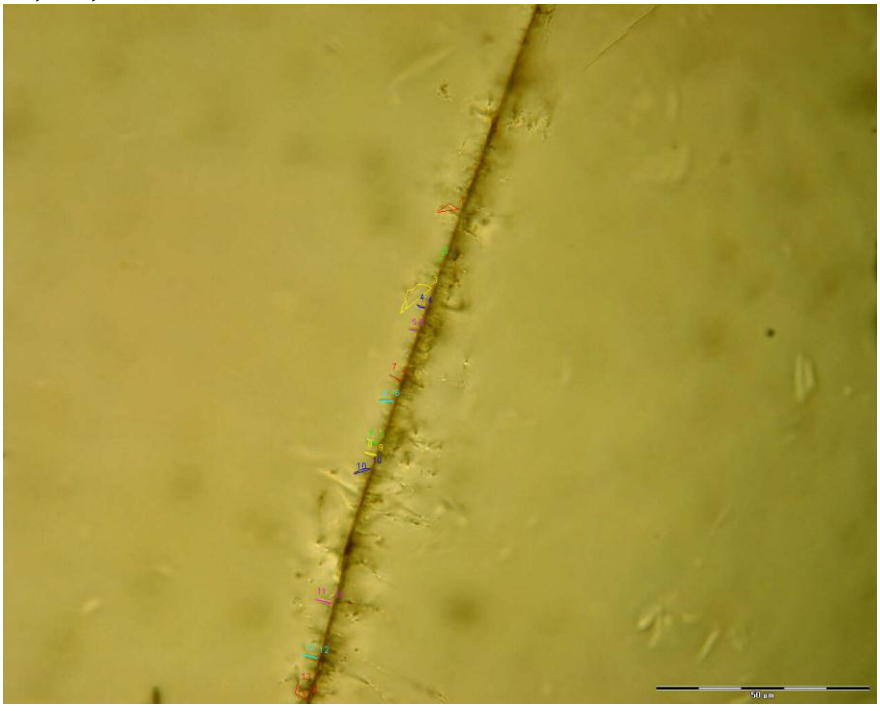

32,110,c

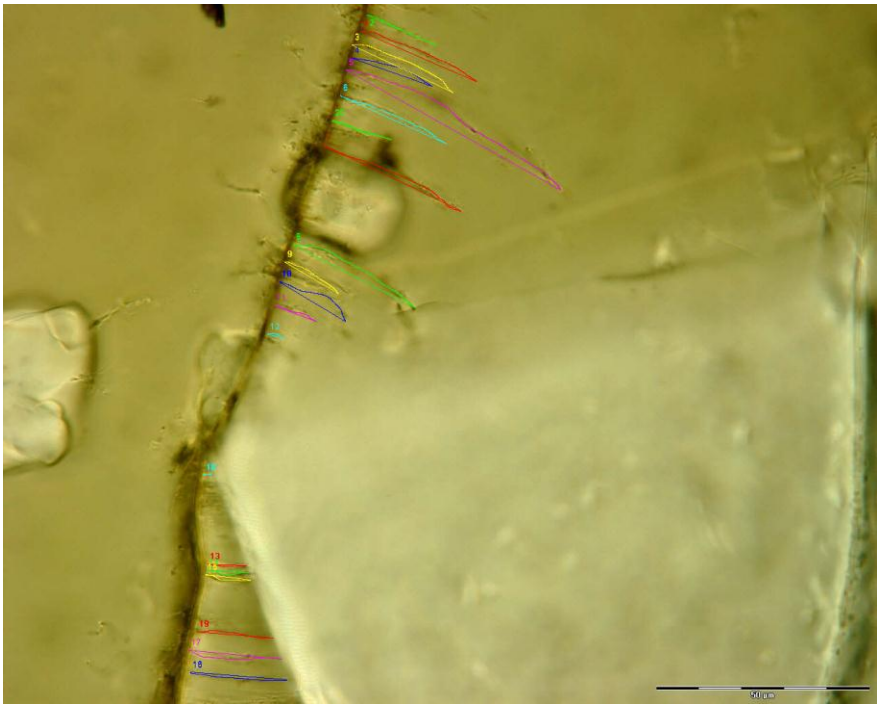

32,110,b

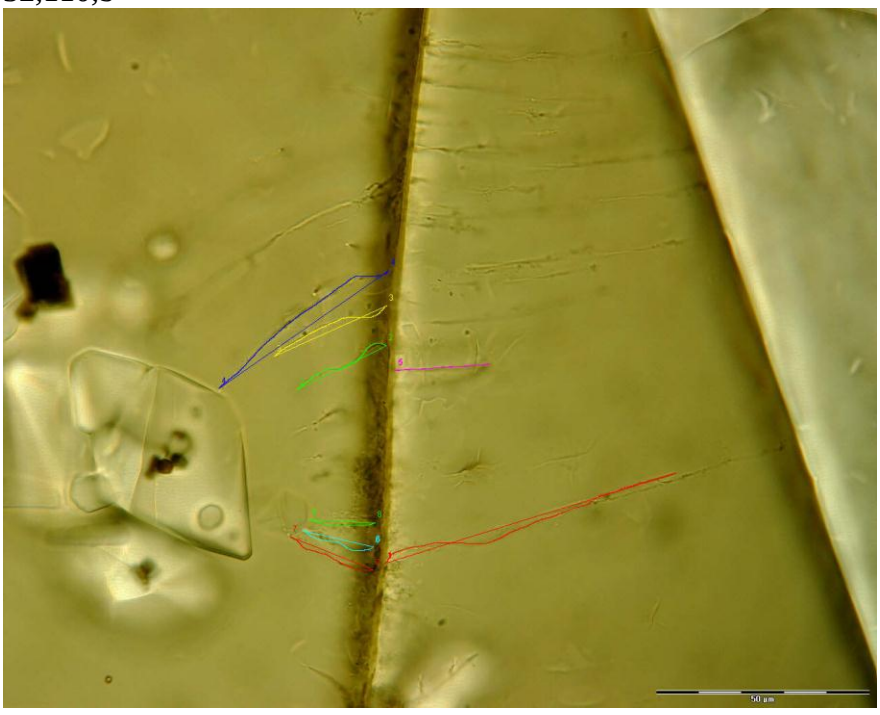

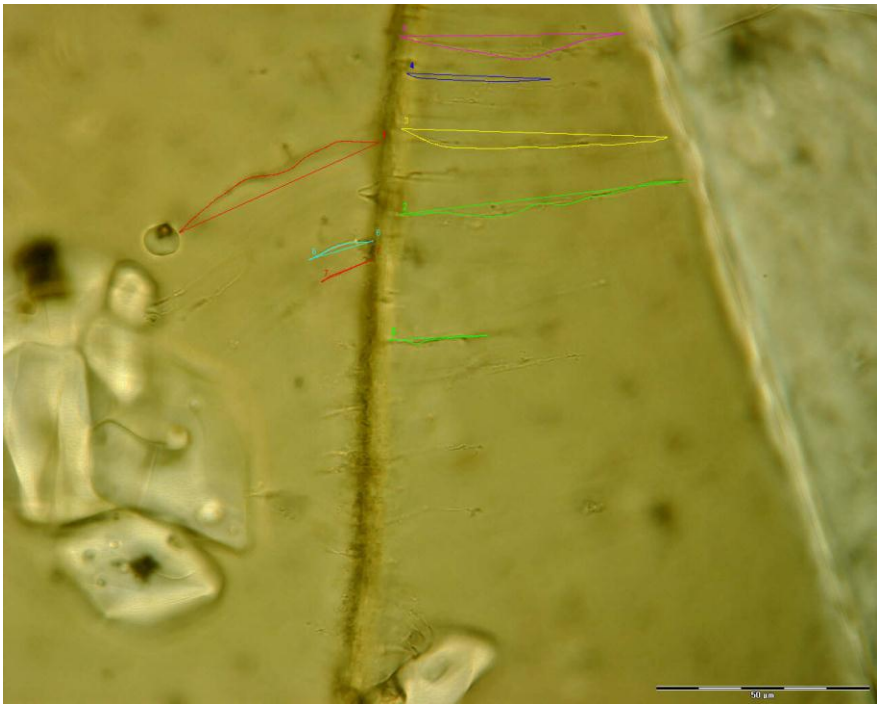

32,110

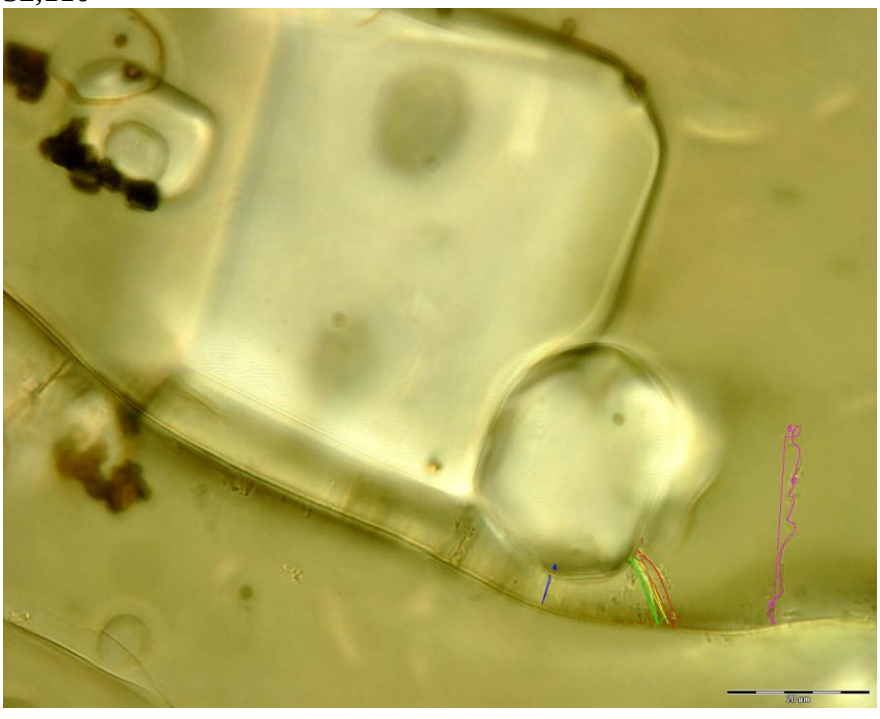

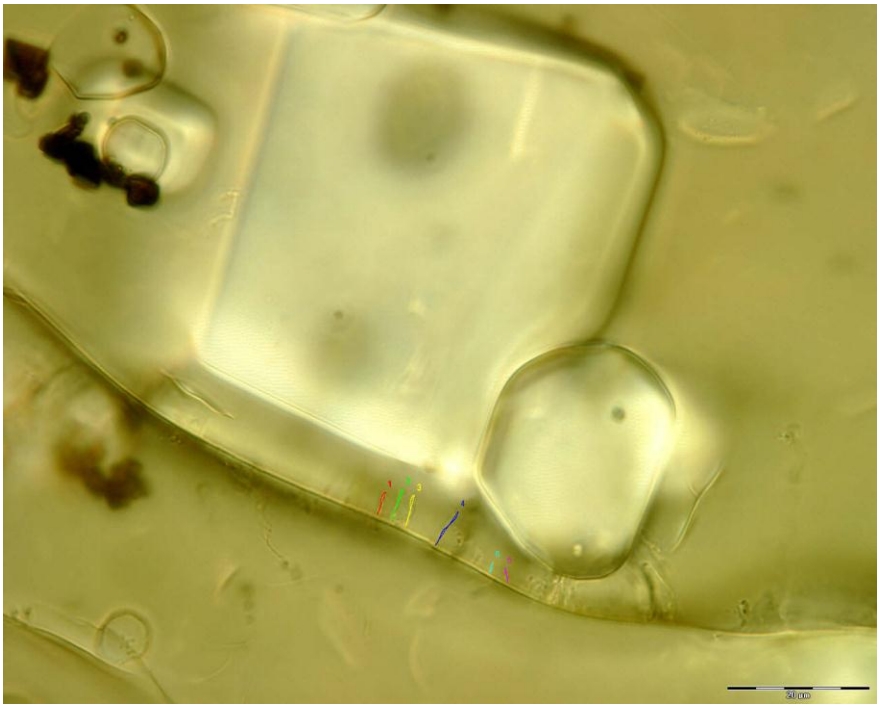

37,103

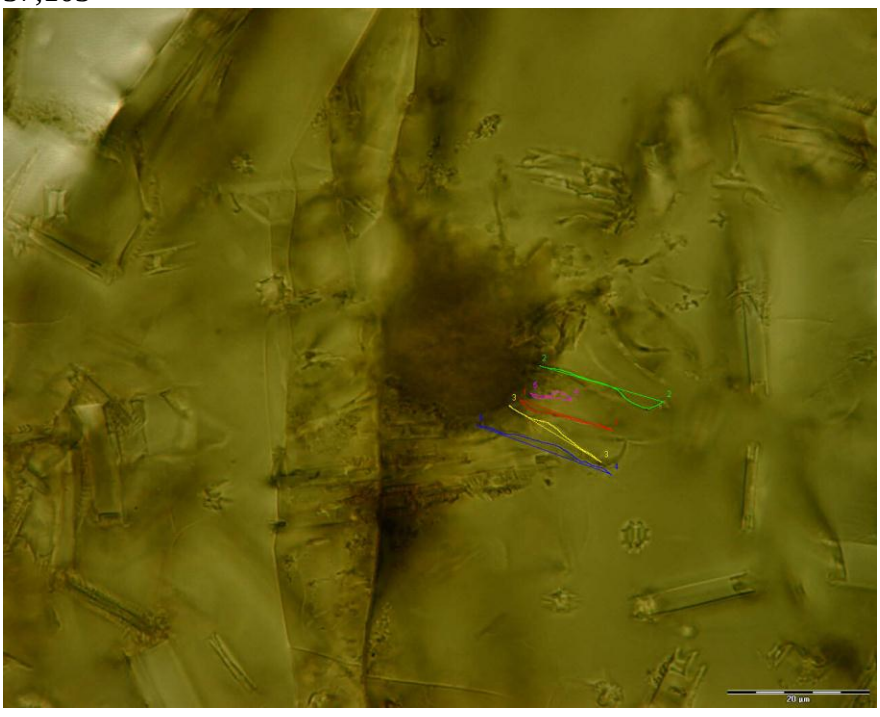

28,111

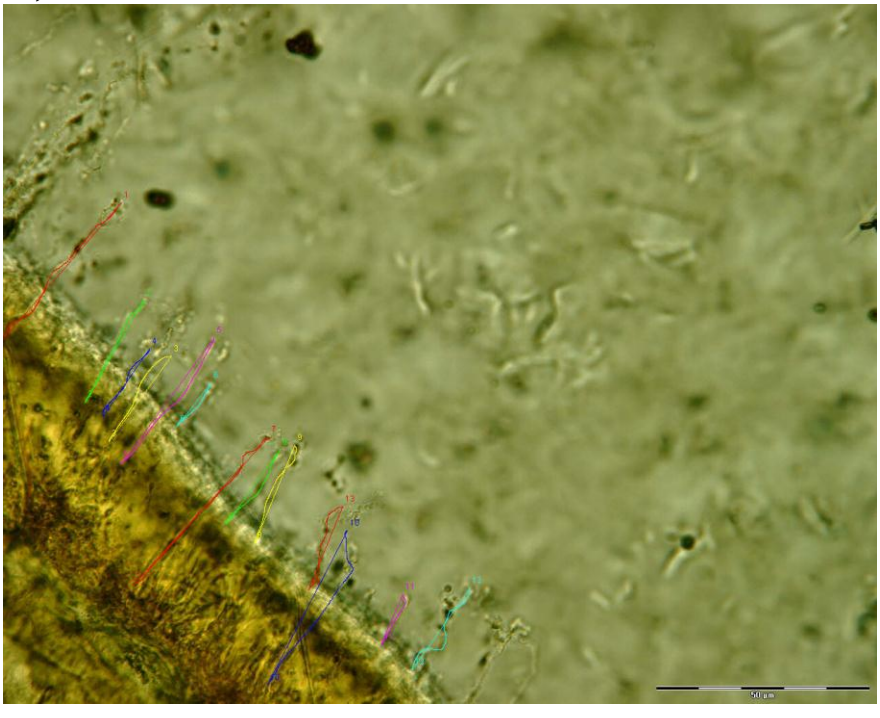

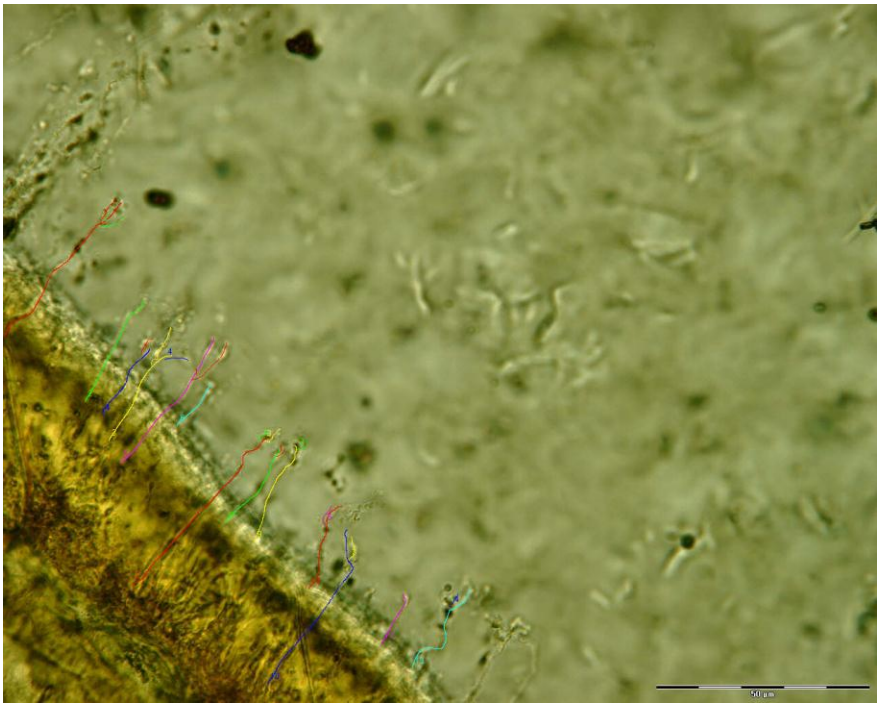

31, 107

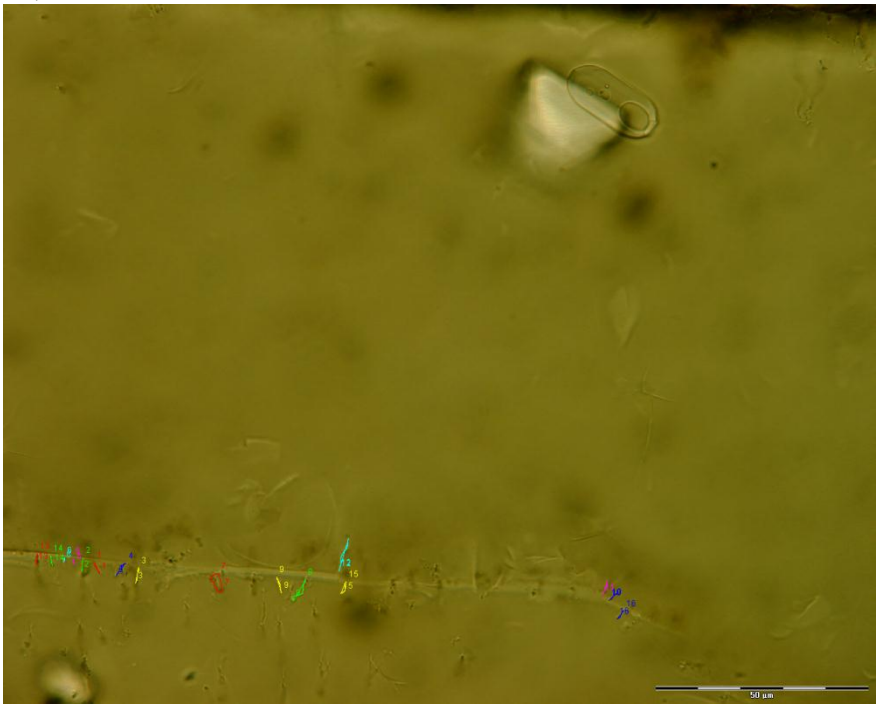

55,118

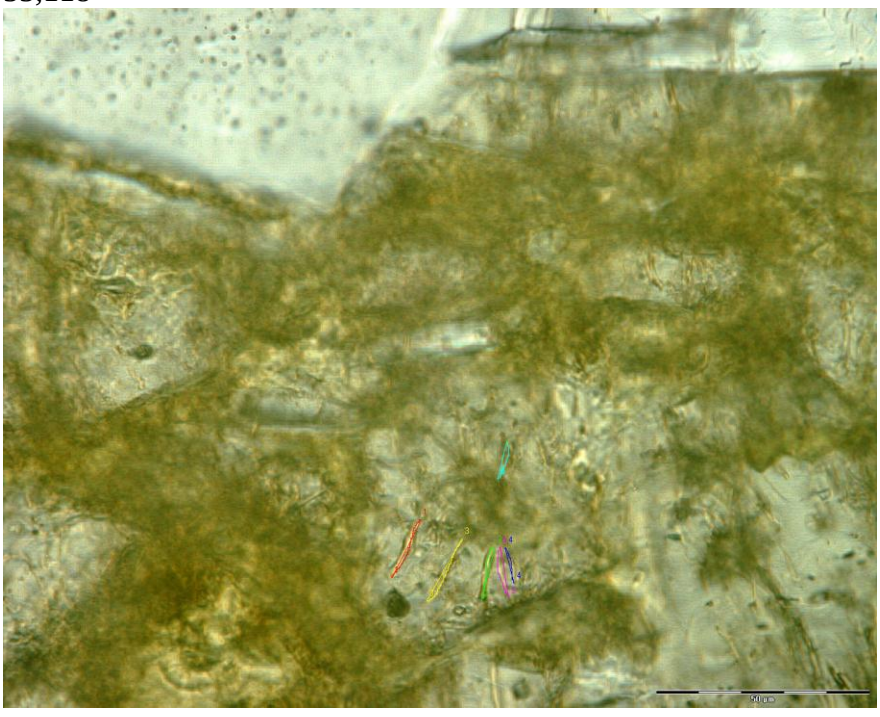

36, 120

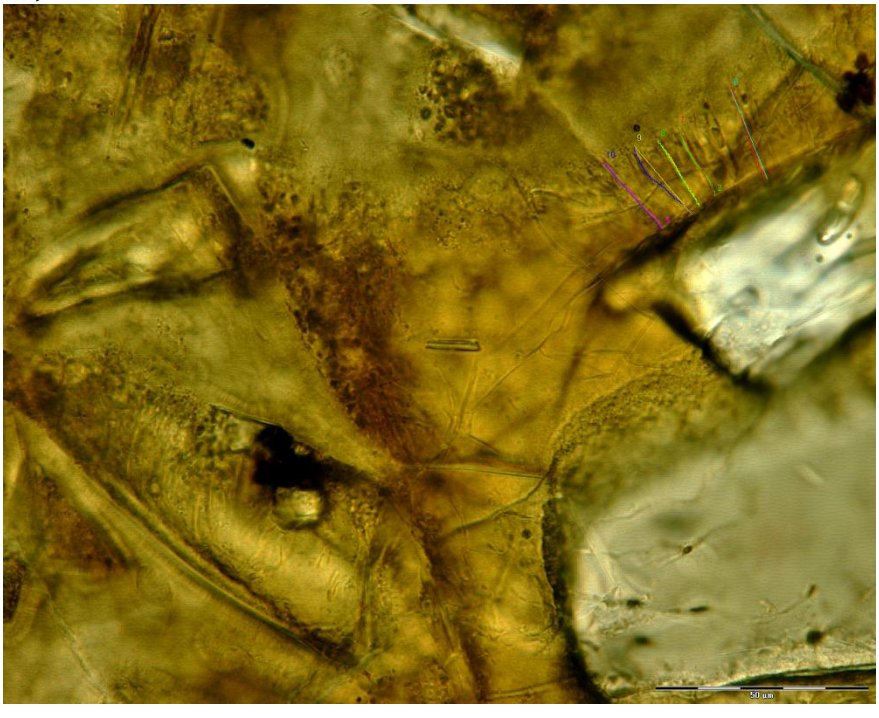

45, 121

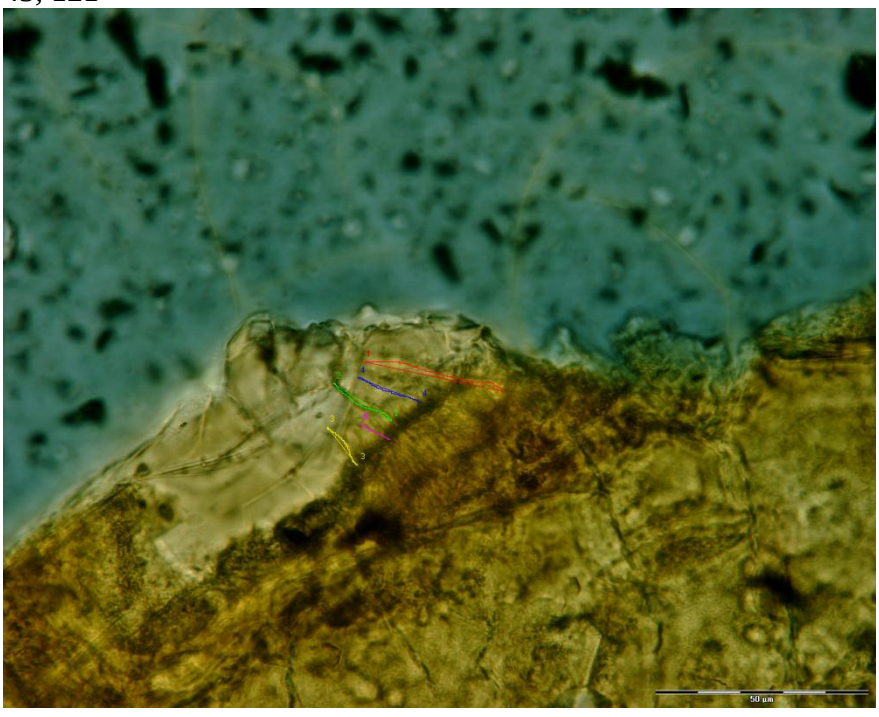

33,112

44,102

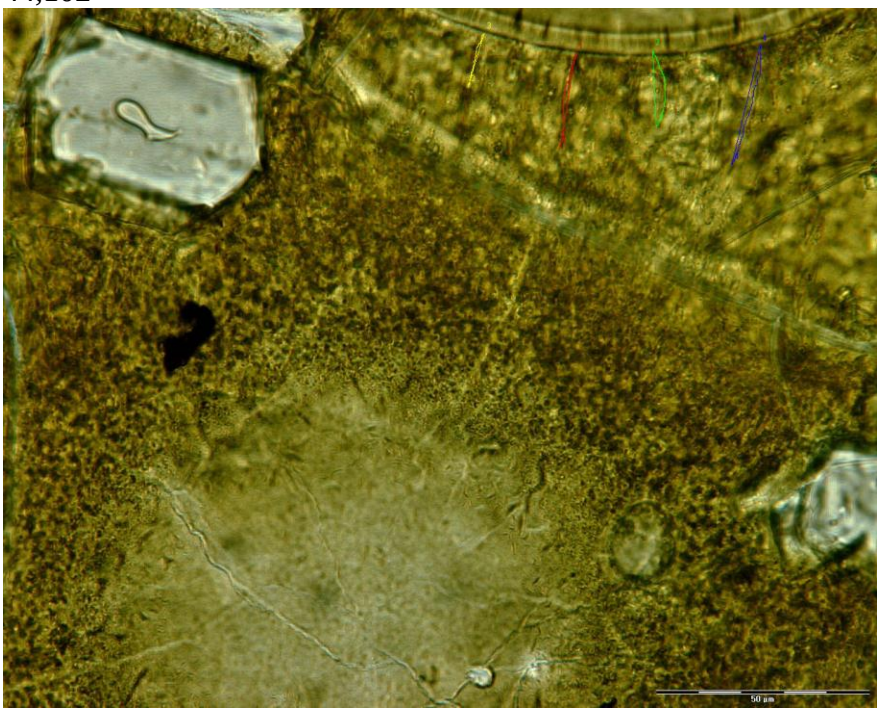

43,108

21,113

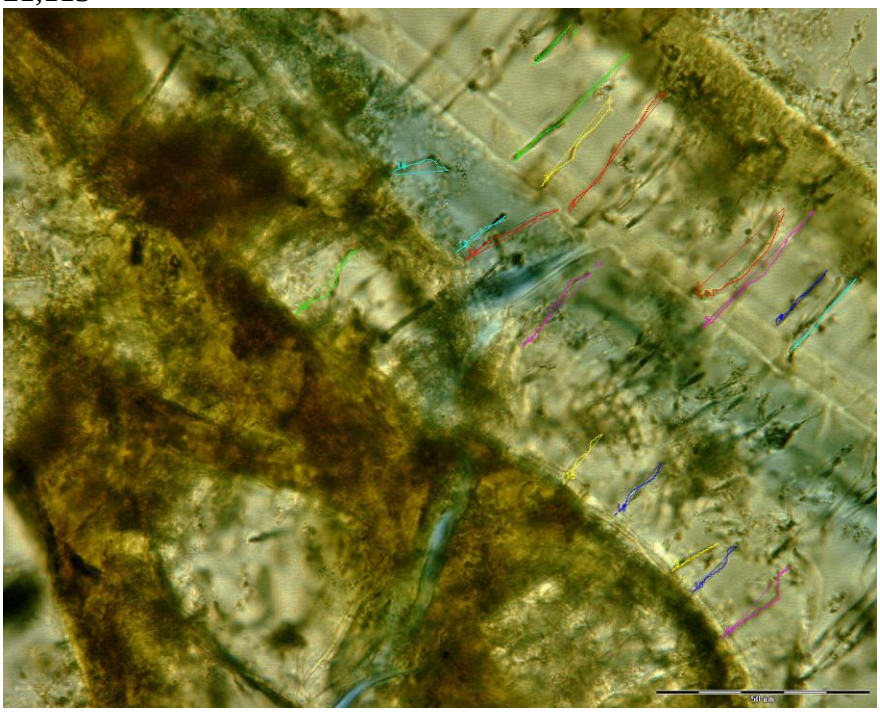

51,111